Continuous-Time Quantum Monte Carlo Studies of Lattice Polarons

by

P E Spencer

A Doctoral Thesis

submitted in partial fulfilment of the requirements

for the award of the degree

Doctor of Philosophy

of

Loughborough University

Supervisor Dr J H Samson

September 2000

Abstract

The polaron problem is studied, on an infinite lattice, using the continuous-time path-integral quantum Monte Carlo scheme The method is based on the Feynman technique to analytically integrate out the phonon degrees of freedom The transformed problem is that of a single electron with retarded self-interaction in imaginary time The Metropolis algorithm is used to sample an ensemble of electron trajectories with twisted (rather than periodic) boundary conditions in imaginary time, which allows dynamic properties of the system to by measured directly The method is numerically "exact", in the sense that there are no systematic errors due to finite system size, trotter decomposition or finite temperature The implementation of the algorithm in continuous imaginary time dramatically increases computational efficiency compared with the traditional discrete imaginary-time algorithms

Various models that differ only in the form or "shape" of the electron-phonon interaction are investigated from the (short range) Holstein model, to the (long range) Frohlich interaction model Furthermore, the effect of "screening" is studied for the Frohlich polaron The ground state energy, effective mass, number of phonons and the isotope exponent are computed for all models, to a high level of statistical accuracy, as functions of electron-phonon coupling strength at various phonon frequencies

The Quantum Monte Carlo results are in excellent agreement with both strong-coupling per-turbation theory (in the small-polaron regime) and with weak-coupling perturbation theory (in the large-polaron regime) The transition between large and small polaron is smooth, and becomes broader as the phonon frequency increases, or as the "spread" of the interaction increases

It is evident from this work that the range of the electron-phonon interaction plays a significant role in determining the properties of the polaron over the entire parameter-space of the system

Acknowledgments.

I would like to thank Dr John H Samson for his helpful advice and guidance throughout the course of this work at Loughborough University I would also like to thank Professor Sasha Alexandrov for regular useful discussions and suggestions Finally, I gratefully acknowledge Dr Pavel Kornilovich for his invaluable explanation, advice and suggestions on the method of continuous-time quantum Monte Carlo

P E Spencer

September 2000

Contents

11 Conclusions and Further Work 106

References 110

Chapter 1

Introduction

1.1 The Polaron Problem

The concept of the polaron can be traced back to Hippel [1] and Landau [2] in the 1930s. A *polaron* is a quasiparticle that is formed as an electron moves *slowly* through a polar crystal. Its constituent parts are the "bare" electron, and the accompanying lattice distortion – induced by the electron in its immediate vicinity, via the Coulomb interaction. The interaction of the electron with the surrounding polarisation (phonon) field results in a reduction of the ground-state energy, and also an enhancement of the Bloch effective mass of the electron.

The Frohlich model [3] was introduced in 1950 in order to study the polaron problem for *weak* electron-phonon coupling. Here the (single) electron interacts only with the (longitudinal) optical vibrational mode of the lattice ions, which is assumed to be dispersionless. This treatment relies on the fact that, for weak coupling, the polaron state is much larger than the associated lattice distance ("large polaron"), allowing the dielectric to be treated as a continuum. Frohlich considered the ground state of the large polaron using second-order perturbation theory.

When the electron-phonon coupling is *strong*, on the other hand, the electron may become "trapped" in the potential well created by the induced lattice distortion. If the reduction of the ground state energy of the polaron is comparable with the half-bandwidth of the "bare" electron, then it is energetically favorable for localised states to exist [4]. If this is the case, then the polaron "radius" is comparable with the associated lattice distance ("small polaron"), and thus the treatment of the lattice as a continuum is no longer valid. In 1954 Frohlich obtained the

1

ground-state energy of the small polaron [5] by using a variational trial wave function – the form of which had been earlier introduced by Pekar [6] Holstein studied the small polaron using a short range electron-phonon interaction [7, 8] More recently, Alexandrov used a perturbation technique (away from the exact extreme-coupling solution obtained by Lang and Firsov [9]) to show that the small polaron can move from site to site, at zero temperature, through the action of zero-point motion [4, 10]

Recently, there has been an increasing amount of experimental evidence to suggest that polarons are present in the high-temperature metal-oxide superconductors [11, 12, 13, 14] and in the magneto-resistance manganites [15, 16, 17] This recent experimental evidence has served to renew theoretical interest in the polaron problem, particularly at intermediate coupling, which is the most physically realistic coupling regime

There is no exact solution to the single polaron problem at intermediate coupling Neither the strong or weak coupling approaches outlined above provides a realistic treatment of the situation at intermediate coupling, where there exists a "self-trapping" transition from large to small polaron This transition has been studied using a variety of different numerical approaches, such as finite-cluster diagonalisation [18, 19, 20], variational methods [21], density matrix renormalisation [22], and various quantum Monte Carlo techniques [23, 24, 25, 26, 27, 28]

In this work, we study the transition from large to small polaron, using the quantum Monte Carlo (QMC) technique recently developed by Kornilovitch [29, 30] In particular, we are interested in the way the form or "shape" of the electron-phonon interaction affects the properties of the polaron We measure various physical properties of the polaron the ground state energy, the number of phonons in the polaron cloud, the effective mass of the polaron, and the exponent of the isotope effect on the effective mass

1.2 Generalised Model Hamiltonian

The model Hamiltonian used in this work describes a single electron interacting with all the ions of an infinite lattice The model Hamiltonian is "generalised", in the sense that no restriction is placed on the form of the electron-phonon interaction The actual "forces" used in the QMC simulations are briefly discussed in section (1 4)

The general electron-phonon model under investigation was recently introduced by Alexandrov and Kornilovitch [30, 31], and is based on the Holstein molecular crystal model [7] The model

Hamiltonian represents a single electron interacting with *all* the ions of an infinite hypercubic lattice, with one vibrational degree of freedom per unit cell The generalised model Hamiltonian reads

$$H = H_e + H_{ph} + H_{e-ph},\tag{1 1}$$

where

$$H_e = -t \sum_{\langle nn' \rangle} c_n^\dagger c_{n'},\tag{1 2}$$

$$H_{ph} = \frac{1}{2M} \sum_m P_m^2 + \frac{M\omega^2}{2} \sum_m \xi_m^2,\tag{1 3}$$

and

$$H_{e-ph} = -\sum_{nm} f_m(n) c_n^\dagger c_n \xi_m\tag{1 4}$$

Let us discuss each term of this model Hamiltonian separately below

The first term of the Hamiltonian, the *free-electron term* H_e, describes the movement of a single electron through the lattice by the process of nearest-neighbour hopping Here the operator $c_n^\dagger$ creates an electron on site n, the operator c_n destroys an electron on site n', and $\langle nn' \rangle$ denotes pairs of nearest-neighbour sites Thus the electron hops from site to nearest-neighbour site with a (nearest-neighbour) *hopping amplitude* of t The electron term, in reciprocal (Bloch) space, is given by [7]

$$H_{el} = \sum_k \varepsilon_k c_k^\dagger c_k,\tag{1 5}$$

where the *free electron dispersion*

$$\varepsilon_k = -2t \sum_{d=1}^{D} \cos(k_d a)\tag{1 6}$$

where a is the lattice constant, k is the wave vector of the electron, and d labels the component of the D dimensional hypercubic lattice Note that we will use t as a convenient base unit of energy

The second term of the Hamiltonian, the *phonon term* H_{ph}, represents the vibrations of the lattice ions Here the operator ξ_m is the displacement of the m'th ion from its equilibrium position, and the operator P_m is its momentum, where $P_m = -i\hbar \partial/\partial \xi_m$ In this model it is assumed that the ions vibrate *independently* of one another (non-interacting Einstein oscillators) Thus, the ions, each having ionic mass M, have the same characteristic (phonon) frequency ω

The final part of the Hamiltonian, the electron-phonon term H_{e-ph}, represents the interaction between the electron and *all* the ions in the lattice The electron-ion interaction is of the "density-displacement" type, where the interaction energy between the electron and the m'th ion is proportional to ξ_m (the displacement of the m'th ion from its equilibrium position) Here $c_n^\dagger c_n$

is the electron number operator, and $f_{\mathbf{m}}(\mathbf{n})$ is interpreted as the *interaction force* between the electron on site $\mathbf{n}$ and the $\mathbf{m}$'th lattice ion. The interpretation of $f_{\mathbf{m}}(\mathbf{n})$ as a force, and the forms of $f_{\mathbf{m}}(\mathbf{n})$ under investigation in this work will be briefly discussed in section (1 4)

The generalised model Hamiltonian is parameterised by two dimensionless quantities, that are used as control parameters. The first is the *dimensionless phonon frequency* or *adiabatic ratio*, defined as

$$\bar{\omega} = \hbar\omega/t \qquad (1\ 7)$$

In the adiabatic limit $\bar{\omega} \ll 1$, the electron moves much more quickly than the phonons. The opposite is true for the anti-adiabatic limit $\bar{\omega} \gg 1$, where the lattice deformation reacts instantaneously to the position of the charge carrier. The second control parameter is related to the small-polaron binding energy E_{p}, derived in chapter (8), which serves as a natural and convenient measure of the strength of the electron-phonon interaction. The dimensionless *electron-phonon coupling constant* is defined as

$$\lambda = \frac{E_{\mathrm{p}}}{zt} = \frac{1}{2M\omega^2 zt}\sum_{\mathbf{m}} f_{\mathbf{m}}^2(0), \qquad (1\ 8)$$

where zt is the bare-electron half bandwidth, with z the lattice coordination number ($z = 2$ for a one-dimensional lattice). The definitions of $\bar{\omega}$ and λ are discussed in more detail in section (5 4)

In the limit of weak coupling $\lambda \ll 1$, the ground state of our generalised model Hamiltonian may be studied using second-order perturbation theory. This treatment is presented in chapter (7). In this limit the lattice ions are only slightly affected by the presence of the electron, and we find band-electron type ("large polaron") states

In the limit of strong coupling $\lambda \gg 1$, on the other hand, the electron is "trapped" on a single site, in a potential well (of "depth" E_p) created by the induced lattice distortion in its immediate vicinity. The ground state is determined using strong-coupling perturbation theory in chapter (8). In this limit we find localised ("small polaron") states

The strong-coupling and weak-coupling perturbation approaches are not able to describe the system at intermediate values of coupling $\lambda \sim 1$, where the transition from large to small polaron occurs. The path integral quantum Monte Carlo method allows us to numerically study the polaron properties of our generalised model Hamiltonian over the *whole* range of λ

1.3   Second-Quantisation

We will find it useful to express the terms H_{ph} and H_{e-ph} of equation (1 1) in second quantised form In order to do so, we must transform the operators ξ_m and P_m into the phonon creation and annihilation operators, $d_m^\dagger$ and d_m respectively It can easily be shown that the choice of

$$d_m = \sqrt{\frac{M\omega}{2\hbar}}\xi_m + \frac{\imath}{\sqrt{2M\omega\hbar}}P_m \quad , \quad d_m^\dagger = \sqrt{\frac{M\omega}{2\hbar}}\xi_m - \frac{\imath}{\sqrt{2M\omega\hbar}}P_m \tag{1 9}$$

satisfies the required fundamental commutator relation $[d_m, d_m^\dagger] = 1$ (given that $[\xi_m, P_m] = \imath\hbar$) One can see from equation (1 9) that

$$\xi_m = \sqrt{\frac{\hbar}{2M\omega}}(d_m + d_m^\dagger) \tag{1 10}$$

and

$$P_m = -\imath\sqrt{\frac{\hbar\omega M}{2}}(d_m - d_m^\dagger) \tag{1 11}$$

Thus, the electron-phonon term H_{e-ph}, equation (1 4), is given in second-quantised form as

$$H_{e-ph} = -\sqrt{\frac{\hbar}{2M\omega}}\sum_{nm} f_m(n)c_n^\dagger c_n \left(d_m^\dagger + d_m\right), \tag{1 12}$$

and the phonon term H_{ph}, equation (1 3), is given by

$$H_{ph} = \hbar\omega \sum_m (d_m^\dagger d_m + \tfrac{1}{2}), \tag{1 13}$$

where the operator $d_m^\dagger d_m$ is the number of phonons on site m

It is worth pointing out that the ground-state energy of the phonon sub-system, which is given by the term $\hbar\omega \sum_m (1/2)$ in equation (1 13), is infinity for an infinite lattice (if $\omega > 0$) This, however, is not a problem due to the fact that the zero of energy is simply a matter of definition – it is only ever *differences* in energy that have physical meaning Thus, whenever necessary, we may shift the ground state of the phonon sub-system to zero by redefining the phonon term as

$$H_{ph} = \frac{1}{2M}\sum_m P_m^2 + \frac{M\omega^2}{2}\sum_m \xi_m^2 - \hbar\omega\sum_m \tfrac{1}{2} \tag{1 14}$$

$$= \hbar\omega \sum_m d_m^\dagger d_m, \tag{1 15}$$

without altering the "physics" of the model in any way

1.4   Electron-Phonon Interaction Force

The electron-phonon interaction force $f_m(n)$ is the force exerted on the m'th oscillator due to the presence of the electron on site n The general aim of this work is to study what role the form of the electron-phonon interaction plays in determining the polaron properties

The interpretation of $f_m(n)$ as a force can be understood from the following argument   Let δU_{mn} be the work done in displacing the m'th ion a small distance ξ_m from its equilibrium position   Then from first principles we may write $\delta U_{mn} = f_m(n)\xi_m$ where $f_m(n)$ is the internal "force" between the m'th ion and the electron on site n

In order to provide some insight, we will briefly mention the various interaction models (distinguished by different forms of $f_m(n)$) that are to be investigated   The different models are

- The ("short-range") Holstein molecular crystal model, with

$$f_m(n) = \kappa \delta_{m,n},\qquad (1\ 16)$$

where κ takes on the dimensionality of force   This interaction is "short-range" in the sense that the electron interacts only with the lattice ion on the site it currently occupies   We will study the Holstein model in chapter (9) for a range of different values of $\bar{\omega}$

- The ("long-range") discrete Frohlich model   This model was recently introduced by Alexandrov and Kornilovitch to describe the polaronic behavior in high-T_c cuprates   The electron interacts with *every* lattice ion with an interaction force of the form

$$f_m(n) = \frac{\kappa}{\left(|m-n|^2 + 1\right)^{3/2}},\qquad (1\ 17)$$

where κ takes on the dimensionality of force, and the lattice constant $a = 1$ The geometry of this model will be discussed in chapter (10)   We will see that the properties of the Holstein and Frohlich polaron are significantly different   The Holstein polaron, for example, is much "heavier" at large couplings than the Frohlich polaron

- The screened (discrete) Frohlich model   It is interesting, at least from a theoretical point of view, to reduce the "spread" of the discrete Frohlich interaction by including, in $f_m(n)$, the screening effect of other electrons in the lattice   The electron-phonon force for the screened Frohlich model is given by

$$f_m(n) = \frac{\kappa}{\left(|m-n|^2 + 1\right)^{3/2}} \exp\left(-\frac{|m-n|}{R_{sc}}\right),\qquad (1\ 18)$$

where the lattice constant $a = 1$, and R_{sc} is known as the *screening length*   Thus the screened Frohlich interaction force is that of the non-screened interaction multiplied by an exponential damping factor   Note that in the limits $R_{sc} \to 0$ and $R_{sc} \to \infty$ equation (1 18) describes the Holstein interaction and the non-screened Frohlich interaction respectively   In chapter (10) we will study two intermediate values of R_{sc} in order to provide further insight into the differences between the Holstein and non-screened Frohlich models

We will avoid imposing restrictions on the form of $f_\mathbf{m}(\mathbf{n})$ throughout the theoretical formulation of the QMC scheme, which is presented in the next few chapters

The term "range" is simply used to indicate the spatial extent of the influence that the interaction force $f_\mathbf{m}(\mathbf{n})$ has on the lattice ions – regardless of the magnitude of the force   Thus, the Holstein interaction is "short range" because the electron interacts only with the site it currently occupies, whereas the screened and non-screened Frohlich interaction is "long range" because it interacts with *all* the ions in the lattice

The term *polaron cloud* refers to the lattice distortion associated with the polaron   Note that, the electron interacts linearly with the oscillators, equation (1 4), and so for the long-range interactions presented above, the polaron cloud extends over a large number of lattice sites   Historically, the terms "large polaron" and "small polaron" refer to the electronic wave function and not to the polaron cloud   Please note that, to avoid confusion, we will continue to follow this convention in this work   Thus, for example, the non-screened Frohlich polaron at $\lambda \to \infty$ is still referred to as a "small polaron" (because the "size" of the localised state is of the order of a lattice constant) even though the polaron cloud extends over many lattice sites

Chapter 2

Path-Integral Approach

2.1 Introduction

We start this chapter by converting the partition function for the system into path-integral representation   This transformation introduces an extra dimension, which may be interpreted as "imaginary time"   We present details of the traditional path-integral Quantum Monte Carlo approach in section (2 5), which is formulated in discrete imaginary time   The reason this method has been so widely adopted is probably due to ease of programming   However, it does suffer from the systematic finite imaginary-time-step error   In section (2 6), we briefly discuss the implementation of the path integral QMC method in *continuous* imaginary time, in which the imaginary-time-step error is completely eliminated

2.2 Path Integral Representation

In this section we determine the quantum statistical partition function for our model Hamiltonian in path integral representation   The standard method of achieving this, which is presented below, is well known in the literature [26, 23, 24]   Here we will consider the path integral from a purely mathematical point of view, and then discuss its intuitive interpretation in the next section

The partition function for our generalised model Hamiltonian is given by

$$Z = \sum_{\mathbf{r}} \int d^N \xi \langle \{\xi_\mathbf{m}\}, \mathbf{r} \mid e^{-\beta H} \mid \{\xi_\mathbf{m}\}, \mathbf{r} \rangle, \qquad (2\ 1)$$

where we have adopted the shorthand

$$\int d^N \xi = \prod_{m=1}^{N} \left[\int_{-\infty}^{\infty} d\xi_m \right] \tag{2 2}$$

Here we have summed over the *discrete* electron states $|\mathbf{r}\rangle$ and integrated over the *continuous* phonon states $|\xi_m\rangle = |\xi_1, \xi_2, \xi_3, \quad , \xi_N\rangle$

In order to form the path integral of the partition function, the Boltzmann factor $e^{-\beta H}$, appearing in equation (2 1), is decomposed into L factors, so that

$$Z = \sum_{\mathbf{r}} \int d^N \xi \langle \{\xi_m\}, \mathbf{r} \mid e^{-\Delta \tau H} e^{-\Delta \tau H} \quad e^{-\Delta \tau H} \mid \{\xi_m\}, \mathbf{r} \rangle, \tag{2 3}$$

where we have defined

$$\Delta \tau = \beta / L, \tag{2 4}$$

and then a complete set of states,

$$\sum_{\mathbf{r}_l} \int d_l^N \mid \{\xi_{m,l}\}, \mathbf{r}_l \rangle \langle \{\xi_{m,l}\}, \mathbf{r}_l \mid = 1, \tag{2 5}$$

is inserted between each pair of factors in equation (2 3) – a total of $(L-1)$ times Thus the partition function in path integral representation is given by

$$Z = \sum_{\{\mathbf{r}_l\}} \int d^{NL} \xi \langle \{\xi_{m,L}\}, \mathbf{r}_L \mid e^{-\Delta \tau H} \mid \{\xi_{m,L-1}\}, \mathbf{r}_{L-1} \rangle \langle \{\xi_{m,L-1}\}, \mathbf{r}_{L-1} \mid \times \tag{2 6}$$

$$\times e^{-\Delta \tau H} \mid \{\xi_{m,1}\}, \mathbf{r}_1 \rangle \langle \{\xi_{m,1}\}, \mathbf{r}_1 \mid e^{-\Delta \tau H} \mid \{\xi_{m,0}\}, \mathbf{r}_0 \rangle$$

$$= \sum_{\{\mathbf{r}_l\}} \int d^{NL} \xi \prod_{l=0}^{L-1} \langle \{\xi_{m,l+1}\}, \mathbf{r}_{l+1} \mid e^{-\Delta \tau H} \mid \{\xi_{m,l}\}, \mathbf{r}_l \rangle, \tag{2 7}$$

where

$$\int d^{NL} \xi = \prod_{m=1}^{N} \prod_{l=0}^{L-1} \left[\int_{-\infty}^{\infty} d\xi_{m,l} \right] \tag{2 8}$$

It is important to realise that the "end-states" in equation (2 7), namely $\langle \{\xi_{m,L}\}, \mathbf{r}_L \mid$ and $\mid \{\xi_{m,L}\}, \mathbf{r}_0 \rangle$, are identified with the states $\langle \{\xi_m\}, \mathbf{r} \mid$ and $\mid \{\xi_m\}, \mathbf{r} \rangle$ from equation (2 1)

2.3 Intuitive Interpretation of the Path Integral

We now discuss a simple intuitive interpretation of the path integral representation of the partition function It is based on the formal similarity between the matrix elements contained in equation (2 7) and the familiar quantum mechanical time-evolution operator,

$$U(t_b, t_a) = e^{-i(t_b - t_a)H/\hbar} \tag{2 9}$$

One can interpret the operator $e^{-\Delta\tau H}$ in equation (2 7) as an "imaginary time evolution operator", that propagates the system through the imaginary time interval $(t_b - t_a) = -i\hbar\Delta\tau$

In forming the path integral we have thus introduced an imaginary time dimension τ with the range $0 \leq \tau \leq \beta$ This range is divided into L *imaginary time slices*, each having width $\Delta\tau = \beta/L$, that are labeled by the *imaginary time index* $0 \leq l \leq L$ The discretisation is illustrated in figure (2 1) Thus, r_l represents the position of the particle in the l'th imaginary time slice, $\xi_{m,l}$ represents the displacement of the oscillator at site m in the l'th time slice, and $f_{m,l}(r_l)$ is the electron-phonon force between the electron (at position r_l) and the m'th ion in the l'th imaginary time slice

The set $\{r_l\}$ constitutes a *single path* or *trajectory* in imaginary time, which is also illustrated in figure (2 1) The whole path integration is then just the sum over all the possible trajectories that takes the particle from the initial state $\mid \{\xi_{m,0}\}, r_0\rangle$ (at imaginary time $\tau_0 = 0$) to the final state $\mid \{\xi_{m,L}\}, r_L\rangle$ (at imaginary time $\tau_L = \beta$) Each of the possible trajectories enter the path integration with a statistical weight given by

$$W = c_1\langle \ \{\xi_{m,l+1}\}, r_{l+1} \mid e^{-\Delta\tau H} \mid \{\xi_{m,l}\}, r_l\rangle, \qquad (2\ 10)$$

where c_1 is a constant Note that the Monte Carlo algorithm evaluates only the *ratio* of weights, and so the constant c_1 (or indeed any other constant multiplier) is of little importance for our purposes

2.4   Evaluation of Matrix Elements

In this section we use the "Trotter decomposition technique", as in [26] and [24], to evaluate the matrix elements $\langle \ \{\xi_{m,l+1}\}, r_{l+1} \mid e^{-\Delta\tau H} \mid \{\xi_{m,l}\}, r_l\rangle$ appearing in our path integral expression for Z, given by equation (2 7) We first break up the generalised model Hamiltonian according to

$$H = H_0 + H_1 + H_{el}, \qquad (2\ 11)$$

where

$$H_0 = \frac{1}{2M} \sum_{m} P_m^2, \qquad (2\ 12)$$

$$H_1 = \frac{M\omega^2}{2} \sum_{m} \xi_m^2 - \sum_{nm} f_m(n) c_n^\dagger c_n \xi_m, \qquad (2\ 13)$$

and

$$H_{el} = -t \sum_{\langle nn'\rangle} c_n^\dagger c_{n'} \qquad (2\ 14)$$

The choice of this particular separation is motivated by the fact that H_1 is diagonal in the chosen set of basis states $\{|\{\xi_{m,l}\}, r_l\rangle\}$ By applying the well known Trotter formula [32],

$$e^{-\Delta\tau H} = e^{-\Delta\tau H_0} e^{-\Delta\tau H_1} e^{-\Delta\tau H_{el}} \left[1 + \mathcal{O}\left(\Delta\tau^2\right)\right], \tag{2 15}$$

and inserting a complete set of states twice, the required matrix element may be written as

$$\langle\{\xi_{m,l+1}\}, r_{l+1}|e^{-\Delta\tau H}|\{\xi_{m,l}\}, r_l\rangle \approx \sum_{r,r'} \int d^{NL}\xi d^{NL}\xi' \langle\{\xi_{m,l+1}\}, r_{l+1}|e^{-\Delta\tau H_0}|\{\xi_m\}, r\rangle$$

$$\times \langle\{\xi_m\}, r|e^{-\Delta\tau H_1}|\{\xi'_m\}, r'\rangle \langle\{\xi'_m\}, r'|e^{-\Delta\tau H_{el}}|\{\xi_{m,l}\}, r_l\rangle \tag{2 16}$$

Note that the error associated with the decomposition in equation (2 15), which results from the fact that the individual elements of the Hamiltonian do not commute, is small for large L, and vanishes in the limit $L \rightarrow \infty$

Let us evaluate the matrix elements of the operators $e^{-\Delta\tau H_0}$, $e^{-\Delta\tau H_1}$ and $e^{-\Delta\tau H_{el}}$, appearing in equation (2 16), separately below Before doing so we first note that the Hilbert space for the system is the direct product of that of the phonon and the electron sub-systems, so that

$$|\{\xi_{m,l}\}, r_l\rangle = |\{\xi_{m,l}\}\rangle |r_l\rangle, \tag{2 17}$$

where the phonon components are orthonormal,

$$\langle\{\xi_{m,l}\} | \{\xi'_{m,l}\}\rangle = \prod_m \langle\xi_{m,l} | \xi'_{m,l}\rangle = \prod_m \delta(\xi_{m,l} - \xi'_{m,l}), \tag{2 18}$$

and form a complete set of states in phonon Hilbert space,

$$I = \int \mathcal{D}\xi \, |\{\xi_{m,l}\}\rangle\langle\{\xi'_{m,l}\}| \tag{2 19}$$

The element H_1 is diagonal in the chosen basis, therefore

$$\langle\{\xi_m\}, r|e^{-\Delta\tau H_1}|\{\xi'_m\}, r'\rangle = e^{-\Delta\tau H_1} \langle r|r'\rangle\langle\{\xi_m\}|\{\xi'_m\}\rangle$$

$$= e^{-\Delta\tau H_1} \delta_{r,r'} \prod_m \delta(\xi_m - \xi'_m) \tag{2 20}$$

The element H_{el} involves only the electron coordinates, so that

$$\langle\{\xi'_m\}, r'|e^{-\Delta\tau H_{el}}|\{\xi_{m,l}\}, r_l\rangle = \langle r'|e^{-\Delta\tau H_{el}}|r_l\rangle\langle\{\xi'_m\}|\{\xi_{m,l}\}\rangle$$

$$= \langle r'|e^{-\Delta\tau H_{el}}|r_l\rangle \prod_m \delta(\xi'_m - \xi_{m,l}) \tag{2 21}$$

We can Fourier transform from the real-space (Wannier) basis $|r\rangle$ to the inverse-space (Bloch) basis $|k\rangle$ using

$$|r\rangle = \frac{1}{\sqrt{N}} \sum_k e^{ik\cdot r}|k\rangle \quad , \quad |k\rangle = \frac{1}{\sqrt{N}} \sum_r e^{-ik\cdot r}|r\rangle \tag{2 22}$$

In Bloch representation, H_{el} is given by equation (1 5), and the matrix element can be written as

$$
\begin{aligned}
\langle\{\xi'_m\},r'|e^{-\Delta\tau H_{el}}|\{\xi_{m,l}\},r_l\rangle &= \frac{1}{N}\sum_{k,k'}e^{-ik\cdot r'}\langle k|e^{-\Delta\tau H_{el}}|k'\rangle e^{ik'\cdot r_l}\prod_m\delta(\xi'_m-\xi_{m,l}) \\
&= \frac{1}{N}\sum_{k,k'}e^{-ik\cdot r'}e^{ik'\cdot r_l}e^{-\Delta\tau H_{el}}\delta_{k,k'}\prod_m\delta(\xi'_m-\xi_{m,l}) \\
&= \frac{1}{N}\sum_k e^{-ik\cdot(r'-r_l)}e^{-\varepsilon_k\Delta\tau}\prod_m\delta(\xi'_m-\xi_{m,l}),
\end{aligned}
\tag{2 23}
$$

where the free electron dispersion ε_k is given by equation (1 6)

The element H_0 depends only on the phonon coordinates, and represents a collection of non-interacting free particles Thus the matrix element for the operator $e^{-\Delta\tau H_0}$ decomposes into the product the matrix elements for each individual oscillator, that is

$$
\begin{aligned}
\langle\{\xi_{m,l+1}\},r_{l+1}|e^{-\Delta\tau H_0}|\{\xi_m\},r\rangle &= \langle r_{l+1}|r\rangle\langle\{\xi_{m,l+1}\}|e^{-\Delta\tau H_0}|\{\xi_m\}\rangle \\
&= \delta_{r_{l+1},r}\prod_m\langle\xi_{m,l+1}|e^{-\Delta\tau P_m^2/2M}|\xi_m\rangle
\end{aligned}
\tag{2 24}
$$

On application of the Fourier transform

$$
|\xi_m\rangle = \int_{-\infty}^{\infty}\frac{dP_m}{\sqrt{2\pi\hbar}}e^{-iP_m\xi_m/\hbar}|P_m\rangle \quad , \quad |P_m\rangle = \int_{-\infty}^{\infty}\frac{d\xi_m}{\sqrt{2\pi\hbar}}e^{-iP_m\xi_m/\hbar}|\xi_m\rangle,
\tag{2 25}
$$

the matrix element appearing in equation (2 24) becomes

$$
\begin{aligned}
\langle\xi_{m,l+1}|e^{-\Delta\tau P_m^2/2M}|\xi_m\rangle &= \int_{-\infty}^{\infty}\frac{dP_m dP'_m}{2\pi\hbar}e^{iP'_m\xi_{m,l+1}/\hbar}\langle P'_m|e^{-\Delta\tau P_m^2/2M}|P_m\rangle e^{iP_m\xi_m/\hbar} \\
&= \int_{-\infty}^{\infty}\frac{dP_m dP'_m}{2\pi\hbar}e^{iP'_m\xi_{m,l+1}/\hbar}e^{iP_m\xi_m/\hbar}e^{-\Delta\tau P_m^2/2M}\delta_{P'_m,P_m} \\
&= \int_{-\infty}^{\infty}\frac{dP_m}{2\pi\hbar}e^{-\Delta\tau P_m^2/2M+i(\xi_{m,l+1}-\xi_m)P_m/\hbar}
\end{aligned}
\tag{2 26}
$$

Here the integral is of the standard Gaussian form

$$
\int_{-\infty}^{\infty}e^{-ax^2+bx} = \sqrt{\frac{\pi}{a}}e^{b^2/4a},
\tag{2 27}
$$

and thus the total matrix element for the operator $e^{-\Delta\tau H_0}$ is given by

$$
\langle\{\xi_{m,l+1}\},r_{l+1}|e^{-\Delta\tau H_0}|\{\xi_m\},r\rangle = \delta_{r_{l+1},r}\left(\frac{M}{2\pi\hbar^2\Delta\tau}\right)^{N/2}\exp\left[-\sum_m\frac{M}{2\hbar^2}\frac{(\xi_{m,l+1}-\xi_m)^2}{\Delta\tau}\right]
\tag{2 28}
$$

On substitution of equations (2 20), (2 23) and (2 28) into equation (2 16), and exercising the various delta functions, the partition function, equation (2 7), reads

$$
Z = \left(\frac{M}{2\pi\hbar^2\Delta\tau}\right)^{N/2}\sum_{\{r_l\}}\int d^{NL}\xi\, e^S\prod_l I(r_{l+1}-r_l),
\tag{2 29}
$$

where the *phonon action* is given by

$$S = \sum_{\mathbf{m},l} \left[-\frac{M}{2\hbar^2} \frac{(\xi_{\mathbf{m},l+1} - \xi_{\mathbf{m},l})^2}{\Delta\tau} - \frac{\Delta\tau M \omega^2}{2} \xi_{\mathbf{m},l}^2 + \Delta\tau f_{\mathbf{m}}(\mathbf{r}_l)\xi_{\mathbf{m},l} \right], \qquad (2\ 30)$$

and the factor

$$I(\mathbf{r}_{l+1} - \mathbf{r}_l) = \frac{1}{N} \sum_{\mathbf{k}} \cos\left[\mathbf{k} \ (\mathbf{r}_{l+1} - \mathbf{r}_l)\right] \exp(-\epsilon_{\mathbf{k}}\Delta\tau), \qquad (2\ 31)$$

represents the purely electronic contribution, where the free electron dispersion ϵ_k was defined in equation (1 6)

The Path Integral QMC method used in this work in based on equation (2 29) In the next section we describe the "traditional" approach, which uses discrete imaginary time Then in section (2 6) we discuss an improved approach that is formulated directly in the continuous imaginary time ($L \to \infty$) limit

2.5   Discrete-Time Path Integral Quantum Monte Carlo

In essence, the path integral Monte Carlo method uses the standard Metropolis algorithm in order to sample the trajectories according to a given statistical weight, such as W In this section we discuss the traditional approach, in which the method is implemented in discrete imaginary time

In 1982 De Raedt and Lagendijk used a discrete imaginary time path integral QMC scheme to study the Holstein polaron [23, 24] The Hamiltonian used here is the same as our generalised model Hamiltonian with an electron-phonon force of $f_{\mathbf{m}}(\mathbf{n}) = \kappa\delta_{\mathbf{m},\mathbf{n}}$ The phonon degrees of freedom are analytically integrated out, using the Feynman technique [33, 37], without making any approximation The integration transforms the problem to that of a single electron with retarded self-interaction (along the imaginary time dimension) The integration is performed using periodic boundary conditions in imaginary time, that is

$$\mid \{\xi_{\mathbf{m},0}\}, \mathbf{r}_0\rangle = \mid \{\xi_{\mathbf{m},L}\}, \mathbf{r}_L\rangle \qquad (2\ 32)$$

The resulting statistical weight ("Monte Carlo weight") reads [1]

$$W = \left[\prod_{l=0}^{L-1} I(\mathbf{r}_{l+1} - \mathbf{r}_l) \right] \exp\left[\sum_{l=0}^{L-1}\sum_{l'=0}^{L-1} F(l - l')\delta_{\mathbf{r}_l,\mathbf{r}_{l'}} \right], \qquad (2\ 33)$$

where

$$F(l - l') = \frac{\Delta\tau^3\hbar^2\kappa^2}{4ML} \sum_{j=0}^{L-1} \frac{\cos\left[2\pi j(l - l')/L\right]}{1 - \cos(2\pi j/L) + \Delta\tau^2(\hbar\omega)^2/2} \qquad (2\ 34)$$

---

[1] The details of the phonon integration are essentially a discretised version of those that will be presented in the following chapter for the case of continuous imaginary-time, and general interaction force

Here $F(l - l')$ is the "memory function" that describes the retarded interaction of the electron with itself

The implementation of the Metropolis algorithm using discrete imaginary time is particularly simple The electron trajectory is represented by the position of the electron in each time slice r_l, where $0 \leq l \leq L$ We will give a detailed discussion of the Metropolis algorithm in chapter (5) The basic structure of the algorithm is as follows

1 Choose an initial trajectory $\{r_l\}$, and evaluate the statistical weight W for this path according to equation (2 33)

2 Randomly choose a time slice l'

3 Propose a small trial change to the trajectory by altering the position $r_{l'}$, by a single site, in a random fashion

4 Evaluate the weight for the trial trajectory W' according to equation (2 33)

5 Accept or reject the proposed change according to the "acceptance ratio", which depends on the ratio W'/W For further details see chapter (5) Note that both accepted and rejected moves contribute to averages in the same way

6 Collect measurements of the required observables if the system has reached equilibrium

7 Repeat steps (2) to (6) until sufficient statistics have been accumulated

After a sufficient number of "warm-up" steps have been completed, the algorithm generates trajectories that statistically appear with the desired probability distribution W, and the system is said to be in equilibrium Due to the fact that the system (after the phonon integration) contains only the electronic degrees of freedom, the size of the lattice has little effect on the efficiency of the algorithm This method gives good statistical results for thermodynamic properties such as the energy and the specific heat

We undertook a brief QMC study of the one dimensional Holstein model using the above discrete imaginary time method Unfortunately, we found that the simulations required an extremely large amount of computational effort to produce results to a reasonable degree of accuracy The main problem was due to the finite-time-step error, which is inherent in the discrete imaginary-time implementation This is a systematic error, introduced by the use of the Trotter formula, equation (2 15), that scales with $(\Delta\tau)^2$ (where $\Delta\tau = \beta/L$) The actual number of time slices used in practice is usually chosen intuitively Increasing the value L decreases the

influence of the finite-time-step error, but increases the computation time required to perform the QMC simulations

We performed simulations for fixed $\hbar\omega/t = 1$ at several different couplings ($\sim \kappa$) The lattice was of size $N = 512$ and the inverse temperature was taken to be $\beta/t = 15$ For each coupling, measurements of energy were accumulated over several series of 3×10^7 Monte Carlo steps Each of these series used a different number of time slices, ranging from $L = 75$ to $L = 150$ We found a significant dependence of the results on L, particularly for large couplings (where the electron-phonon interaction is dominant)

In principle, one could extrapolate the results (for each series) to the $L \to \infty$ limit by performing $1/L^2$ scaling However, to produce results to a reasonable accuracy, this process would require a very large amount of computational effort (and data analysis)

The implications of the finite-time-step error has lead to the recent development of continuous imaginary time QMC algorithms The scheme completely eliminates the finite-time step error by working directly in the limit $L \to \infty$ This is the subject of the next section

2.6 Continuous Imaginary Time

Traditionally, path integral QMC has been implemented using discrete imaginary time The reason why this method has been so widely adopted is probably due to ease of programming However, as we have already discussed, the major drawback in the discrete imaginary time scheme is due to the systematic finite-time-step error

Recently, QMC schemes have been developed that are implemented in *continuous* imaginary time, for general quantum mechanical lattice models [34, 35, 36] The continuous time QMC scheme is formulated directly in the $L \to \infty$ limit, which completely eliminates the finite-time-step error In this approach the trajectory is characterised by a series of "kinks", where a kink is defined as the point in imaginary time at which the system state changes This is illustrated in figure (2 2) The Metropolis algorithm is used to accept or reject proposed changes to the trajectory The trial changes to the trajectory are based on processes involving the addition or deletion of single kinks We will discuss the continuous imaginary time QMC scheme in detail in chapter (5)

Let us now take the limit of continuous imaginary time ($L \to \infty$) The coordinates r_i and

$\xi_{\mathbf{m},l}$ become functions of continuous imaginary time τ, that is, $\mathbf{r}(\tau)$ and $\xi_{\mathbf{m}}(\tau)$ respectively The path integration in equation (2 7) is written as

$$\lim_{L \to \infty} \sum_{\{\mathbf{r}_l\}} \int d^{NL}\xi = \int \mathcal{D}\xi\mathcal{D}\mathbf{r}, \qquad (2\ 35)$$

which represents integration over all possible trajectories that start with state $|\{\xi_{\mathbf{m}}(0)\}, \mathbf{r}(0)\rangle$ and end with state $|\{\xi_{\mathbf{m}}(\beta)\}, \mathbf{r}(\beta)\rangle$ The phonon action, equation (2 30), tends to the integral

$$S = \sum_{\mathbf{m}} \int_0^{\beta} d\tau \left[-\frac{M}{2\hbar^2}\dot{\xi}_{\mathbf{m}}^2(\tau) - \frac{M\omega^2}{2}\xi_{\mathbf{m}}^2(\tau) + f_{\mathbf{m}}(\mathbf{r}(\tau))\xi_{\mathbf{m}}(\tau) \right], \qquad (2\ 36)$$

where $\dot{\xi}_{\mathbf{m}}(\tau) = \partial\xi_{\mathbf{m}}(\tau)/\partial\tau$ From this point on we will work in continuous imaginary time

Our next task is to integrate out the phonon degrees of freedom in equation (2 36) This will be performed using periodic boundary conditions (in imaginary time), as in [26] and [24], in chapter (3), and then using twisted boundary conditions in chapter (4) The use of twisted boundary conditions allows us to directly compute dynamic properties of the system, such as the effective mass and the isotope exponent (in addition to static properties such as the energy and the number of phonons)

The phonon action (after the phonon coordinates have been integrated out) and the electronic contribution, equation (2 31), will be incorporated into the continuous time QMC scheme in chapter (5) The resulting algorithm is "numerically exact" (no finite-time-step error), and is much more efficient than the discrete imaginary time scheme The increase in efficiency is due to the fact that the computation involves running over a relatively small number of kinks, rather than a large number of imaginary time slices
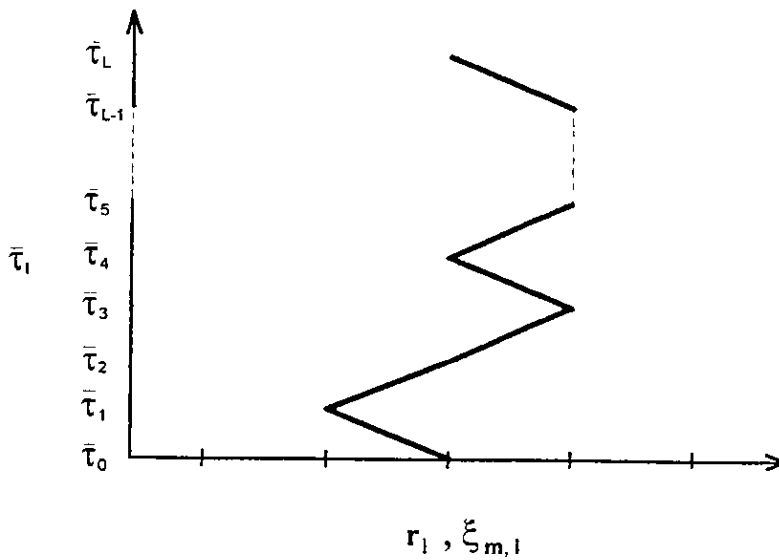
Figure 2 1 The intuitive interpretation of the path integral in discrete imaginary time A single path is represented by the position of the electron r_l, and the displacement of each ion $\xi_{m,l}$, in all of the L imaginary time slices, where $0 \leq l \leq L$ The path integration is the sum over all possible paths that have an initial state of $|\ \{\xi_{m,0}\}, r_0\rangle$ (at imaginary time $\tau_0 = 0$) and a final state of $|\ \{\xi_{m,L}\}, r_L\rangle$ (at $\tau_L = \beta$) Each of these possible paths contribute to the path integration with weight W
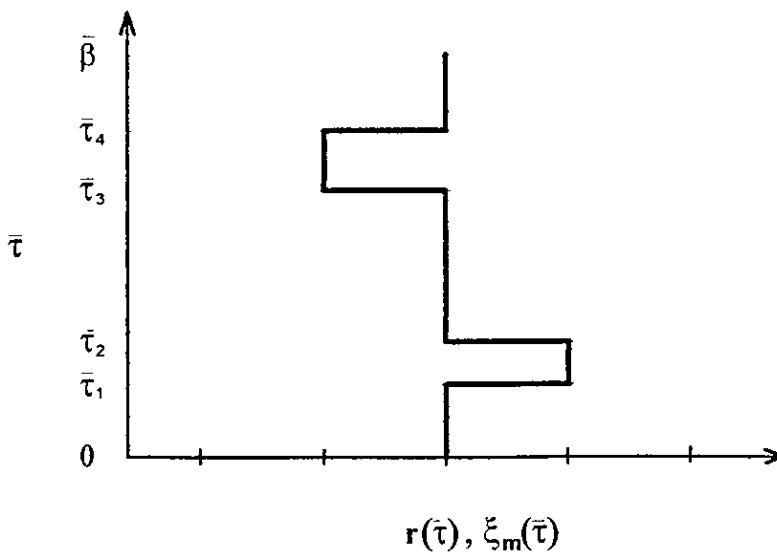
Figure 2 2 The path integral in continuous imaginary time τ Points in imaginary time at which the system state changes are known as kinks Here the trajectory is characterised by a series of four kinks at imaginary times $\tau_1, \tau_2 \quad \tau_4$

Chapter 3

Phonon Integration with Periodic Boundary Conditions

3.1 Introduction

In the previous chapter we determined the path integral expression for our generalised model Hamiltonian in continuous imaginary time. Our aim now is to analytically integrate out the phonon degrees of freedom. That is, we are concerned with performing the *phonon path integral*

$$I = \int \mathcal{D}\xi \exp\left(\sum_{\mathbf{m}} S_{\mathbf{m}}\right), \tag{3 1}$$

where

$$S_{\mathbf{m}} = \int_0^\beta d\tau \left[-\frac{M}{2\hbar^2}\dot{\xi}_{\mathbf{m}}^2(\tau) - \frac{M\omega^2}{2}\xi_{\mathbf{m}}^2(\tau) + f_{\mathbf{m}}(\mathbf{r}(\tau))\xi_{\mathbf{m}}(\tau) \right], \tag{3 2}$$

with $\dot{\xi}_{\mathbf{m}}(\tau) \equiv \delta\xi_{\mathbf{m}}(\tau)/\delta\tau$. Here $\int \mathcal{D}\xi$ indicates integration over all possible trajectories which start from $\xi_{\mathbf{m}}(0)$ and end on $\xi_{\mathbf{m}}(\beta)$. Note that, by design, we placed no restrictions on the values that $\xi_{\mathbf{m}}(0)$ and $\xi_{\mathbf{m}}(\beta)$ take. As we shall see, after integration, the system has only the electronic degrees of freedom, which is ideal for practical QMC simulation. The phonon degrees of freedom remain in the system, taking the form of a retarded interaction (along the imaginary time dimension) of the electron with itself.

As explained in section (2 3), the QMC algorithm samples trajectories that appear with a statistical weight (Monte Carlo weight) that is proportional to the partition function of the system. For our purposes, then, the Monte Carlo weight is the quantity that is of primary

18

interest In this chapter, we will consider the "normal" (thermodynamic) partition function Z In this case, we notice from equations (2 1) and (2 8) that the trajectories must start and end with the same state, and thus we must perform the phonon path integration using *periodic boundary conditions in imaginary time*, that is

$$\{\xi_m(0)\} = \{\xi_m(\beta)\} \tag{3 3}$$

In the next chapter we will consider a different "projected" partition function, the use of which allows us to directly compute the dynamic properties of the system In this case the integration must be performed under twisted boundary conditions in imaginary time

The method used here to perform the phonon integration is known as the "Feynman technique", which consists of the following three steps [37, 32]

- The variational principle is used in order to determine the classical path, that links $\xi_m(0)$ to $\xi_m(\beta)$

- The (quantum mechanical) trajectory is measured from the classical path, by introducing so called "quantum fluctuations" It turns out that, in this representation, the phonon coordinates in S_m, equation (3 2), are described only in terms of the end points of the trajectory, $\xi_m(0)$ and $\xi_m(\beta)$

- With S_m formulated in terms of the end points, one can analytically perform the path integral, equation (3 1), by making use of the well known Gaussian integral formula

$$\int_{-\infty}^{\infty} \exp(-ax^2 + bx + c)dx = \left(\frac{\pi}{a}\right)^{\frac{1}{2}} \exp\left(\frac{b^2}{4a} + c\right), \tag{3 4}$$

subject to the appropriate boundary conditions (in imaginary time) In the case of periodic boundary conditions, equation (3 4) can be directly applied However, as we shall see in the next chapter, the use of twisted boundary requires us to first decompose the action into Fourier components

3.2 The Classical Trajectory

The classical trajectory $\bar{\xi}_m(\tau)$ may be determined by making use of the (variational) *principle of least action* This states that of all of the possible trajectories $\{\xi_m(\tau)\}$, the classical path is the trajectory for which the action is an extremum [37] Thus, if the classical path is altered by a small amount $\delta\xi_m(\tau)$, the action remains unchanged to the first order in $\delta\xi_m(\tau)$, that is

$$S_m\left[\bar{\xi}_m(\tau) + \delta\xi_m(\tau)\right] - S_m\left[\bar{\xi}_m(\tau)\right] = 0, \tag{3 5}$$

provided that $\delta\xi_m$ is sufficiently small. On substitution of the phonon action, equation (3 2), into equation (3 5), and neglecting terms involving the second order in $\delta\xi_m(\tau)$, we find that the classical trajectory satisfies

$$\int_0^\beta d\tau \left[-\frac{M}{\hbar^2}\ddot{\bar{\xi}}_m(\tau)\delta\xi_m(\tau) - M\omega^2\bar{\xi}_m(\tau)\delta\xi_m(\tau) + f_m(\mathbf{r}(\tau))\delta\xi_m(\tau) \right] = 0 \qquad (3\ 6)$$

The first term of equation (3 6) can be integrated by parts, so that

$$-\frac{M}{\hbar^2}\left[\dot{\bar{\xi}}_m(\tau)\delta\xi_m(\tau) \right]_0^\beta + \int_0^\beta d\tau \left[\frac{M}{\hbar^2}\dot{\bar{\xi}}_m(\tau)\dot{\delta\xi}_m(\tau) - M\omega^2\bar{\xi}_m(\tau)\delta\xi_m(\tau) + f_m(\mathbf{r}(\tau))\delta\xi_m(\tau) \right] = 0$$
$$(3\ 7)$$

The fact that the path integration involves only those possible trajectories that start at $\xi_m(0)$ and end at $\xi_m(\beta)$ means that

$$\delta\xi_m(0) = \delta\xi_m(\beta) = 0, \qquad (3\ 8)$$

and so the first term of equation (3 7) is equal to zero. Other than at the end-points, the value of $\delta\xi_m(\tau)$ is arbitrary. Therefore, in order for the integral in equation (3 7) to vanish, the classical trajectory requires that

$$-\ddot{\bar{\xi}}_m(\tau) + (\hbar\omega)^2\bar{\xi}_m(\tau) = \frac{\hbar^2}{M}f_m(\mathbf{r}(\tau)) \qquad (3\ 9)$$

Equation (3 9) is of a standard form that can be solved by using the well known *Green's function* to describe the particular non-homogeneous part of the solution (the details of which can be found in many mathematical text books, for example [38]) The classical trajectory is given by

$$\bar{\xi}_m(\tau) = \xi_m \frac{\sinh[\hbar\omega(\beta - \tau)]}{\sinh(\hbar\omega\beta)} + \xi_m'\frac{\sinh(\hbar\omega\tau)}{\sinh(\hbar\omega\beta)} + \frac{\hbar^2}{M}\int_0^\beta d\tau' f(\mathbf{r}(\tau))G(\tau, \tau')f(\mathbf{r}(\tau')), \qquad (3\ 10)$$

where we have explicitly represented the start and the end of the trajectory (boundary conditions) as

$$\xi_m = \xi_m(0) = \bar{\xi}_m(0) \quad , \quad \xi_m' = \xi_m(\beta) = \bar{\xi}_m(\beta), \qquad (3\ 11)$$

and the Green's function is given by

$$G(\tau, \tau') = \frac{1}{\hbar\omega\sinh(\hbar\omega\beta)} \begin{cases} \sinh(\hbar\omega\tau)\sinh[\hbar\omega(\beta - \tau')] & 0 < \tau < \tau' \\ \sinh[\hbar\omega(\beta - \tau)]\sinh(\hbar\omega\tau') & \tau' < \tau < \beta \end{cases} \qquad (3\ 12)$$

3.2 Action in Terms of End-Points

We have found the classical (straight line) trajectory $\bar{\xi}_m(\tau)$ by extremising the action. The probability amplitude for the "actual" trajectories to be "close" to the classical path is large, and becomes smaller as the difference between the two increases. Thus, it is reasonable to think

of the trajectory $\xi_m(\tau)$ as being "mainly" the classical path, plus a small deviation (or *quantum fluctuation*) from it

As we shall see below, if we measure the trajectory from the classical path, it turns out that the phonon coordinates enter the action only via the end-points of the trajectory, ξ_m and ξ'_m. The motivation for expressing the action in terms of the end-points is that it allows us to integrate out the phonon degrees of freedom by making use of the Gaussian formula, equation (3 4)

Let us decompose the trajectory according to

$$\xi_m(\tau) = \bar{\xi}_m(\tau) + \eta_m(\tau) \tag{3 13}$$

(and so $\dot{\xi}_m(\tau) = \dot{\bar{\xi}}_m(\tau) + \dot{\eta}_m(\tau)$), where $\bar{\xi}_m(\tau)$ is the classical path and $\eta_m(\tau)$ is the deviation (quantum fluctuation) from the classical path   On substitution of equation (3 13) into equation (3 2), and after rearrangement, the action may be written as

$$S_m = S_m^{(cl)} + S_m^{(fl)} + S_m^{(mix)} \tag{3 14}$$

where

$$S_m^{(cl)} = \int_0^\beta d\tau \left[-\frac{M}{2\hbar^2}\dot{\bar{\xi}}_m^2(\tau) - \frac{M\omega^2}{2}\bar{\xi}^2{}_m(\tau) + f_m(\mathbf{r}(\tau))\bar{\xi}_m(\tau) \right], \tag{3 15}$$

$$S_m^{(fl)} = \int_0^\beta d\tau \left[-\frac{M}{2\hbar^2}\dot{\eta}_m^2(\tau) - \frac{M\omega^2}{2}\eta_m^2(\tau) \right], \tag{3 16}$$

$$S_m^{(mix)} = \int_0^\beta d\tau \left[-\frac{M}{\hbar^2}\dot{\bar{\xi}}_m(\tau)\dot{\eta}_m(\tau) - M\omega^2\bar{\xi}_m(\tau)\eta_m(\tau) + f_m(\mathbf{r}(\tau))\eta_m(\tau) \right] \tag{3 17}$$

The first term of $S_m^{(mix)}$ may be integrated by parts, so that equation (3 17) becomes

$$S_m^{(mix)} = \int_0^\beta d\tau \left[-\frac{M}{\hbar^2}\ddot{\bar{\xi}}_m(\tau) - M\omega^2\bar{\xi}_m(\tau) + f_m(\mathbf{r}(\tau)) \right] \eta_m(\tau), \tag{3 18}$$

which is equal to zero due to equation (3 9) Now let us look at the fluctuation term $S_m^{(fl)}$ The path integral of $S_m^{(fl)}$ (over the shifted variable $\eta_m(\tau)$) can be performed analytically by making use of a discrete Fourier transform The result turns out to be a constant [1], so that the path integral of interest, equation (3 1), can be written as

$$I = c_{mix} \sum_{\{\mathbf{r}(\tau)\}} \int \mathcal{D}\xi \exp\left(\sum_m S_m^{(cl)} \right) \tag{3 19}$$

Note that c_{mix} is unimportant for QMC simulation due to the fact that the Metropolis test requires only the *ratio* of weights to be evaluated The classical part $S_m^{(cl)}$ can be simplified by integrating the first term of equation (3 15) by parts, so that

$$S_m^{(cl)} = -\frac{M}{2\hbar^2}\left[\dot{\bar{\xi}}'_m\bar{\xi}'_m - \dot{\bar{\xi}}_m\bar{\xi}_m\right] + \int_0^\beta d\tau \left[\frac{M}{2\hbar^2}\ddot{\bar{\xi}}_m(\tau)\bar{\xi}_m(\tau) - \frac{M\omega^2}{2}\bar{\xi}_m^2(\tau) + f_m(\mathbf{r}(\tau))\bar{\xi}_m(\tau) \right]$$

$$= -\frac{M}{2\hbar^2}\left[\dot{\bar{\xi}}'_m\bar{\xi}'_m - \dot{\bar{\xi}}_m\bar{\xi}_m\right] + \frac{1}{2}\int_0^\beta d\tau f_m(\mathbf{r}(\tau))\bar{\xi}_m(\tau) \tag{3 20}$$

---

[1] The details of the calculation can be found in textbooks on the subject, for example section 2 4 of [32]

where we have made use of equation (3 9)

Finally, we wish to substitute the expression for the classical trajectory $\bar{\xi}_{\mathbf{m}}(\tau)$, equation (3 10), together with $\bar{\xi}_{\mathbf{m}} = \bar{\xi}(0)$ and $\bar{\xi}'_{\mathbf{m}} = \bar{\xi}(\beta)$, into equation (3 20)   Accordingly, the derivative of $\bar{\xi}_{\mathbf{m}}(\tau)$ is

$$
\bar{\xi}_{\mathbf{m}}(\tau) = \frac{\hbar\omega\cosh(\hbar\omega\tau)}{\sinh(\hbar\omega\beta)}\xi'_{\mathbf{m}} + \frac{\hbar^2}{M}\frac{\cosh(\hbar\omega\tau)}{\sinh(\hbar\omega\beta)}\int_\tau^\beta d\tau'\sinh[\hbar\omega(\beta-\tau')]f_{\mathbf{m}}(\mathbf{r}(\tau'))
$$
$$
- \frac{\hbar\omega\cosh[\hbar\omega(\beta-\tau)]}{\sinh(\hbar\omega\beta)}\xi_{\mathbf{m}} - \frac{\hbar^2}{M}\frac{\cosh[\hbar\omega(\beta-\tau)]}{\sinh(\hbar\omega\beta)}\int_0^\tau d\tau'\sinh(\hbar\omega\tau')f_{\mathbf{m}}(\mathbf{r}(\tau')), \quad (3\ 21)
$$

so that

$$
\bar{\xi}_{\mathbf{m}} = -\xi_{\mathbf{m}}\frac{\hbar\omega\cosh(\hbar\omega\beta)}{\sinh(\hbar\omega\beta)} + \xi'_{\mathbf{m}}\frac{\hbar\omega}{\sinh(\hbar\omega\beta)} + \frac{\hbar^2}{M}\int_0^\beta d\tau'\frac{\sinh[\hbar\omega(\beta-\tau')]}{\sinh(\hbar\omega\beta)}f_{\mathbf{m}}(\mathbf{r}(\tau')), \quad (3\ 22)
$$

and

$$
\bar{\xi}'_{\mathbf{m}} = -\xi_{\mathbf{m}}\frac{\hbar\omega}{\sinh(\hbar\omega\beta)} + \xi'_{\mathbf{m}}\frac{\hbar\omega\cosh(\hbar\omega\beta)}{\sinh(\hbar\omega\beta)} - \frac{\hbar^2}{M}\int_0^\beta d\tau'\frac{\sinh(\hbar\omega\tau')}{\sinh(\hbar\omega\beta)}f_{\mathbf{m}}(\mathbf{r}(\tau')) \quad (3\ 23)
$$

Thus, the action in terms of the end-points is given by

$$
S_{\mathbf{m}}^{(\mathrm{cl})} = \frac{M\omega}{2\hbar\sinh(\hbar\omega\beta)}\left\{-[\xi_{\mathbf{m}}^2 + \xi'^2_{\mathbf{m}}]\cosh(\hbar\omega\beta) + 2\xi_{\mathbf{m}}\xi'_{\mathbf{m}}\right\} + \xi_{\mathbf{m}}B_{\mathbf{m}}(\tau) + \xi'_{\mathbf{m}}C_{\mathbf{m}}(\tau)
$$
$$
+ \frac{\hbar^2}{2M}\int_0^\beta\int_0^\beta d\tau d\tau' f_{\mathbf{m}}(\mathbf{r}(\tau))G(\tau,\tau')f_{\mathbf{m}}(\mathbf{r}(\tau')), \quad (3\ 24)
$$

where

$$
B_{\mathbf{m}}(\tau) \equiv \int_0^\beta d\tau\frac{\sinh(\hbar\omega(\beta-\tau))}{\sinh(\hbar\omega\beta)}f_{\mathbf{m}}(\mathbf{r}(\tau)), \quad (3\ 25)
$$

and

$$
C_{\mathbf{m}}(\tau) \equiv \int_0^\beta d\tau\frac{\sinh(\hbar\omega\tau)}{\sinh(\hbar\omega\beta)}f_{\mathbf{m}}(\mathbf{r}(\tau)), \quad (3\ 26)
$$

with the Greens function $G(\tau,\tau')$ given by equation (3 12)

In the expression for the phonon path integral, equation (3 19), the phonon subsystem is represented only via $\xi_{\mathbf{m}}$ and $\xi'_{\mathbf{m}}$ from within $S_{\mathbf{m}}^{(\mathrm{cl})}$, equation (3 24)   In this form, the phonon coordinates can be integrated out of the system completely using Gaussian integration

Thus far we have not imposed any boundary conditions on the imaginary-time dimension (that is, no restrictions have been placed on the values of $\xi_{\mathbf{m}}$ and $\xi'_{\mathbf{m}}$)   In the next section we will perform the Gaussian integration using periodic boundary conditions in imaginary time, as in [26] and [24]   Then in the next chapter we will perform the phonon integration using twisted boundary conditions in imaginary time, which allows the Monte Carlo scheme to directly calculate dynamic properties such as the effective mass and the isotope exponent

3.4 Integration using Periodic Boundary Conditions

In this section wish to perform the Gaussian integration of the phonon coordinates – for the special case of when periodic boundary conditions are imposed upon the trajectory This corresponds to the "normal" partition function Z, given by equation (2 8) In this case the integration is particularly simply because the Gaussian integral formula given by equation (3 4) can be applied directly We are interested in performing the path integral

$$I_{per} = \int_{per} \mathcal{D}\xi \exp\left(\sum_m S_m^{(cl)}\right), \tag{3 27}$$

where $\int_{per} \mathcal{D}\xi$ denotes integration over all trajectories that are subject to the condition

$$\xi_m = \xi'_m \tag{3 28}$$

Under these boundary condition $S_m^{(cl)}$, equation (3 24), can be written in the form

$$S_m^{(cl)} = \frac{M\omega[\cosh(\hbar\omega\beta) - 1]}{\hbar\sinh\hbar\omega\beta}\xi_m^2 + (B_m + C_m)\xi_m + \frac{\hbar^2}{2M}\int_0^\beta\!\!\int_0^\beta d\tau d\tau' f_m(\mathbf{r}(\tau))G(\tau,\tau')f_m(\mathbf{r}(\tau')), \tag{3 29}$$

where B_m and C_m are defined in equations (3 25) and (3 26) respectively, and $G(\tau, \tau')$, equation (3 12), is not dependent on ξ_m

The fact that equation (3 29) depends on the single phonon coordinate ξ_m allows us to decompose the path integral, equation (3 27), into the product of one-variable integrals, that is

$$I_{per} = \prod_m \int_{-\infty}^\infty d\xi_m \exp\left(S_m^{(cl)}\right) \tag{3 30}$$

Note that this decomposition can not be done for the case of twisted boundary conditions Now the Gaussian integral formula, equation (3 4) can be applied directly to give

$$I_{per} = e^{A_{per}} \prod_m \left\{ \frac{\pi\hbar\sinh(\hbar\omega\beta)}{M\omega[\cosh(\hbar\omega\beta) - 1]} \right\}^{1/2}, \tag{3 31}$$

where

$$A_{per} = \frac{\hbar(B_m + C_m)^2 \sinh(\hbar\omega\beta)}{4M\omega[\cosh(\hbar\omega\beta) - 1]} + \frac{\hbar^2}{2M}\int_0^\beta\!\!\int_0^\beta d\tau d\tau' f_m(\mathbf{r}(\tau))G(\tau,\tau')f_m(\mathbf{r}(\tau')) \tag{3 32}$$

The phonon coordinates have now been integrated out The above result for A_{per} may be simplified by bringing the first and second terms of equation (3 32) to a similar form, and canceling out common terms Accordingly, on application of the identity $2\sinh^2(x/2) = \cosh x - 1$, and the hyperbolic factor formulae, the first term of equation (3 32) takes the form

$$(B_m + C_m)^2 = \left\{ \int_0^\beta d\tau \left[\frac{\sinh[\hbar\omega(\beta-\tau)]}{\sinh(\hbar\omega\beta)}f_m(\mathbf{r}(\tau)) + \frac{\sinh(\hbar\omega\tau)}{\sinh(\hbar\omega\beta)}f_m(\mathbf{r}(\tau)) \right] \right\}^2$$

$$= \frac{1}{\sinh^2(\hbar\omega\beta)} \left\{ \int_0^\beta d\tau \, 2f_{\mathbf{m}}(\mathbf{r}(\tau)) \sinh(\hbar\omega\beta/2) \cosh[\hbar\omega(\beta/2-\tau)] \right\}^2$$

$$= \frac{4\sinh^2(\hbar\omega\beta/2)}{\sinh^2(\hbar\omega\beta)} \int_0^\beta\int_0^\beta d\tau d\tau' \, f_{\mathbf{m}}(\mathbf{r}(\tau))f_{\mathbf{m}}(\mathbf{r}(\tau')) \cosh[\hbar\omega(\beta/2-\tau)] \cosh[\hbar\omega(\beta/2-\tau')]$$

$$= \frac{2\sinh^2(\hbar\omega\beta/2)}{\sinh^2(\hbar\omega\beta)} \int_0^\beta\int_0^\beta d\tau d\tau' \, f_{\mathbf{m}}(\mathbf{r}(\tau))f_{\mathbf{m}}[\mathbf{r}(\tau')] \left\{ \cosh[\hbar\omega(\beta-\tau-\tau')] + \cosh[\hbar\omega(-\tau'+\tau)] \right\}$$

$$= \frac{\cosh(\hbar\omega\beta)-1}{\sinh^2(\hbar\omega\beta)} \int_0^\beta\int_0^\beta d\tau d\tau' \, f_{\mathbf{m}}(\mathbf{r}(\tau))f_{\mathbf{m}}(\mathbf{r}(\tau')) \left\{ \cosh[\hbar\omega(\beta-\tau-\tau')] + \cosh[\hbar\omega(-\tau'+\tau)] \right\}$$

$$\text{(3 33)}$$

Given that the Green's function may be written in the form,

$$G(\tau,\tau') = \frac{1}{2\hbar\omega\sinh\hbar\omega\beta} \left\{ \begin{array}{ll} \cosh[\hbar\omega(\beta+\tau-\tau')] - \cosh[\hbar\omega(-\beta+\tau+\tau')] & 0 < \tau < \tau' \\ \cosh[\hbar\omega(\beta-\tau+\tau')] - \cosh[\hbar\omega(\beta-\tau-\tau')] & \tau' < \tau < \beta \end{array} \right. , \quad \text{(3 34)}$$

one can see that equation (3 33) shares common terms with the second term of equation (3 32)

Now let us substitute equations (3 33) and (3 34) into equation (3 32) After canceling out the common terms, for the case when $\tau < \tau'$, we see that

$$A_{\text{per}}_{\tau<\tau'} = \frac{\hbar}{4M\omega\sinh(\hbar\omega\beta)} \int_0^\beta d\tau'\int_0^{\tau'} d\tau \left\{ \cosh[\hbar\omega(\beta+\tau-\tau')] - \cosh[\hbar\omega(-\beta+\tau+\tau')] \right.$$
$$\left. + \cosh[\hbar\omega(\beta-\tau-\tau')] + \cosh[\hbar\omega(-\tau+\tau')] \right\} \sum_{\mathbf{m}} f_{\mathbf{m}}(\mathbf{r}(\tau))f_{\mathbf{m}}(\mathbf{r}(\tau'))$$

$$= \frac{\hbar}{2M\omega\sinh(\hbar\omega\beta)} \int_0^\beta d\tau'\int_0^{\tau'} d\tau \left\{ \cosh(\hbar\omega\beta/2) + \cosh[\hbar\omega(\beta/2+\tau-\tau')] \right\} \sum_{\mathbf{m}} f_{\mathbf{m}}(\mathbf{r}(\tau))f_{\mathbf{m}}(\mathbf{r}(\tau'))$$

$$= \frac{\hbar}{4M\omega} \int_0^\beta d\tau'\int_0^{\tau'} d\tau \frac{\cosh\hbar\omega(\beta/2+\tau-\tau')]}{\sinh(\hbar\omega\beta/2)} \sum_{\mathbf{m}} f_{\mathbf{m}}(\mathbf{r}(\tau))f_{\mathbf{m}}(\mathbf{r}(\tau')) \quad \text{(3 35)}$$

In a similar way, the result for $\tau > \tau'$ reads

$$A_{\text{per}}_{\tau>\tau'} = \frac{\hbar}{4M\omega} \int_0^\beta d\tau'\int_{\tau'}^\beta d\tau \frac{\cosh[\hbar\omega(\beta/2-\tau+\tau')]}{\sinh(\hbar\omega\beta/2)} \sum_{\mathbf{m}} f_{\mathbf{m}}(\mathbf{r}(\tau))f_{\mathbf{m}}(\mathbf{r}(\tau')) \quad \text{(3 36)}$$

Finally, on substitution of the simplified expression for A_{per}, equations (3 35) and (3 36), into equation (3 31), the result (for periodic boundary conditions $\xi_{\mathbf{m}} = \xi'_{\mathbf{m}}$) is given by

$$I_{\text{per}} = \left\{ \frac{\pi\hbar\sinh(\hbar\omega\beta)}{M\omega[\cosh(\hbar\omega\beta) - 1]} \right\}^{N/2} \exp A_{\text{per}}, \quad \text{(3 37)}$$

where

$$A_{\text{per}} = \frac{\hbar}{4M\omega} \int_0^\beta\int_0^\beta d\tau d\tau' \frac{\cosh[\hbar\omega(\beta/2-|\tau'-\tau|)]}{\sinh(\hbar\omega\beta/2)} \sum_{\mathbf{m}} f_{\mathbf{m}}(\mathbf{r}(\tau))f_{\mathbf{m}}(\mathbf{r}(\tau')) \quad \text{(3 38)}$$

One can see that equation (3 38) does not contain any phonon degrees of freedom We have transformed the problem from that of an electron interacting with many phonons, to that of an electron with retarded self-interaction The fact that the system contains only one (electronic) degree of freedom is ideal for QMC simulation -- because the amount of computation required to carry out each Monte Carlo step is minimised

Chapter 4

Twisted Boundary Conditions and Effective Mass

4.1 Introduction

In the previous chapter we integrated out the phonon degrees of freedom using periodic boundary conditions in imaginary time. This transforms the problem to that of a single electron with retarded self-interaction, which allows the QMC method to be applied effectively. In this chapter we again perform the phonon integration, but this time using *twisted* boundary conditions in imaginary time, which corresponds to the use of a modified expression for the partition function. The motivation for the use of twisted boundary conditions is that it allows us to directly compute the effective mass from the QMC simulations. Let us start by defining the the "total momentum" of the system and, using this, the effective mass of the polaron.

The *total momentum* $\mathbf{P}$ of the system is defined as the sum of the momentum of the electron and the momenta of the phonons, that is

$$\hat{\mathbf{P}} = \hat{\mathbf{p}} + \sum_{\mathbf{q}} \hbar \mathbf{q} \hat{n}_{\mathbf{q}}, \tag{4 1}$$

where $\hat{\mathbf{p}}$ is the electron momentum operator, and $\hat{n}_{\mathbf{q}}$ is the phonon number operator corresponding to phonons of wave number $\mathbf{q}$. In any translationally invariant quantum system, such as that considered in the present calculations, the total momentum is a conserved quantity (within the first Brillouin zone). Thus, with reference to the partition function given by equation (2 7), an initial state $\mid \{\xi_{\mathbf{m}}\}, \mathbf{r}\rangle$ with a particular total momentum $\mathbf{P}$, will evolve and end with the same

25

P

The concept of the *effective mass* is useful because it allows us to interpret the dynamics of the polaron in an intuitive manner. The difference between the behaviour of the polaron (which depends on the interaction with its environment) and that described by the free-electron dispersion relation (no interaction), is taken into account by replacing the bare electron mass m_0 with an effective mass m^*. The effective mass of the polaron is defined in the "usual" way as

$$\frac{1}{m_d^*} = \lim_{\beta \to \infty} \frac{\partial^2 E(\mathbf{P})}{\partial P_d^2}, \tag{4 2}$$

where $1 \leq d \leq D$ labels the dimension of the D dimensional system, and $E(\mathbf{P})$ is the energy of the polaron for total momentum $\mathbf{P}$. It should be stressed that the effective mass only has meaning in the low temperature limit $\beta \to \infty$, which corresponds to the lowest energy state $E_0(\mathbf{P})$. The effective mass is related to the curvature of the polaron dispersion curve,

$$E_0(\mathbf{P}) = E_0(0) + \sum_{d=1}^{D} \frac{P_d^2}{2m_d^*}, \tag{4 3}$$

which is shown graphically in figure (4 1). Note that the ground state energy $E_0(0)$ occurs at $\mathbf{P} = 0$. The effective mass of the polaron is greater than the bare electron mass as a result of the electron-phonon interaction.

An efficient method which allows the direct measurement of the effective mass from QMC simulations has recently been developed by Kornilovitch [29, 30]. It considers electron trajectories with *twisted* boundary conditions in imaginary time (in a similar way to Feynmans calculation of the Frohlich polaron effective mass [37]). The twisted boundary conditions result from the use of the modified partition function described in the next section.

4.2 Partition Function for Fixed Total Momentum

Given that the total momentum $\mathbf{P}$ is a conserved quantity, it is reasonable to divide the total partition function Z into a number of *partial partition functions* $Z_\mathbf{P}$, each of which involves only those states with a fixed total momentum $\mathbf{P}$. Accordingly, we define

$$Z = \sum_\mathbf{P} Z_\mathbf{P}, \tag{4 4}$$

with

$$Z_\mathbf{P} = \sum_i \langle i \mid e^{-\beta H} \mid i \rangle \delta_{\mathbf{P}, \mathbf{P}_i}, \tag{4 5}$$

where i numbers states of a complete basis, and $\mathbf{P}_i$ is the total momentum of state $\mid i \rangle$. Kornilovitch and Pike [29] showed that equation (4 5) can be brought to a similar form to that of

the original partition function, namely

$$Z_{\mathbf{P}} = \sum_{\Delta \mathbf{r}} e^{i\mathbf{P} \cdot \Delta \mathbf{r}/\hbar} Z_{\Delta \mathbf{r}}, \tag{4 6}$$

with

$$Z_{\Delta \mathbf{r}} = \int d^N \xi \langle \{\xi_{\mathbf{m}+\mathbf{r}'-\mathbf{r}}\}, \mathbf{r}' \mid e^{-\beta H} \mid \{\xi_{\mathbf{m}}\}, \mathbf{r} \rangle, \tag{4 7}$$

where $\int d^N \xi$ is defined in equation (2 2) In equation (4 6), the summation includes all possible values of $\Delta \mathbf{r} = \mathbf{r}' - \mathbf{r}$ One can see that the essential difference between $Z_{\mathbf{P}}$ and Z is in the "bra" state $\langle \{\xi_{\mathbf{m}+\Delta \mathbf{r}}\}, \mathbf{r} + \Delta \mathbf{r} \mid$

In chapter (1 2), we formed the path integral of the "normal" partition function Z, given by equation (2 1), evaluated the matrix elements, and took the limit of continuous imaginary time In the process, we imposed *no* restrictions on the end-points of the trajectory (the boundary conditions in imaginary time), which correspond to the "bra" and "ket" appearing in equation (2 1) The "normal" partition function Z is properly represented in the formalism given in chapter (1 2) by imposing periodic boundary conditions in imaginary time (the end states are the same) A comparison of equations (2 1) and (4 6) shows that the *same* formalism can be used for $Z_{\mathbf{P}}$ In this case, we must impose twisted boundary conditions in imaginary time, that is

$$\mid \{\xi_{\mathbf{m}}(0)\}, \mathbf{r}(0) \rangle = \mid \{\xi_{\mathbf{m}}\}, \mathbf{r} \rangle$$
$$\mid \{\xi_{\mathbf{m}}(\beta)\}, \mathbf{r}(\beta) \rangle = \mid \{\xi_{\mathbf{m}+\Delta \mathbf{r}}\}, \mathbf{r} + \Delta \mathbf{r} \rangle \tag{4 8}$$

Thus, we require the QMC simulations to sample trajectories for which the final state (at $\tau = \beta$) is the initial state (at $\tau = 0$) with all the coordinates (both electron and phonons) shifted by $\Delta \mathbf{r}$

The use of $Z_{\mathbf{P}}$, rather than Z, thus allows us to compute properties for a particular value of $\mathbf{P}$ As can be seen from equation (4 6), the path integral now involves the extra weight factor $e^{i\mathbf{P} \cdot \Delta \mathbf{r}/\hbar}$ Please note that in this work we will *only* consider the case for $\mathbf{P} = 0$, which corresponds to the ground state of the system, with energy $E_0(0)$ For $\mathbf{P} = 0$, the factor $e^{i\mathbf{P} \cdot \Delta \mathbf{r}/\hbar}$ is always unity and so

$$Z_{\mathbf{P}=0} = \sum_{\Delta \mathbf{r}} Z_{\Delta \mathbf{r}} \tag{4 9}$$

It should be pointed out that at non-zero values of $\mathbf{P}$, the extra factor $e^{i\mathbf{P} \cdot \Delta \mathbf{r}/\hbar}$ introduces the complication of the *sign problem* The sign problem occurs when the Monte Carlo weight used in the Metropolis Algorithm in not always positive-definite [1] In practice, the presence of the sign problem in a QMC simulation tends to produce large statistical fluctuations in the quantities measured This reduces the rate of convergence, and thus increases the computational

---

[1] A more detailed discussion of the sign-problem can be found in most text books on the subject of Monte Carlo, for example see [40]

effort required to produce accurate results By restricting ourselves to the case of $\mathbf{P} = 0$, where the Monte Carlo weight is always positive-definite, we do not have this added complication

Kornilovitch used the continuous time path integral QMC method to obtain the energy at non-zero values of $\mathbf{P}$ for lattice polarons [39] It was shown there that the measurement of $E_0(\mathbf{P}) - E_0(0)$, which depends on the logarithm of $\langle e^{i\mathbf{P} \ \Delta\mathbf{r}/\hbar} \rangle = \langle \cos(\mathbf{P} \ \Delta\mathbf{r}/\hbar) \rangle$, is statistically stable enough to determine the whole polaron spectrum, provided that the electron-phonon coupling is not too small

4.3 Effective Mass

Generally speaking, the thermodynamic properties of the system, such as the energy, are readily extracted from QMC simulations However, obtaining the (real time) dynamical properties, such as the effective mass, is not as straightforward In fact, it usually involves some kind of analytical continuation from imaginary time to real time [29] This is because QMC simulations yields direct information relating to imaginary-time correlation functions only However, in this section it is shown that, by the use of twisted boundary conditions in imaginary time, the effective mass can be *inferred directly* from the imaginary-time simulations

The effective mass is defined, by equation (4 2), in the low temperature limit $\beta \rightarrow \infty$ In this limit the partition function (for fixed total momentum) $Z_{\mathbf{P}}$ is dominated by the lowest eigenstate $E_0(\mathbf{P})$, that is

$$Z_{\mathbf{P}} = e^{-\beta E_0(\mathbf{P})}, \tag{4 10}$$

where $E_0(\mathbf{P})$ is given by equation (4 3) As mentioned in the previous section, we are restricting ourselves to the case of $\mathbf{P} = 0$, which eliminates the sign problem At $\mathbf{P} = 0$ (and $\beta \rightarrow \infty$) we notice from equations (4 6) and (4 10) that

$$Z_{\mathbf{P}=0} = \sum_{\Delta\mathbf{r}} Z_{\Delta\mathbf{r}} = e^{-\beta E_0(0)} \tag{4 11}$$

We wish to combine equations (4 10) and (4 6) in order to form an expression for m_d^*, in terms of $Z_{\Delta\mathbf{r}}$, at $\mathbf{P} = 0$ However, the fact that the effective mass is a second order quantity (with respect to $\mathbf{P}$) means that we must consider the neighbourhood around $\mathbf{P} = 0$ Expanding equations (4 10) and (4 6) for small $\mathbf{P}$ yields

$$Z_{\mathbf{P}} = e^{-\beta E_0(0)} \left(1 - \sum_{d=1}^{D} \frac{\beta P_d^2}{2m_d^*} + \quad \right)$$

$$= \sum_{\Delta \mathbf{r}} Z_{\Delta \mathbf{r}} - \sum_{\Delta \mathbf{r}} \sum_{d=1}^{D} \frac{\beta P_d^2}{2m_d^*} Z_{\Delta \mathbf{r}} + \quad , \tag{4 12}$$

where we have made use of equation (4 11), and

$$Z_{\mathbf{P}} = \sum_{\Delta \mathbf{r}} Z_{\Delta \mathbf{r}} \left[1 + \frac{\imath}{\hbar} \sum_{d=1}^{D} P_d \Delta r_d - \frac{1}{2} \left(\sum_{d=1}^{D} \frac{P_d \Delta r_d}{\hbar} \right)^2 + \quad \right]$$

$$= \sum_{\Delta \mathbf{r}} Z_{\Delta \mathbf{r}} - \sum_{\Delta \mathbf{r}} \sum_{d=1}^{D} \frac{P_d^2 (\Delta r_d)^2}{2\hbar^2} Z_{\Delta \mathbf{r}} + \quad , \tag{4 13}$$

where terms involving the linear order of Δr_d sum to zero Now, on combining equations (4 12) and (4 13), the inverse effective mass is given by

$$\frac{1}{m_d^*} = \frac{1}{\beta \hbar^2} \frac{\sum_{\Delta \mathbf{r}} (\Delta r_d)^2 Z_{\Delta \mathbf{r}}}{\sum_{\Delta \mathbf{r}} Z_{\Delta \mathbf{r}}} \tag{4 14}$$

Finally, it is convenient to measure the inverse effective mass in terms of the the bare electron mass $m_{0,d}$ By comparing the dispersion relation for a free electron,

$$\varepsilon_{\mathbf{k}} = \varepsilon_0 + \sum_{d=1}^{D} \frac{k_d^2}{2m_{0,d}}, \tag{4 15}$$

with the expansion of equation (1 6) for small $\mathbf{k}$,

$$\varepsilon_{\mathbf{k}} = -\sum_{d=1}^{D} 2t + \sum_{d=1}^{D} \frac{t k_d^2 a^2}{\hbar^2} - \quad , \tag{4 16}$$

we deduce that the bare electron mass can be written as

$$m_{0,d} = \frac{\hbar^2}{2ta^2} \tag{4 17}$$

Thus, the effective mass in relation to the bare electron mass is given by

$$\frac{m_{0,d}}{m_d^*} = \frac{1}{2\beta t a^2} \frac{\sum_{\Delta \mathbf{r}} (\Delta r_d)^2 Z_{\Delta \mathbf{r}}}{\sum_{\Delta \mathbf{r}} Z_{\Delta \mathbf{r}}}, \tag{4 18}$$

which is the statistical average of Δr_d over trajectories at $\mathbf{P} = 0$

Thus, by imposing twisted boundary conditions in imaginary time, the effective mass can now be obtained directly from the QMC simulations – simply by computing the arithmetic average of $\Delta \mathbf{r}$ within the QMC simulation

4.4 Fourier Decomposition

In this section we will analytically integrate out the phonon degrees of freedom from the system, using Gaussian integration, for the case of twisted boundary conditions in imaginary time As

explained in the previous section, the twisted boundary conditions correspond to the use of the partition function for fixed total momentum Z_P. Thus, we wish to perform the path integral

$$I_{\text{tw}} = \int_{\text{tw}} \mathcal{D}\xi \exp \sum_{\text{m}} S_{\text{m}}^{(\text{cl})}, \qquad (4\ 19)$$

where $S_{\text{m}}^{(cl)}$ is the action in terms of the end-points, equation (3 24), which we derived with no restrictions placed on the boundary conditions. The shorthand $\int_{\text{tw}} \mathcal{D}\xi$ in equation (4 19) denotes integration over all trajectories, subject to the constraint

$$\xi_{\text{m}}(0) = \xi_{\text{m}} \qquad (4\ 20)$$

$$\xi_{\text{m}}(\beta) = \xi_{\text{m}-\Delta\text{r}} \qquad (4\ 21)$$

On imposition of these boundary conditions, the action may be written in the form

$$\sum_{\text{m}} S_{\text{m}} = -\rho \sum_{\text{m}} \left(\xi_{\text{m}}^2 + \xi_{\text{m}-\Delta\text{r}}^2\right) + 2\sigma \sum_{\text{m}} \xi_{\text{m}}\xi_{\text{m}-\Delta\text{r}} + \sum_{\text{m}} \left(B_{\text{m}}\xi_{\text{m}} + C_{\text{m}}\xi_{\text{m}-\Delta\text{r}}\right) + \varpi, \qquad (4\ 22)$$

with

$$\rho = \frac{M\omega \cosh(\hbar\omega\beta)}{2\hbar \sinh(\hbar\omega\beta)}, \qquad (4\ 23)$$

$$\sigma = \frac{M\omega}{2\hbar \sinh(\hbar\omega\beta)}, \qquad (4\ 24)$$

and

$$\varpi = \sum_{\text{m}} \frac{\hbar^2}{2M} \int_0^\beta \int_0^\beta d\tau d\tau' f_{\text{m}}(\mathbf{r}(\tau)) G(\tau, \tau') f(\mathbf{r}(\tau')), \qquad (4\ 25)$$

where $G(\tau, \tau')$, B_{m} and C_{m} are defined in equations (3 12), (3 25) and (3 26) respectively

In contrast to the phonon integration using periodic boundary conditions, we can not directly apply the Gaussian integral formula, equation (3 4), due to the fact that equation (4 22) contains the mixed variable term $\xi_{\text{m}}\xi_{\text{m}-\Delta\text{r}}$. However, we may proceed by transforming ξ_{m} and $\xi_{\text{m}-\Delta\text{r}}$ into Fourier components, which will separate the mixed term (diagonalise the action), and allow the Gaussian integral formula to be applied. It is convenient to use a Fourier transformation of the form

$$\xi_{\text{m}} = \frac{1}{\sqrt{DN}} \sum_{\text{q}} (a_{\text{q}} + ib_{\text{q}})e^{i\mathbf{q}\ \text{m}}, \qquad (4\ 26)$$

and so

$$\xi_{\text{m}-\Delta\text{r}} = \frac{1}{\sqrt{DN}} \sum_{\text{q}} (a_{\text{q}} + ib_{\text{q}})e^{i\mathbf{q}\ (\text{m}-\Delta\text{r})}, \qquad (4\ 27)$$

where N is the number of sites, and D is the number of dimensions. Note that the transformation must preserve the number of independent degrees of freedom of the system. Thus the sum of the number of independent degrees of freedom arising from the a_{q} and b_{q} must be equal to DN, that is $DN/2$ each

When we shortly come to represent the action in terms of $a_{\mathbf{q}}$ and $b_{\mathbf{q}}$, we can simplify matters by noticing that $a_{\mathbf{q}}$ is an even function, and $b_{\mathbf{q}}$ an odd function, of $\mathbf{q}$ To show this we use the fact that $\xi_{\mathbf{m}}$ is real,

$$\xi_{\mathbf{m}} = \xi_{\mathbf{m}}^{*} = \frac{1}{\sqrt{DN}} \sum_{\mathbf{q}} (a_{\mathbf{q}} - \imath b_{\mathbf{q}}) e^{-\imath \mathbf{q} \cdot \mathbf{m}}, \tag{4 28}$$

and also that $\xi_{\mathbf{m}}$ is symmetrical about $\mathbf{q} = 0$, so that

$$\xi_{\mathbf{m}}_{(\mathbf{q} \to -\mathbf{q})} = \frac{1}{\sqrt{DN}} \sum_{\mathbf{q}} (a_{-\mathbf{q}} + \imath b_{-\mathbf{q}}) e^{-\imath \mathbf{q} \cdot \mathbf{m}} \tag{4 29}$$

On combining equations (4 28) and (4 29), we see that $a_{\mathbf{q}}$ is indeed an even function of $\mathbf{q}$,

$$a_{-\mathbf{q}} = a_{\mathbf{q}}, \tag{4 30}$$

and $b_{\mathbf{q}}$ an odd function of $\mathbf{q}$,

$$b_{-\mathbf{q}} = -b_{\mathbf{q}} \tag{4 31}$$

This knowledge is useful because summations over $\mathbf{q}$ may be simplified by making use of the following property of odd and even functions If $f(\mathbf{q})$ and $f'(\mathbf{q})$ are either odd $(f(-\mathbf{q}) = -f(\mathbf{q}))$ or even $(f(-\mathbf{q}) = f(\mathbf{q}))$ functions of $\mathbf{q}$ then

$$\sum_{\mathbf{q}} f(\mathbf{q}) f'(\mathbf{q}) = \frac{1}{2} \left[\sum_{\mathbf{q}} f(\mathbf{q}) f'(\mathbf{q}) + \sum_{\mathbf{q}} f(-\mathbf{q}) f'(-\mathbf{q}) \right]$$

$$= \begin{cases} \sum_{\mathbf{q}} f(\mathbf{q}) f'(\mathbf{q}) & \text{if } f(\mathbf{q}) \text{ and } f'(\mathbf{q}) \text{ are both odd or both even} \\ 0 & \text{otherwise} \end{cases} \tag{4 32}$$

Now let us express equation (4 22) in terms of the Fourier components $a_{\mathbf{q}}$ and $b_{\mathbf{q}}$ The quantity $\sum_{\mathbf{m}} \xi_{\mathbf{m}} \xi_{\mathbf{m} - \Delta \mathbf{r}}$ appearing in equation (4 22) transforms to

$$\sum_{\mathbf{m}} \xi_{\mathbf{m}} \xi_{\mathbf{m} - \Delta \mathbf{r}} = \frac{1}{DN} \sum_{\mathbf{m}} \sum_{\mathbf{q}, \mathbf{q}'} (a_{\mathbf{q}} + \imath b_{-\mathbf{q}})(a_{\mathbf{q}'} + \imath b_{\mathbf{q}'}) e^{-\imath \mathbf{m} \cdot (\mathbf{q} + \mathbf{q}')} e^{-\imath \mathbf{q}' \cdot \Delta \mathbf{r}}$$

$$= \sum_{\mathbf{q}, \mathbf{q}'} (a_{\mathbf{q}} + \imath b_{-\mathbf{q}})(a_{\mathbf{q}'} + \imath b_{\mathbf{q}'}) \delta_{\mathbf{q}, -\mathbf{q}'} e^{-\imath \mathbf{q}' \cdot \Delta \mathbf{r}}$$

$$= \sum_{\mathbf{q}} (a_{\mathbf{q}} + \imath b_{-\mathbf{q}})(a_{-\mathbf{q}} + \imath b_{-\mathbf{q}}) [\cos(\mathbf{q} \cdot \Delta \mathbf{r}) + \imath \sin(\mathbf{q} \cdot \Delta \mathbf{r})]$$

$$= \sum_{\mathbf{q}} (a_{\mathbf{q}}^{2} + b_{\mathbf{q}}^{2}) \cos(\mathbf{q} \cdot \Delta \mathbf{r}), \tag{4 33}$$

where we have used the fact that $a_{\mathbf{q}}^{2}$ and $b_{\mathbf{q}}^{2}$ are both even functions of $\mathbf{q}$ In a similar way we find that

$$\sum_{\mathbf{m}} \xi_{\mathbf{m}}^{2} = \sum_{\mathbf{m}} \xi_{\mathbf{m} - \Delta \mathbf{r}}^{2} = \sum_{\mathbf{k}} (a_{\mathbf{q}}^{2} + b_{\mathbf{q}}^{2}), \tag{4 34}$$

which can also be inferred from Parseval's theorem On substitution of equations (4 26), (4 27), (4 33) and (4 34) into equation (4 22), the action in terms of the Fourier components is given by

$$\sum_{\mathbf{q}} S_{\mathbf{q}} = -2 \sum_{\mathbf{q}} [\rho - \sigma \cos(\mathbf{q} \cdot \Delta \mathbf{r})](a_{\mathbf{q}}^{2} + b_{\mathbf{q}}^{2}) + \frac{1}{\sqrt{DN}} \sum_{\mathbf{q}} \sum_{\mathbf{m}} \left[B_{\mathbf{m}} e^{\imath \mathbf{q} \cdot \mathbf{m}} + C_{\mathbf{m}} e^{\imath \mathbf{q} \cdot (\mathbf{m} - \Delta \mathbf{r})} \right] a_{\mathbf{q}}$$

$$+ \frac{1}{\sqrt{DN}} \sum_{\mathbf{q}} \sum_{\mathbf{m}} \left[\imath B_{\mathbf{m}} e^{\imath \mathbf{q} \cdot \mathbf{m}} + \imath C_{\mathbf{m}} e^{\imath \mathbf{q} \cdot (\mathbf{m} - \Delta \mathbf{r})} \right] b_{\mathbf{q}} + \varpi$$

$$= -2 \sum_{\mathbf{q}} [\rho - \sigma \cos(\mathbf{q} \cdot \Delta \mathbf{r})](a_{\mathbf{q}}^2 + b_{\mathbf{q}}^2) + \frac{1}{\sqrt{DN}} \sum_{\mathbf{m}} \left\{ B_{\mathbf{m}} \cos(\mathbf{q} \cdot \mathbf{m}) + C_{\mathbf{m}} \cos[\mathbf{q} \cdot (\mathbf{m} - \Delta \mathbf{r})] \right\} a_{\mathbf{q}}$$

$$+ \frac{1}{\sqrt{DN}} \sum_{\mathbf{m}} \left\{ B_{\mathbf{m}} \sin(\mathbf{q} \cdot \mathbf{m}) + C_{\mathbf{m}} \sin[\mathbf{q}(\mathbf{m} - \Delta \mathbf{r})] \right\} b_{\mathbf{q}} + \varpi, \qquad (4\ 35)$$

where we have used the identity $e^{\imath x} = \cos x + \imath \sin x$ One can see from equation (4 35) that now the action (in terms of the Fourier components) does not involve any mixed terms Thus, using this diagonal form, we can now proceed to integrate out the phonon coordinates by applying the Gaussian integration formula

4.5   Integration with Twisted Boundary Conditions

In this section we will perform the integration over the phonon degrees of freedom, and then take the low temperature limit $\beta \to \infty$, in which the effective mass is defined

In terms of the Fourier components $a_{\mathbf{q}}$ and $b_{\mathbf{q}}$, the path integral over the phonon coordinates that we wish to perform, equation (4 19), is given by

$$I_{\text{tw}} = \int_{\text{tw}} \mathcal{D}a_{\mathbf{q}} \mathcal{D}b_{\mathbf{q}} \exp \left(\sum_{\mathbf{q}} S_{\mathbf{q}} \right)$$

$$= \prod_{\mathbf{q}} \int_{\text{tw}} da_{\mathbf{q}} db_{\mathbf{q}} \exp \left(S_{\mathbf{q}} \right), \qquad (4\ 36)$$

where we have used the fact that $S_{\mathbf{q}}$, given by equation (4 22), is diagonal in this representation We can now directly apply the Gaussian integral formula, equation (3 4), to each separate Fourier component (of which there are $DN/2$ for $a_{\mathbf{q}}$, and $DN/2$ for $b_{\mathbf{q}}$) The result is

$$I_{\text{tw}} = \left[\prod_{\mathbf{q}} \frac{\pi}{2[\rho - \sigma \cos(\mathbf{q} \cdot \Delta \mathbf{r})]} \right] \exp A_{\text{tw}}$$

$$= \left[\frac{\pi \hbar \sinh(\hbar \omega \beta)}{M \omega [\cosh(\hbar \omega \beta) - \cos(\mathbf{q} \cdot \Delta \mathbf{r})]} \right]^{DN/2} \exp A_{\text{tw}}, \qquad (4\ 37)$$

where

$$A_{\text{tw}} = \sum_{\mathbf{q}} \frac{1}{8dN[\rho - \sigma \cos(\mathbf{q} \cdot \Delta \mathbf{r})]} \left\{ \left(\sum_{\mathbf{m}} B_{\mathbf{m}} \cos(\mathbf{q} \cdot \mathbf{m}) + \sum_{\mathbf{m}'} C_{\mathbf{m}'} \cos[\mathbf{q} \cdot (\mathbf{m}' - \Delta \mathbf{r})] \right)^2 \right.$$

$$\left. + \left(\sum_{\mathbf{m}} B_{\mathbf{m}} \sin(\mathbf{q} \cdot \mathbf{m}) + \sum_{\mathbf{m}'} C_{\mathbf{m}'} \sin[\mathbf{q} \cdot (\mathbf{m}' - \Delta \mathbf{r})] \right)^2 \right\} + \varpi \quad (4\ 38)$$

The contents of the braces in equation (4 38) can be expanded and simplified according to

$$\left(\sum_{\mathbf{m}} B_{\mathbf{m}} \cos(\mathbf{q} \cdot \mathbf{m}) + \sum_{\mathbf{m}'} C_{\mathbf{m}'} \cos[\mathbf{q} \cdot (\mathbf{m}' - \Delta \mathbf{r})] \right)^2 + \left(\sum_{\mathbf{m}} B_{\mathbf{m}} \sin(\mathbf{q} \cdot \mathbf{m}) + \sum_{\mathbf{m}'} C_{\mathbf{m}'} \sin[\mathbf{q} \cdot (\mathbf{m}' - \Delta \mathbf{r})] \right)^2$$

$$
\begin{aligned}
&= \sum_{\mathbf{mm'}} \big\{ B_{\mathbf{m}} B_{\mathbf{m'}} \cos[\mathbf{q} \ (\mathbf{m} - \mathbf{m'})] + B_{\mathbf{m}} C_{\mathbf{m'}} \cos[\mathbf{q} \ (\mathbf{m} - \mathbf{m'} + \Delta \mathbf{r})] \\
&\qquad\qquad + C_{\mathbf{m}} B_{\mathbf{m'}} \cos[\mathbf{q} \ (\mathbf{m} - \mathbf{m'} - \Delta \mathbf{r})] + C_{\mathbf{m}} C_{\mathbf{m'}} \cos[\mathbf{q} \ (\mathbf{m} - \mathbf{m'})] \big\} \\
&= \sum_{\mathbf{mm'}} [B_{\mathbf{m}} B_{\mathbf{m'}} \delta_{\mathbf{m},\mathbf{m'}} + B_{\mathbf{m}} C_{\mathbf{m'}} \delta_{\mathbf{m},\mathbf{m'}-\Delta \mathbf{r}} + B_{\mathbf{m'}} C_{\mathbf{m}} \delta_{-\mathbf{m'},\mathbf{m}+\Delta \mathbf{r}} + B_{\mathbf{m}} B_{\mathbf{m'}} \delta_{\mathbf{m},\mathbf{m'}}] \\
&= \sum_{\mathbf{m}} [B_{\mathbf{m}}^2 + 2 B_{\mathbf{m}} C_{\mathbf{m}} + C_{\mathbf{m}}^2] \\
&= \sum_{\mathbf{m}} \big[(B_{\mathbf{m}} + C_{\mathbf{m}})^2 + 2 B_{\mathbf{m}} (C_{\mathbf{m}-\Delta \mathbf{r}} - C_{\mathbf{m}}) \big] ,
\end{aligned}
\tag{4 39}
$$

so that

$$
A_{\mathrm{tw}} = \frac{\hbar \sinh(\hbar\omega\beta) \sum_{\mathbf{m}} B_{\mathbf{m}}(C_{\mathbf{m}-\Delta \mathbf{r}} - C_{\mathbf{m}})}{2 M \omega [\cosh(\hbar\omega\beta) - \cos(\mathbf{q} \ \Delta \mathbf{r})]} + \frac{\hbar \sinh(\hbar\omega\beta) \sum_{\mathbf{m}} (B_{\mathbf{m}} + C_{\mathbf{m}})^2}{4 M \omega [\cosh(\hbar\omega\beta) - \cos(\mathbf{q} \ \Delta \mathbf{r})]}
$$
$$
+ \sum_{\mathbf{m}} \frac{\hbar^2}{2M} \int_0^\beta \int_0^\beta d\tau d\tau' f_{\mathbf{m}}(\mathbf{r}(\tau)) G(\tau, \tau') f(\mathbf{r}(\tau')) \tag{4 40}
$$

Thus the phonon degrees of freedom have been integrated out   The result represents a single electron with retarded self interaction along the imaginary time dimension   Notice that if we set $\Delta \mathbf{r} = 0$ in equation (4 40), the result correctly reduces to the expression previously found using periodic boundary conditions, given by equation (3 37)

The final step is to take the limit of low temperature $\beta \to \infty$, which corresponds to the ground state of the system (where the effective mass is defined)   This limit is equivalent to

$$
\frac{1}{2} e^{\hbar\omega\beta} = \cosh \hbar\omega\beta = \sinh \hbar\omega\beta \gg 1 \tag{4 41}
$$

Note that, since both β and ω will be used as parameters in our QMC simulations, the condition $e^{\hbar\omega\beta} \gg 1$ is easily realisable in practice   The quantities $B_{\mathbf{m}}$ and $C_{\mathbf{m}}$, given by equations (3 25) and (3 26) respectively, become

$$
B_{\mathbf{m}} = \int_0^\beta d\tau e^{-\hbar\omega\beta} \big(e^{\hbar\omega(\beta-\tau)} - e^{\hbar\omega(\beta-\tau)} \big) f_{\mathbf{m}}(\mathbf{r}(\tau)) \tag{4 42}
$$

$$
= \int_0^\beta d\tau \big(e^{-\hbar\omega\tau} - e^{-\hbar\omega(2\beta-\tau)} \big) f_{\mathbf{m}}(\mathbf{r}(\tau)) \tag{4 43}
$$

$$
\approx \int_0^\beta d\tau e^{-\hbar\omega\tau} f_{\mathbf{m}}(\mathbf{r}(\tau)), \tag{4 44}
$$

and in a similar way

$$
C_{\mathbf{m}} \approx \int_0^\beta d\tau e^{-\hbar\omega(\beta-\tau)} f_{\mathbf{m}}(\mathbf{r}(\tau)) \tag{4 45}
$$

Notice that the sum of the second and third terms appearing in equation (4 40) is exactly the same as the result we previously obtained for periodic boundary conditions I_{per}, given by equation (3 37)   Thus, in the low temperature limit we can write

$$
I_{\mathrm{tw}} = \exp A_{\mathrm{tw}} \left(\frac{\pi \hbar}{M \omega} \right)^{DN/2} , \tag{4 46}
$$

where

$$A_{\text{tw}} = A_{\text{per}} + \Delta A, \tag{4 47}$$

with

$$
\begin{aligned}
\Delta A &= \frac{\hbar}{2M\omega} \sum_{\mathbf{m}} B_{\mathbf{m}}(C_{\mathbf{m}-\Delta\mathbf{r}} - C_{\mathbf{m}}) \\
&= \frac{\hbar}{2M\omega} \int_0^\beta \int_0^\beta d\tau d\tau' e^{-\hbar\omega\tau} e^{-\hbar\omega(\beta-\tau')} \sum_{\mathbf{m}} f_{\mathbf{m}}(\mathbf{r}(\tau)) \left[f_{\mathbf{m}+\Delta\mathbf{r}}(\mathbf{r}(\tau')) - f_{\mathbf{m}}(\mathbf{r}(\tau')) \right]
\end{aligned} \tag{4 48}
$$

and

$$
A_{\text{per}} = \frac{\hbar}{4M\omega} \int_0^\beta \int_0^\beta d\tau d\tau'\, e^{\hbar\omega\frac{\beta}{2}} \left(e^{\hbar\omega(\frac{\beta}{2} - |\tau-\tau'|)} + e^{-\hbar\omega(\frac{\beta}{2} - |\tau-\tau'|)} \right) \sum_{\mathbf{m}} f_{\mathbf{m}}(\mathbf{r}(\tau)) f_{\mathbf{m}}(\mathbf{r}(\tau'))
\tag{4 49}
$$

Equation (4 46) then forms the basis for the QMC scheme used in this work, which we will develop into a form that is suitable for implementation in the following chapter
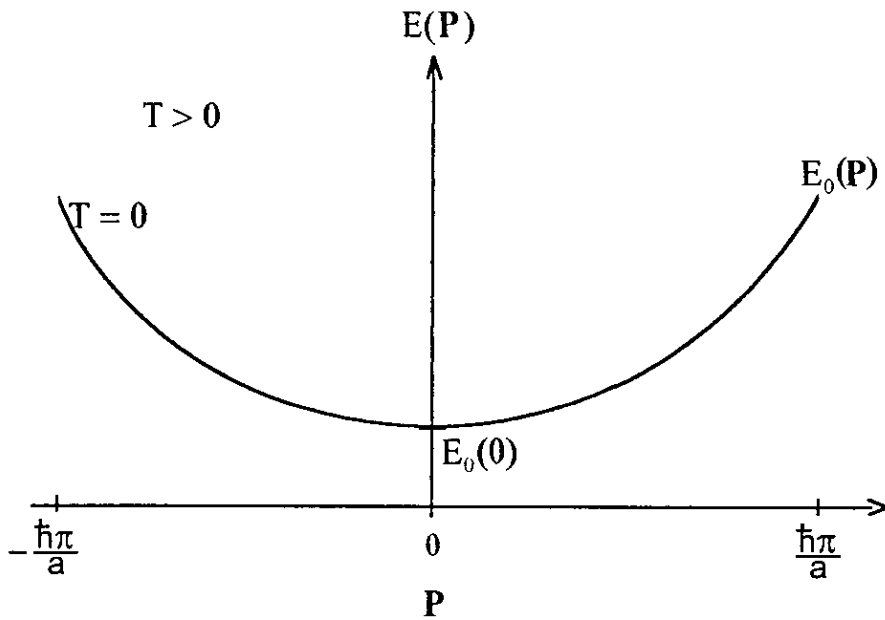
Figure 4 1   The dispersion curve for a (one dimensional) polaron with effective mass m^* The dotted line represents the curve at finite temperatures   The solid line $E_0(\mathbf{P})$ represents the curve in the low temperature limit $\beta \to \infty$, where the lowest eigenstate dominates   The ground state energy $E_0(0)$ occurs at $\mathbf{P} = 0$ The definition of effective mass only has meaning for $\beta \to \infty$

Chapter 5

Continuous-Time Monte Carlo Scheme.

5.1 Introduction

In chapter (2) we discussed the traditional approach to path-integral QMC simulation, in which the imaginary-time dimension is (artificially) decomposed into a large number of imaginary-time slices, each having width $\Delta\tau$. The trajectory is then represented by the position of the electron in each imaginary-time slice. The reason this method has been so widely adopted is probably ease of programming. However, as we discussed, the use of discrete imaginary time inherently introduces the problematic finite-time-step error, which is a *systematic* error that scales with $(\Delta\tau)^2$.

The desire to eliminate this finite-time-step error has encouraged the recent development of path-integral QMC methods that are implemented *directly* in the limit of continuous imaginary time. Here, the trajectory is represented by a series of "kinks" in an otherwise straight-line trajectory. Changes to the trajectory are generated by processes that involve the addition and deletion of kinks. The use of continuous imaginary time has two major advantages over the traditional approach.

1. The systematic finite-time-step error is entirely eliminated, which renders the scheme – in the numerical sense – "exact".

2 The Monte Carlo weight, used in the Metropolis algorithm, now involves the integration over kinks, rather than imaginary-time slices Generally speaking, the number of kinks is significantly smaller than the corresponding number of imaginary-time slices This leads a dramatic increase in the efficiency of the algorithm

We start this chapter by presenting the basic structure of the Metropolis Monte Carlo algorithm, from a general point of view Then, in section (5 3), we discuss the implementation of the algorithm in continuous imaginary time, for the specific case of our lattice model The expression for the action, equation (4 47) is transformed into dimensionless form in section (5 4), which is necessary for practical QMC simulation Finally, we present three "tricks" that increase the efficiency of the continuous-imaginary-time algorithm for our particular model

1 An analytical integration over kinks

2 The identification of factors involving exponential functions, that are common to the various quantities to be evaluated during the QMC simulation

3 The use of a "look-up table" involving the interaction force $f_{\mathbf{m}}(\mathbf{n})$

The resulting continuous-imaginary-time QMC algorithm is significantly more efficient than the corresponding discrete-imaginary-time algorithm

5.2   Metropolis Monte Carlo Algorithm

The aim in Monte Carlo simulation is to generate a random set of states according to a desired probability distribution (Monte Carlo weight) W This is achieved by the use of a *Markov chain*, which generates a random walk through state space Given that the system is in a state μ, a single Markov process (Monte Carlo step) generates a new state μ', using information about the states μ and μ' only It does so in a random fashion according to a *transition probability* $P(\mu \to \mu')$

The transition probabilities $P(\mu \to \mu')$ are chosen in such a way as to ensure that the Markov chain will generate states which appear with the desired probability distribution $W(\mu)$ -- after a sufficiently large number of Monte Carlo steps have been performed It is well known that the Markov chain will (eventually) generate states according to $W(\mu)$ for any $P(\mu \to \mu')$ that satisfies the following three conditions [40]

1   The transition probabilities must obey the usual sum rule of probabilities,

$$\sum_{\mu'} P(\mu \to \mu') = 1,$$ (5 1)

where the probability of staying in the same state $P(\mu \to \mu)$ is not necessarily zero

2   $P(\mu \to \mu')$ must satisfy the *condition of detailed balance*,

$$W(\mu)P(\mu \to \mu') = W(\mu')P(\mu' \to \mu)$$ (5 2)

3   $P(\mu \to \mu')$ must be *ergodic*, which means that it is always possible to move from one state of the system to any other state in a finite number of Markov processes, and thus all of state space can be sampled

The Metropolis (rejection) algorithm is a particular way of specifying $P(\mu \to \mu')$ such that the above three conditions are simultaneously satisfied   The transition probability is split into two parts,

$$P(\mu \to \mu') = g(\mu \to \mu')a(\mu \to \mu'),$$ (5 3)

where $g(\mu \to \mu')$ is known as the *sampling distribution* and $a(\mu \to \mu')$ as the *acceptance probability*   In practice, we have considerable freedom in the way in which the Monte Carlo algorithm constructs a new state μ' from μ, and on the sampling distribution $g(\mu \to \mu')$ The only constraint on the choice of $g(\mu \to \mu')$ is that $P(\mu \to \mu')$ should remain ergodic

Given, then, that a new state has been generated, the change is accepted or rejected with acceptance probability $a(\mu \to \mu')$ We choose $a(\mu \to \mu')$ such that the detailed balance equation (5 2) is still satisfied, which can now be written as

$$\frac{a(\mu \to \mu')}{a(\mu' \to \mu)} = \frac{g(\mu' \to \mu)}{g(\mu \to \mu')} \frac{W(\mu')}{W(\mu)}$$ (5 4)

In order to produce an efficient algorithm, the acceptance probabilities $0 \le a(\mu \to \mu') \le 1$ should be as close to unity as possible   A low acceptance probability would mean that changes would be accepted rarely   One way to achieve this is to set the larger of $a(\mu \to \mu')$ and $a(\mu' \to \mu)$ to unity, and adjust the other such that the ratio of the two satisfies equation (5 4), that is

$$a(\mu \to \mu') = \min\left[1, \frac{g(\mu' \to \mu)}{g(\mu \to \mu')} \frac{W(\mu')}{W(\mu)}\right]$$ (5 5)

This method of maximising the acceptance probabilities is due to Metropolis [41, 40]

A general Metropolis algorithm will contain at least the following steps

1   Choose an initial state of the system

2 *Propose* a small change to the system, from state μ to μ' The selection probabilities $g(\mu \to \mu')$ will depend on the method chosen to generate the proposed changes

3 Accept or reject the proposed change according to the acceptance ratio $a(\mu \to \mu')$ In practice, this can be achieved with the aid of a random number $0 \leq r < 1$, generated from a uniform distribution If $r < a(\mu \to \mu')$, then the proposed change should be accepted, otherwise it should rejected (leaving the state unchanged)

4 If the system has reached "equilibrium" (explained below), then accumulate averages of the required observable quantities

5 Repeat steps (2) to (4) until the statistical errors in the accumulated averages have reduced to an acceptable level

The system is said to be in equilibrium when the algorithm generates states that appear according to the desired probability distribution $W(\mu)$ The number of Monte Carlo steps required for the system to reach equilibrium ("warm-up period") can not be determined in advance However, one can estimate the point at which the system reaches equilibrium by considering how the measured quantities evolve with "time" (the number of Monte Carlo steps performed) In equilibrium, the measured quantities tend to fluctuate around a narrow range of values It is important that the data used to produce averages is accumulated after equilibrium has been reached Note that, once the system is in equilibrium, the "memory" of the initial state has been lost Thus, the choice of the initial state of the system is quite arbitrary

An important consideration in the design of a Monte Carlo algorithm is the size of the proposed change to the system, on each Monte Carlo step In equilibrium, only a small subset of states are important A dramatic alteration to the state of the system would result in a very low acceptance ratio (ratio of the number of accepted changes to the total number of proposed changes), and produce large statistical fluctuations in the measured quantities It is thus, in general, preferable to consider small changes to the state of the system – only increasing the size of the change if the warm-up period is found to be impractically long

5.3 Continuous-Time Monte Carlo Scheme.

A path-integral QMC scheme, that is implemented in continuous imaginary-time, has recently been developed for systems with a discrete basis [42, 43] In this scheme, the electron trajectory is viewed as finite intervals of imaginary time, in which the system remains in a particular state,

with sporadic transitions to other states The points in imaginary time at which the state of
the system changes are called "kinks" An example of a one-dimensional trajectory is shown in
figure (5 1)

It is necessary, in this method, to consider the statistics governing different *types* of kinks
independently of one another For a hypercubic lattice with nearest-neighbour hopping, there are
$2D$ different types of kinks – each corresponding to an electron hop to one of the $2D$ nearest-
neighbours In the one-dimensional case, we must treat the statistics governing *left* and *right*
kinks separately Proposed changes to the shape of the trajectory are generated by the addition
or deletion of kinks One may also consider other processes that alter the shape of the trajectory,
such as changing the type of a kink (e g   left or right for one-dimension), changing a kink's
position in imaginary time, or changing the order in which the kinks appear

In our implementation of the above continuous-time method we only consider the processes
of addition and deletion of kinks This is sufficient in practice, due to the fact that the other
processes mentioned above can always be formed by combining addition and deletion processes
Furthermore, we only consider the addition and deletion of *single* kinks, because our model is
restricted to nearest-neighbour hopping

The Monte Carlo weight for our model is given by

$$w(N_s) = w_{\mathrm{el}}(N_s) \ w_{\mathrm{ph}}(N_s), \tag{5 6}$$

where N_s is the number of kinks of type s, $w_{\mathrm{el}}(N_s)$ is the weight induced by the electron sub-
system, and $w_{\mathrm{ph}}(N_s)$ the weight from the phonon subsystem Note that $w_{\mathrm{ph}}(N_s)$, and therefore
$w(N_s)$, also depends on the position in imaginary time at which each kink occurs The individual
weights $w_{\mathrm{el}}(N_s)$ and $w_{\mathrm{ph}}(N_s)$ originate from the factors $\prod_l I(\mathbf{r}_{l+1} - \mathbf{r}_l)$ and e^S, respectively, in
equation (2 29) Note that any multiplicative constants involved in $w(N_s)$ are unimportant due
to the fact that the Metropolis algorithm evaluates the ratio of weights only In the absence of
any electron-phonon interaction, the probability that the electron trajectory consists of N_s kinks
of sort s is given by the Poisson distribution [30] [1]

$$w_{\mathrm{el}}(N_s) = \frac{(t\beta)^{N_s} e^{-t\beta}}{N_s!} \tag{5 7}$$

The phonon-induced weight $w(N_s)$ is given by the factor $e^{A_{\mathrm{tw}}}$ appearing in equation (4 46) Thus,
the total Monte Carlo weight is given by

$$w(N_s) = \frac{(t\beta)^{N_s} e^{-t\beta}}{N_s!} \exp[A_{\mathrm{tw}}(N_s)] \tag{5 8}$$

---

[1] Imagine that the imaginary-time dimension $[0, \beta]$ is split into a large number of small time intervals If we
regard each time interval as a separate "experiment", then the probability of an "event" (one kink) occurring in
a particular time-slice is very small Under these circumstances, the expected (finite) number of kinks, over the
entire trajectory, is governed by the Poisson distribution

Let us now consider the selection probability to propose the addition or deletion of a kink (of type s), $g(N_s \rightarrow N_s + 1)$ and $g(N_s + 1 \rightarrow N_s)$ respectively In the case of $N_s \geq 1$ (one or more kinks exist), we choose $g(N_s + 1 \rightarrow N_s) = g(N_s \rightarrow N_s + 1) = 1/2$, and so the acceptance probability, equation (5 5), is given by

$$a_{\text{add}}(N_s \rightarrow N_s + 1) = \min\left(1, \frac{t\beta}{N_s + 1} \exp[A_{\text{tw}}(N_s + 1) - A_{\text{tw}}(N_s)]\right) \tag{5 9}$$

$$a_{\text{rem}}(N_s + 1 \rightarrow N_s) = \min\left(1, \frac{N_s + 1}{t\beta} \exp[A_{\text{tw}}(N_s) - A_{\text{tw}}(N_s + 1)]\right) \tag{5 10}$$

However, in the case of $N_s = 0$, we can only add a kink, and thus $g(0 \rightarrow 1) = 1$ The other sampling distribution involved in equation (5 5) is $g(1 \rightarrow 0) = 1/2$ Thus, for $N_s = 0$, the acceptance probabilities are given by

$$a_{\text{add}}(0 \rightarrow 1) = \min\left(1, \frac{t\beta}{2} \exp[A_{\text{tw}}(1) - A_{\text{tw}}(0)]\right) \tag{5 11}$$

$$a_{\text{rem}}(1 \rightarrow 0) = \min\left(1, \frac{2}{t\beta} \exp[A_{\text{tw}}(0) - A_{\text{tw}}(1)]\right) \tag{5 12}$$

The corresponding (single kink) continuous-imaginary-time QMC algorithm has the following structure

1 Select a kink type in a random fashion In the case of a one-dimensional system, this could be either a left kink or a right kink

2 Propose a change to the trajectory by randomly selecting whether to add a new kink (at a random imaginary time) or to remove an existing kink (selected in a random fashion) This is done according to the selection probabilities $g(N_s + 1 \rightarrow N_s)$ and $g(N_s \rightarrow N_s + 1)$

3 Accept or reject the change proposed above, with probability $a_{\text{add}}(N_s \rightarrow N_s + 1)$ if adding a kink, or $a_{\text{rem}}(N_s + 1 \rightarrow N_s)$ if removing a kink

4 If the change has been accepted in step (3), then the *entire* trajectory that lies "above" the kink (i e from the imaginary time of the kink to β) should be shifted across [2] This is shown graphically in figures (5 2) and (5 2) If, on the other hand, the proposed change has been rejected in step (3), then the trajectory should be left untouched

One can see from equations (5 9) to (5 12), that the major computational task in the algorithm is to calculate the phonon induced weight $\exp A(N_s)$ for the configuration of kinks, upon each Monte Carlo step

---

[2]Unlike similar schemes [44, 42], we do not need to create kink anti-kink pairs, due to the fact that we are employing twisted, rather than periodic, boundary conditions

5.4   Dimensionless Representation.

The model Hamiltonian, equation (1 1), contains three, non-independent, dimensioned control parameters ω, t and $f_{\mathbf{m}}(\mathbf{n})$ In order to successfully implement the QMC algorithm, we would like to use these three quantities to form two *independent* and *dimensionless* control parameters   There is considerable freedom as to how these dimensionless quantities may be defined   The action, equation (4 47), as well as any other quantities that need to be evaluated in the QMC algorithm, must then be transformed into this dimensionless representation

Let us take the hopping integral t as the base unit of energy   This naturally gives rise to the definition of the *dimensionless phonon frequency* (adiabatic parameter) as

$$\bar{\omega} = \frac{\hbar\omega}{t} \tag{5 13}$$

As the second dimensionless parameter, it is convenient to define the *electron-phonon coupling strength* as

$$\lambda = \frac{E_p}{zt} = \frac{1}{2M\omega^2 zt} \sum_{\mathbf{m}} f_{\mathbf{m}}^2(0), \tag{5 14}$$

where E_p is the "small-polaronic shift", which will be derived later in chapter (8), M is the ionic mass, and z is the co-ordination number   Note that λ represents the ratio of the energy of the completely localised state to that of a free electron   The results of the QMC simulations will be presented in terms of $\bar{\omega}$ and λ for each model studied

Now let us cast the additional dimensioned parameters – β, τ and $f_{\mathbf{m}}(\mathbf{n})$ – into dimensionless form   The above choice of t as the unit of energy leads to the definition of the *dimensionless inverse-temperature* as

$$\bar{\beta} = t\beta, \tag{5 15}$$

which has the effect of re-scaling the imaginary-time dimension, so that the *dimensionless imaginary time*

$$\bar{\tau} = t\tau \tag{5 16}$$

is in the range $0 \leq \bar{\tau} \leq \bar{\beta}$ The dimensioned electron-phonon interaction force $f_{\mathbf{m}}(\mathbf{n})$ may be decomposed into the product of two parts,

$$f_{\mathbf{m}}(\mathbf{n}) = \kappa \bar{f}_{\mathbf{m}}(\mathbf{n}), \tag{5 17}$$

where κ takes the dimensions of force, and $\bar{f}_{\mathbf{m}}(\mathbf{n})$ is dimensionless and represents the *shape* or *form* of the electron-phonon interaction   In terms of the dimensionless control parameters, λ and $\bar{\omega}$, equation (5 17) is given by

$$f_{\mathbf{m}}(\mathbf{n}) = \left(\frac{2z\lambda M t^3 \bar{\omega}^2}{\hbar^2 \sum_{\mathbf{m}} \bar{f}_{\mathbf{m}}^2(0)} \right)^{1/2} \bar{f}_{\mathbf{m}}(\mathbf{n}), \tag{5 18}$$

where we see that the interaction shape $\bar{f}_\mathbf{m}(\mathbf{n})$ is defined up to an arbitrary constant

Thus, the action, equation (4 47), in dimensionless representation, is given by

$$A_\mathrm{tw} = A_\mathrm{per} + \Delta A, \tag{5 19}$$

with

$$A_\mathrm{per} = \frac{z\lambda\bar{\omega}}{2\Phi_0(0,0)} \int_0^{\bar{\beta}}\int_0^{\bar{\beta}} d\bar{\tau}\,d\bar{\tau}'\,e^{\bar{\omega}\frac{\bar{\beta}}{2}} \left(e^{\bar{\omega}\left(\frac{\bar{\beta}}{2}-|\bar{\tau}-\bar{\tau}'|\right)} + e^{-\bar{\omega}\left(\frac{\bar{\beta}}{2}-|\bar{\tau}-\bar{\tau}'|\right)} \right) \Phi_0\left(\mathbf{r}(\bar{\tau}),\mathbf{r}(\bar{\tau}')\right), \tag{5 20}$$

and

$$\Delta A = \frac{z\lambda\bar{\omega}}{\Phi_0(0,0)} \int_0^{\bar{\beta}}\int_0^{\bar{\beta}} d\bar{\tau}\,d\bar{\tau}'\,e^{-\bar{\omega}\bar{\tau}}e^{-\bar{\omega}(\bar{\beta}-\bar{\tau}')} \left[\Phi_{\Delta\mathbf{r}}\left(\mathbf{r}(\bar{\tau}),\mathbf{r}(\bar{\tau}')\right) - \Phi_0\left(\mathbf{r}(\bar{\tau}),\mathbf{r}(\bar{\tau}')\right)\right], \tag{5 21}$$

where we have introduced the shorthand for the *lattice summation*

$$\Phi_{\Delta\mathbf{r}}\left(\mathbf{r}(\bar{\tau}),\mathbf{r}(\bar{\tau}')\right) = \sum_\mathbf{m} \bar{f}_\mathbf{m}(\mathbf{r}(\bar{\tau}))\bar{f}_{\mathbf{m}+\Delta\mathbf{r}}(\mathbf{r}(\bar{\tau}')) \tag{5 22}$$

5.5   Analytical Integration Over Kinks.

The Metropolis algorithm requires the action to be computed on each and every Monte Carlo step, in order to evaluate the acceptance ratios   It is therefore extremely important that our algorithm should be designed in such a way that the action is computed efficiently   The double integration in equations (5 20) and (5 21) would require a large amount of computational effort to evaluate numerically   However, the representation of the trajectory as a series of single kinks, between which the trajectory is a straight line, allows us to "break up" the double integration into segments, such that the integration can be treated analytically within each segment   The double integration can then be computed, in an efficient way, by summing up the individual contributions from each segment

There are also two further "tricks" that we have employed, in order to increase the overall efficiency of the algorithm   The first is to generate a "look-up table" of values in advance of the simulation proper   This is explained fully in section (5 6)   The second trick is to identify common factors in the final expressions for the action and the other quantities that are to be evaluated   The algorithm evaluates these factors only when a new kink is added, and then "carries" them around through the simulation, until the kink is deleted   An exponential function that is evaluated on every Monte Carlo step constitutes a large amount of computational effort (compared with operations such as multiplication or addition)   Thus, the most important influence in the choice of these factors is the reduction in the overall number of exponential functions that must be computed   The three factors that were chosen – K_1, K_2 and K_3 – are introduced below

Let us "break up" the area of integration of the double integrals, appearing in equations (5 20) and (5 21), into segments according to

$$\int_0^{\bar{\beta}}\int_0^{\bar{\beta}}d\bar{\tau}d\bar{\tau}' = \sum_{j=1}^{N_s+1}\sum_{k=1}^{N_s+1}\int_{\bar{\tau}_{j-1}}^{\bar{\tau}_j}\int_{\bar{\tau}_{k-1}}^{\bar{\tau}_k}d\bar{\tau}d\bar{\tau}',\tag{5 23}$$

which is shown graphically in figure (5 4)   Each rectangular segment is specified by four times, $[\bar{\tau}_{j-1},\bar{\tau}_j,\bar{\tau}_{k-1},\bar{\tau}_k]$, each of which correspond to the position of a kink in imaginary-time   The important point is that in the range $[\bar{\tau}_{j-1},\bar{\tau}_j]$, the electron has a fixed position of $\mathbf{r}(\bar{\tau}) = \mathbf{r}(\bar{\tau}_{j-1})$ Similarly, in the range $[\bar{\tau}_{k-1},\bar{\tau}_j]$, the position is fixed at $\mathbf{r}(\bar{\tau}') = \mathbf{r}(\bar{\tau}_{k-1})$ Thus, *within each segment* the lattice summations

$$\Phi_{\Delta\mathbf{r}}(\mathbf{r}(\bar{\tau}_{j-1}),\mathbf{r}(\bar{\tau}_{k-1})) = \sum_{\mathbf{m}}\bar{f}_{\mathbf{m}}(\mathbf{r}_{\bar{\tau}_{j-1}})\bar{f}_{\mathbf{m}+\Delta\mathbf{r}}(\mathbf{r}_{\bar{\tau}_{k-1}}),\tag{5 24}$$

in equations (5 20) and (5 21), are in fact *constant*   Thus, the integral can be treated analytically within each segment

We can reduce the necessary computation further by treating the diagonal and off-diagonal segments, shown in figure (5 4), separately   Accordingly, we can express equation (5 24) as

$$\int_0^{\bar{\beta}}\int_0^{\bar{\beta}}d\bar{\tau}d\bar{\tau}' = 2\sum_{j=1}^{N_s}\sum_{k=j+1}^{N_s+1}\int_{\bar{\tau}_{j-1}}^{\bar{\tau}_j}\int_{\bar{\tau}_{k-1}}^{\bar{\tau}_k}d\bar{\tau}d\bar{\tau}' + \sum_{j=1}^{N_s+1}\int_{\bar{\tau}_{j-1}}^{\bar{\tau}_j}\int_{\bar{\tau}_{j-1}}^{\bar{\tau}_j}d\bar{\tau}d\bar{\tau}'\tag{5 25}$$

The factor of 2 in the first term of equation (5 25) is due to the fact that we must consider *pairs* of off-diagonal segments   one in the lower triangle $(0 \le \bar{\tau} < \bar{\tau}' \le \bar{\beta})$, and the other in the upper triangle $(0 \le \bar{\tau} < \bar{\tau}' \le \bar{\beta})$ On application of equation (5 25) to the double integral appearing in equations (5 20) and (5 21), we may express the action in the form

$$A = 2\sum_{j=1}^{N_s}\sum_{k=j+1}^{N_s+1}A_{jk} + \sum_{j=1}^{N_s+1}A_{jj},\tag{5 26}$$

where

$$A_{jk} = \frac{z\lambda\bar{\omega}}{2\Phi_0(0,0)}\left\{2\Delta A'\left[\Phi_{\Delta\mathbf{r}}(\mathbf{r}(\bar{\tau}_{j-1}),\mathbf{r}(\bar{\tau}_{k-1})) - \Phi_0(\mathbf{r}(\bar{\tau}_{j-1}),\mathbf{r}(\bar{\tau}_{k-1}))\right]\right.$$
$$\left. +A'_{\text{per}}\Phi_0(\mathbf{r}(\bar{\tau}_{j-1}),\mathbf{r}(\bar{\tau}_{k-1}))\right\},\tag{5 27}$$

with

$$A'_{\text{per}} = \int_{\bar{\tau}_{j-1}}^{\bar{\tau}_j}\int_{\bar{\tau}_{k-1}}^{\bar{\tau}_k}d\bar{\tau}d\bar{\tau}'e^{-\bar{\omega}\bar{\beta}/2}\left(e^{\bar{\omega}(\bar{\beta}/2-|\bar{\tau}-\bar{\tau}'|)} + e^{-\bar{\omega}(\bar{\beta}/2-|\bar{\tau}-\bar{\tau}'|)}\right),\tag{5 28}$$

and

$$\Delta A' = \int_{\bar{\tau}_{j-1}}^{\bar{\tau}_j}\int_{\bar{\tau}_{k-1}}^{\bar{\tau}_k}d\bar{\tau}d\bar{\tau}'e^{-\bar{\omega}\bar{\tau}}e^{-\bar{\omega}(\bar{\beta}-\bar{\tau}')}\tag{5 29}$$

Let us now perform the double integration, in the expressions for A'_{per} and $\Delta A'$, and thus find A_{jk} and A_{jj} Note that, when performing the integrations, we must consider the lower triangle

$(0 \leq \bar{\tau} < \bar{\tau}' \leq \bar{\beta})$ and the upper triangle $(0 \leq \bar{\tau}' < \bar{\tau} \leq \bar{\beta})$ separately We present the details of the integration below in a brief form, because the calculation involves a large amount of algebraic manipulation

Consider first the contribution from the off-diagonal segment A_{jk} Integrating the expression for $\Delta A'$, first in the lower triangle $(0 \leq \bar{\tau} < \bar{\tau}' \leq \bar{\beta})$, and then in the upper triangle $(0 \leq \bar{\tau}' < \bar{\tau} \leq \bar{\beta})$, we find that

$$\underset{\bar{\tau}<\bar{\tau}'}{\Delta A'} = -\frac{1}{\bar{\omega}^2}e^{-\bar{\omega}\bar{\beta}}\left(e^{-\bar{\omega}\bar{\tau}_j} - e^{-\bar{\omega}\bar{\tau}_{j-1}}\right)\left(e^{\bar{\omega}\bar{\tau}_k} - e^{\bar{\omega}\bar{\tau}_{k-1}}\right)$$
$$= K_1(\bar{\tau}_j, \bar{\tau}_{j-1})K_1(\bar{\tau}_k, \bar{\tau}_{k-1})e^{-\bar{\omega}(\bar{\beta}-\bar{\tau}_k+\bar{\tau}_{j-1})}, \tag{5 30}$$

and

$$\underset{\bar{\tau}>\bar{\tau}'}{\Delta A'} = K_1(\bar{\tau}_j, \bar{\tau}_{j-1})K_1(\bar{\tau}_k, \bar{\tau}_{k-1})e^{-\bar{\omega}(\bar{\beta}-\bar{\tau}_j+\bar{\tau}_{k-1})}, \tag{5 31}$$

where we have defined the factor

$$K_1(\bar{\tau}_j, \bar{\tau}_{j-1}) = \frac{1}{\bar{\omega}}(1 - e^{-\bar{\omega}(\bar{\tau}_j - \bar{\tau}_{j-1})}) \tag{5 32}$$

Equation (5 31) vanishes in the low-temperature limit $e^{-\bar{\omega}\bar{\beta}} \to 0$, due to the fact that $\bar{\omega}(\bar{\beta} - \bar{\tau}_j + \bar{\tau}_{k-1}) < \bar{\omega}\bar{\beta}$ in the upper triangle $(\bar{\tau}' < \bar{\tau})$ In a similar way, on integration of the expression for A'_{per} we find that

$$\underset{(\bar{\tau}<\bar{\tau}')}{A'_{per}} = \underset{(\bar{\tau}>\bar{\tau}')}{A'_{per}} = -\frac{1}{\bar{\omega}^2}\left(1 - e^{-\bar{\omega}\bar{\beta}}\right)\left(e^{\bar{\omega}\bar{\tau}_j} - e^{\bar{\omega}\bar{\tau}_{j-1}}\right)\left(e^{-\bar{\omega}\bar{\tau}_k} - e^{-\bar{\omega}\bar{\tau}_{k-1}}\right) \tag{5 33}$$

$$= K_1(\bar{\tau}_j, \bar{\tau}_{j-1})K_1(\bar{\tau}_k, \bar{\tau}_{k-1})\left(e^{-\bar{\omega}(\bar{\beta}-\bar{\tau}_k+\bar{\tau}_{j-1})} + e^{-\bar{\omega}(\bar{\tau}_{k-1}-\bar{\tau}_j)}\right) \tag{5 34}$$

Thus, the total contribution due to an off-diagonal pair of segments, after a cancellation of terms, is given by

$$A_{jk} = \frac{z\lambda\bar{\omega}}{2\Phi_0(0,0)}K_1(\bar{\tau}_j, \bar{\tau}_{j-1})K_1(\bar{\tau}_k, \bar{\tau}_{k-1})\Big[e^{-\bar{\omega}(\bar{\tau}_{k-1}-\bar{\tau}_j)}\Phi_0(\mathbf{r}(\bar{\tau}_{j-1}), \mathbf{r}(\bar{\tau}_{k-1}))$$
$$+ e^{-\bar{\omega}(\bar{\beta}-\bar{\tau}_k+\bar{\tau}_{j-1})}\Phi_{\Delta\mathbf{r}}(\mathbf{r}(\bar{\tau}_{j-1}), \mathbf{r}(\bar{\tau}_{k-1}))\Big] \tag{5 35}$$

The contribution to the diagonal segments A_{jj} can be found in a similar way to A_{jk} above The result reads

$$A_{jj} = \frac{z\lambda\bar{\omega}}{2\Phi_0(0,0)}\left[K_2(\bar{\tau}_j, \bar{\tau}_{j-1})\Phi_0(\mathbf{r}(\bar{\tau}_{j-1}), \mathbf{r}(\bar{\tau}_{j-1})) + K_3(\bar{\tau}_j, \bar{\tau}_{j-1})\Phi_{\Delta\mathbf{r}}(\mathbf{r}(\bar{\tau}_{j-1}), \mathbf{r}(\bar{\tau}_{j-1}))\right], \tag{5 36}$$

where we have defined the factors

$$K_2(\bar{\tau}_j, \bar{\tau}_{j-1}) = \frac{2}{\bar{\omega}^2}(\bar{\omega}(\bar{\tau}_j - \bar{\tau}_{j-1}) - 1 + e^{-\bar{\omega}(\bar{\tau}_j - \bar{\tau}_{j-1})}), \tag{5 37}$$

and

$$K_3(\bar{\tau}_j, \bar{\tau}_{j-1}) = \frac{2}{\bar{\omega}^2}e^{-\bar{\omega}(\bar{\beta}+\bar{\tau}_{j-1}-\bar{\tau}_j)} \tag{5 38}$$

Thus, the Monte Carlo simulation computes the action by summing the diagonal A_{jj} and the off-diagonal A_{jk} elements, given by equations (5 36) and (5 35) respectively, according to equation (5 26) This is much more efficient than computing the double integral appearing in equations (5 20) and (5 21) numerically

5.6   Look-Up Table for the Interaction Force.

The various models studied in this work differ only in the shape of the electron-phonon interaction force $f_m(n)$ – the force that exists between the electron on site n and the oscillator at site m The interaction force enters the expression for the action, in equations (5 36) and (5 35), only via the four lattice summations, which have the general form

$$\Phi_{\Delta r}(r_1, r_2) = \sum_m \bar{f}_m(r_1) \bar{f}_{m+\Delta r}(r_2) \tag{5 39}$$

In all the models we intend to study in this work, $f_m(n)$ depends only on the *relative* lattice distance $|m - n|$, in which case we can express equation (5 39) as

$$\Phi_{\Delta r}(r_1, r_2) = \sum_m f(m - r_1) f(m + \Delta r - r_2) \tag{5 40}$$

Furthermore, in all the models we study, $f_m(n)$ is either zero, or else tends to zero, at large distance Thus, we can replace the summation variable in equation (5 40) by $m' = m - r_1$, so

$$\Phi(r') = \sum_{m'} f(m') f(m' - r'), \tag{5 41}$$

where we see that the lattice summation is a function of the single variable $r' = r_2 - r_1 - \Delta r$

It makes sense to evaluate the value of $\Phi(r')$ for all possible values of $(r_2 - r_1 - \Delta r)$ in advance of the simulation proper, and store this information in a look-up table The look-up table for a D-dimensional system requires a D-dimensional array, which is then accessed, whenever required, from within the simulation proper This increases the efficiency of the algorithm, particularly when the interaction force involves an exponential function

The fact that $f_m(n)$ enters the formalism only via $\Phi(r')$ is, in itself, a major practical advantage of this method The actual program code used to simulate the various models is exactly the same, apart from the definition of the look-up table Thus, the method handles different models in an entirely "consistent" manner

Including the above definition of $\Phi(r')$, the action, given by equations (5 26), (5 35) and (5 36),

ıs gıven by

$$A = \frac{z\lambda\bar{\omega}}{2\Phi(0)} \left\{ \sum_{\jmath=1}^{N_s+1} [K_2(\bar{\tau}_\jmath, \bar{\tau}_{\jmath-1})\Phi(0) + K_3(\bar{\tau}_\jmath, \bar{\tau}_{\jmath-1})\Phi(-\Delta\mathbf{r})] \right.$$

$$+ 2\sum_{\jmath=1}^{N_s} \sum_{k=\jmath+1}^{N_s+1} K_1(\bar{\tau}_\jmath, \bar{\tau}_{\jmath-1}) K_1(\bar{\tau}_k, \bar{\tau}_{k-1}) \left[e^{-\bar{\omega}(\bar{\tau}_{k-1}-\bar{\tau}_\jmath)} \Phi(\mathbf{r}_{\bar{\tau}_{k-1}} - \mathbf{r}_{\bar{\tau}_{\jmath-1}}) \right.$$

$$\left. \left. + e^{-\bar{\omega}(\bar{\beta}-\bar{\tau}_k+\bar{\tau}_{\jmath-1})} \Phi(\mathbf{r}_{\bar{\tau}_{k-1}} - \mathbf{r}_{\bar{\tau}_{\jmath-1}} - \Delta\mathbf{r}) \right] \right\}, \qquad (5\ 42)$$

where the factors K_1, K_2 and K_3 were defined ıs equatıons (5 32), (5 37) and (5 38) respectıvely Equatıon (5 42), then, together wıth the algorıthm presented ın sectıon (5 3), defines the contınuous ımagınary-tıme path ıntegral QMC scheme used ın thıs work
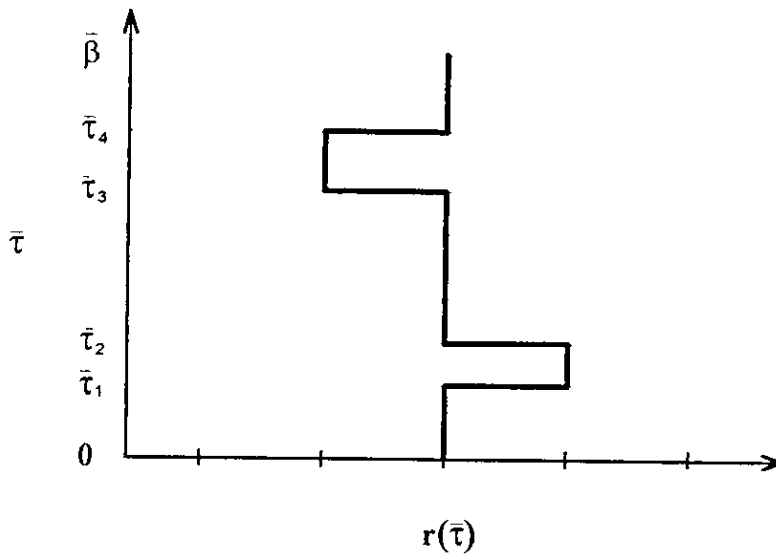
Figure 5 1 A one-dimensional election trajectory represented in continuous imaginary time The points in imaginary time at which the electron jumps to a neighbouring site is called a kink In this example there are four kinks occurring at imaginary times $\bar{\tau}_1$, $\bar{\tau}_2$, $\bar{\tau}_3$ and $\bar{\tau}_4$
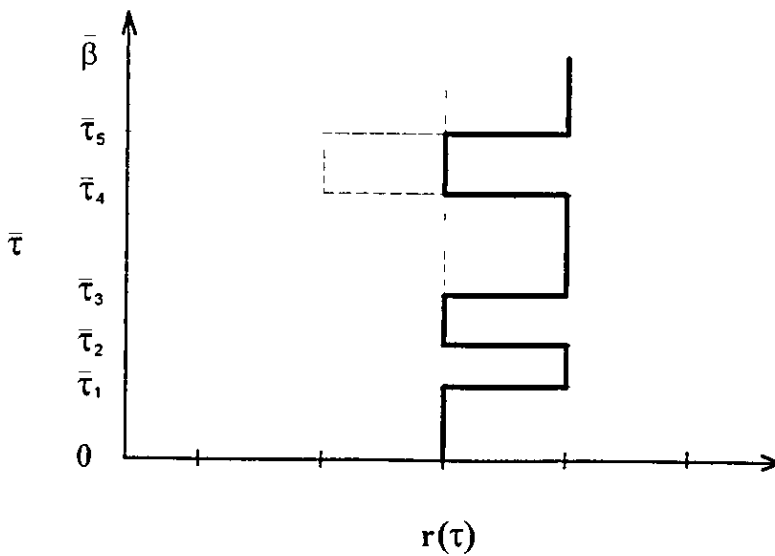
Figure 5 2 The addition of a right kink, at imaginary time $\bar{\tau}_3$, to the trajectory shown in figure (5 1) The entire trajectory from $\bar{\tau}_3$ to $\bar{\beta}$ is shifted in the direction of the kink by one lattice space
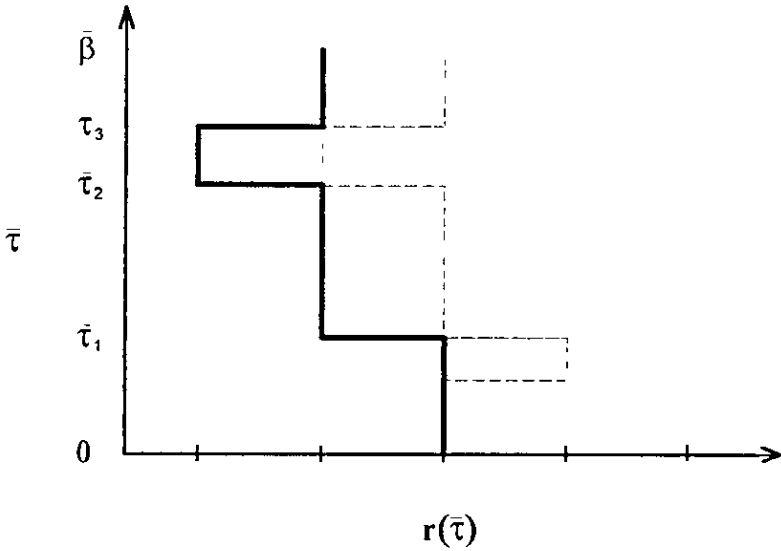
Figure 5 3 The deletion of the kink that was at imaginary time $\bar{\tau}_1$, from the trajectory shown in figure (5 1)   The entire trajectory from where the kink was to $\bar{\beta}$ is shifted in the opposite direction of the kink by one lattice space
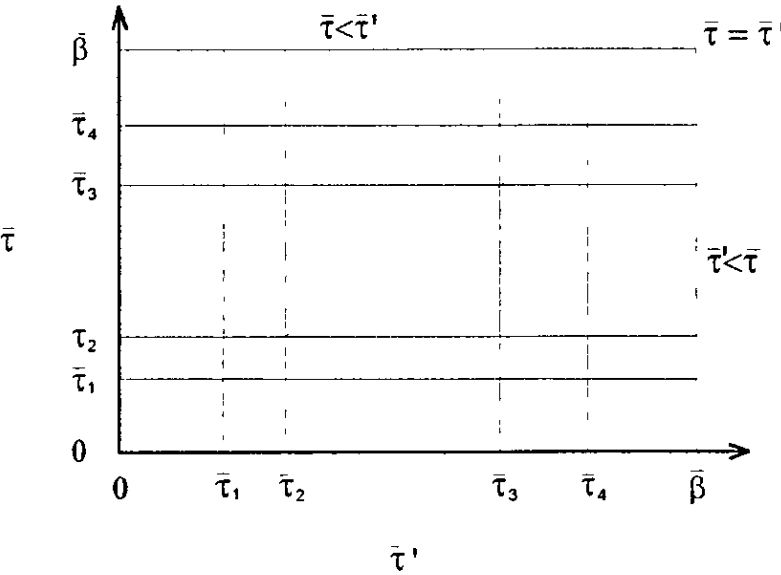
Figure 5 4 Splitting up the area of integration of the action, equation (5 19), into segments Within each segment, both $r(\bar{\tau})$ and $1(\bar{\tau}')$ are constant

Chapter 6

Physical Observables

6.1 Introduction

In the context of our QMC scheme, the expectation value for a physical observable M is the statistical average over trajectories at $\mathbf{P} = 0$, which corresponds to the ground state of the system. This can be written as

$$\langle M \rangle_0 = \frac{\int_{\mathrm{tw}} \mathcal{D}\mathbf{r} \mathcal{D}\xi \; M(\xi_{\mathbf{m}}(\tau), \mathbf{r}(\tau)) w}{\int_{\mathrm{tw}} \mathcal{D}\mathbf{r} \mathcal{D}\xi \; w}, \tag{6 1}$$

with

$$w = \langle \{\xi_{\mathbf{m}+\Delta\mathbf{r}}\}, \mathbf{r} + \Delta\mathbf{r} \mid e^{-\beta H} \mid \{\xi_{\mathbf{m}}\}, \mathbf{r} \rangle, \tag{6 2}$$

where $\int_{\mathrm{tw}} \mathcal{D}\mathbf{r} \mathcal{D}\xi$ denotes integration over all possible trajectories, and values of $\Delta\mathbf{r}$, subject to twisted boundary conditions in imaginary time. Each of the possible trajectories enter the path integral with a statistical weight given by w. As we discussed in section (4 2), the use of twisted boundary conditions in imaginary time introduces an extra factor $e^{i\mathbf{P} \cdot \Delta\mathbf{r}/\hbar}$ in w. In this work, we are restricting ourselves to the case when $\mathbf{P} = 0$, which means that $e^{i\mathbf{P} \cdot \Delta\mathbf{r}/\hbar}$ is always unity, and thus there is no sign problem.

In chapter (4), we analytically integrated out the phonon degrees of freedom, and then in section (5 5) performed an integration over kinks. The resulting expression for the action A, given by equation (5 42), is in a form that can be easily incorporated into the QMC algorithm. In terms of A, the expectation value, equation (6 1), is given by

$$\langle M \rangle_0 = \frac{\int_{\mathrm{tw}} \mathcal{D}\mathbf{r} \; M w_{\mathrm{el}} e^A}{\int_{\mathrm{tw}} \mathcal{D}\mathbf{r} \; w_{\mathrm{el}} e^A}, \tag{6 3}$$

with

$$w = w_{el} \; e^{A},$$

(6 4)

where w_{el} is the electron-induced weight, equation (5 7), and the factor e^{A} is the phonon-induced weight

In this chapter, we consider four physical observables that can be extracted directly from our QMC simulations the ground state energy, the effective mass, the number of phonons, and the isotope exponent on the effective mass The effective mass has previously been studied using path-integral QMC, for the Holstein, Frohlich and Jahn-Teller polaron, by Kornilovitch [30, 31, 45] Both the isotope exponent and the number of phonons -- to the best of our knowledge -- have not previously been measured using path-integral QMC In the following chapters, we will study the above four observables, using several different forms of the electron-phonon interaction force $f_m(m)$

As we shall see, the energy, the number of phonons and the isotope exponent are all related to the partial derivative of A with respect to either β or ω After performing the partial derivatives, the resulting expressions -- with a form similar to that of the action -- can be easily incorporated into the QMC scheme In the final section of this chapter, we will discuss the practical details of the QMC simulations

6.2   Ground State Energy and Effective Mass

In the low-temperature limit $\beta \to \infty$, the lowest eigenstate of the system dominates, and so the partition function, for a particular total momentum $\mathbf{P}$, is given by equation (4 10) On differentiation of equation (4 10) with respect to β, we see that the energy of the lowest eigenstate may be written in the form

$$E_0(\mathbf{P}) = -\frac{1}{Z_{\mathbf{P}}} \frac{\partial Z_{\mathbf{P}}}{\partial \beta}$$

(6 5)

Using the present shorthand, the definition of $Z_{\mathbf{P}}$, equation (4 6), is written as

$$Z_{\mathbf{P}} = \int_{tw} \mathcal{D}\mathbf{r}\mathcal{D}\xi e^{i\mathbf{P} \; \Delta\mathbf{r}/\hbar} w,$$

(6 6)

so that the energy, at $\mathbf{P} = 0$, is given by

$$E_0(0) = -\frac{\int_{tw} \mathcal{D}\mathbf{r}\mathcal{D}\xi \left(\frac{\partial w}{\partial \beta} \frac{1}{w} \right) w}{\int_{tw} \mathcal{D}\mathbf{r}\mathcal{D}\xi w}$$

$$= -\left\langle \frac{1}{w} \frac{\partial w}{\partial \beta} \right\rangle_0,$$

(6 7)

which is the energy of the ground state The explicit form of the energy estimator in equation (6 7) is given by [30]

$$\frac{\partial w}{\partial \beta} \frac{1}{w} = \frac{\partial A}{\partial \beta} + \frac{1}{\beta} \sum_s N_s,$$ (6 8)

which follows the corresponding finite-imaginary-time energy estimator [24] in the limit of continuous imaginary time Here, N_s is the number of kinks of type s Thus, the total ground state energy is given by

$$E_0(0) = -\left\langle \frac{\partial A}{\partial \beta} \right\rangle_0 - \frac{1}{\beta} \left\langle \sum_s N_s \right\rangle_0,$$ (6 9)

where the first term estimates the potential energy, and the second term the kinetic energy of the polaron [24] The potential energy involves the partial derivative with respect to β We will perform this differentiation later in section (6 6)

In section (4 3), we derived an expression for expectation value of the effective mass Using the present shorthand, we may write equation (4 18) as

$$\frac{m_{0,d}}{m_d^*} = \frac{1}{2\beta} \left\langle (\Delta r_d)^2 \right\rangle_0,$$ (6 10)

where $\Delta r_d = r_d(\beta) - r_d(0)$ is measured in units of the lattice constant a Here, m_d^* is the effective mass of the polaron, $m_{0,d}$ is the bare electron mass, and d labels the dimension of the D-dimensional system

6.3   Number of Phonons in the Polaron Cloud

The effective mass of the polaron is larger than the bare electron mass This is due to the associated lattice deformation – or the equivalent "cloud" of virtual phonons – that surrounds the polaron [1] Thus, the number of virtual phonons in the polaron cloud N_{ph} is a quantity of interest The value of N_{ph} is given by the expectation value of the phonon number operator

$$N_{ph} = \left\langle \sum_m d_m^\dagger d_m \right\rangle_0,$$ (6 11)

where the shorthand of the angled brackets is defined in equations (6 1) and (6 3)

In section (1 3), we transformed the terms H_{ph} and H_{el-ph} of the model Hamiltonian, equation (1 1), into second-quantised form In this representation, the model Hamiltonian reads

$$H = -t \sum_{<nn'>} c_n^\dagger c_{n'} - \left(2t\hbar^2\lambda\omega\right)^{1/2} \sum_{nm} f_m(\mathbf{n})c_n^\dagger c_n \left(d_m^\dagger + d_m\right) + \hbar\omega \sum_m d_m^\dagger d_m$$ (6 12)

[1] The electron continually emits and absorbs virtual phonons The term "virtual" refers to the fact that, in order not to violate energy conservation, an emitted phonon may only exist for a time $\sim 2\pi/\omega$ (given by the uncertainty principle), after which it *must* be reabsorbed

Here, we notice that the phonon number operator can be isolated by taking the partial differential of H with respect to $\hbar\omega$, that is

$$\left.\frac{\partial H}{\partial(\hbar\omega)}\right|_{\lambda_\omega} = \sum_{\mathbf{m}} d_{\mathbf{m}}^\dagger d_{\mathbf{m}}, \tag{6 13}$$

Note that the constraint of holding $\lambda\omega$ fixed is absolutely necessary – otherwise the differentiation would yield a non-zero term involving $\sum_{\mathbf{m}} \left(d_{\mathbf{m}}^\dagger + d_{\mathbf{m}}\right)$

We can relate equation (6 13) to the action by considering the derivative of free energy with respect to $\hbar\omega$ (keeping $\lambda\omega$ fixed) Accordingly, the free energy, at $\mathbf{P} = 0$, is defined as

$$\begin{aligned} F_0 &= -\frac{1}{\beta} \ln Z_0 \\ &= -\frac{1}{\beta} \ln \left\{ \int_{\mathrm{tw}} \mathcal{D}\mathbf{r}\mathcal{D}\xi w \right\}, \end{aligned} \tag{6 14}$$

where we have used equation (6 6), and so the derivative is given by

$$\left.\frac{\partial F_0}{\partial(\hbar\omega)}\right|_{\lambda_\omega} = -\frac{1}{\beta} \frac{\int_{\mathrm{tw}} \mathcal{D}\mathbf{r}\mathcal{D}\xi \left.\frac{\partial w}{\partial(\hbar\omega)}\right|_{\lambda_\omega}}{\int_{\mathrm{tw}} \mathcal{D}\mathbf{r}\mathcal{D}\xi w} \tag{6 15}$$

If we evaluate the quantity $\partial w/\partial(\hbar\omega)|_{\lambda_\omega}$ appearing in equation (6 15), using the definition of w as given by equation (6 2), then we get

$$\begin{aligned} \left.\frac{\partial w}{\partial(\hbar\omega)}\right|_{\lambda_\omega} &= -\langle\{\xi_{\mathbf{m}+\Delta\mathbf{r}}\}, \mathbf{r}+\Delta\mathbf{r} \,|\, \beta e^{-\beta H} \left.\frac{\partial H}{\partial(\hbar\omega)}\right|_{\lambda_\omega} |\, \{\xi_{\mathbf{m}}\}, \mathbf{r}\rangle \\ &= -\beta\langle\{\xi_{\mathbf{m}+\Delta\mathbf{r}}\}, \mathbf{r}+\Delta\mathbf{r} \,|\, e^{-\beta H} \sum_{\mathbf{m}} d_{\mathbf{m}}^\dagger d_{\mathbf{m}} \,|\, \{\xi_{\mathbf{m}}\}, \mathbf{r}\rangle, \end{aligned} \tag{6 16}$$

where we have made use of equation (6 13), and so equation (6 15) becomes

$$\left.\frac{\partial F_0}{\partial(\hbar\omega)}\right|_{\lambda_\omega} = \left\langle \sum_{\mathbf{m}} d_{\mathbf{m}}^\dagger d_{\mathbf{m}} \right\rangle_0 = N_{\mathrm{ph}} \tag{6 17}$$

We can also evaluate the quantity $\partial w/\partial(\hbar\omega)|_{\lambda_\omega}$ that appears in equation (6 15), using the definition of w as given in equation (6 4), which gives

$$\left.\frac{\partial w}{\partial(\hbar\omega)}\right|_{\lambda_\omega} = w_{\mathrm{el}}\, e^A \left.\frac{\partial A}{\partial(\hbar\omega)}\right|_{\lambda_\omega}, \tag{6 18}$$

and so

$$\left.\frac{\partial F_0}{\partial(\hbar\omega)}\right|_{\lambda_\omega} = -\frac{1}{\beta} \left\langle \left.\frac{\partial A}{\partial(\hbar\omega)}\right|_{\lambda_\omega} \right\rangle_0 \tag{6 19}$$

On combining equations (6 19) and (6 17), the number of virtual phonons in the polaron cloud can be expressed as

$$\begin{aligned} N_{\mathrm{ph}} &= \left\langle \sum_{\mathbf{m}} d_{\mathbf{m}}^\dagger d_{\mathbf{m}} \right\rangle_0 = -\frac{1}{\beta} \left\langle \left.\frac{\partial A}{\partial(\hbar\omega)}\right|_{\lambda_\omega} \right\rangle_0 \\ &= -\frac{1}{\beta} \left\langle \left.\frac{\partial A}{\partial(\bar\omega)}\right|_{\lambda_{\bar\omega}} \right\rangle_0 \end{aligned} \tag{6 20}$$

Thus, the number of phonons depends on the partial derivative of A with respect to $\bar\omega$, holding the product $\lambda\bar\omega$ constant We will consider this derivative later in section (6 6)

6.4   The Isotope Effect

The *isotope effect* was discovered in 1950, for the metal mercury, by Maxwell [46] and Reynolds *et al* [47] They observed a dependence on the experimentally measured value of the superconducting transition temperature T_c for different isotopes of the same metal – in which the mass of the lattice ions M changes, without any change in the electronic configuration of the ion The dependence was found (empirically) to be

$$T_c \propto \frac{1}{M^\alpha},$$

(6 21)

where α is known as the *isotope exponent on T_c* On differentiation of equation (6 21) with respect to M, we see that

$$\frac{dT_c}{dM} = -c_T \frac{\alpha}{M^{\alpha+1}} = -\left(c_T \frac{1}{M^\alpha}\right) \frac{\alpha}{M} = -\frac{T_c \alpha}{M},$$

(6 22)

where c_T is the constant of proportionality Thus, the isotope exponent on T_c may be written in the form

$$\alpha = -\frac{M}{T_c} \frac{dT_c}{dM} = -\frac{d\ln T_c}{d\ln M}$$

(6 23)

The isotope effect is also observable in other experimentally measured quantities, such as the the critical field [46, 47]

The isotope exponent on T_c, for the classical (low temperature) superconductors, has an experimentally measured value of $\alpha \leq 0\,5$ In some cases, such as lead, α is very close to $0\,5$, which is in excellent agreement with the BCS prediction that $kT_c \approx M^{-1/2}$ [48] However, α can range all the way down to zero, or even have a small negative value The discrepancy from the BCS prediction is due to the effects of Coulomb repulsion and the anharmonicity of phonons The presence of an experimentally measured finite isotope effect demonstrates that phonons are involved in the pairing mechanism in classical superconductors

The isotope effects observed in high-T_c metal oxides are very different from those observed in the conventional BCS superconductors [49, 50, 51] In order to exchange the oxygen ion mass in these materials, samples are subjected to ^{16}O and ^{18}O isotope diffusion The oxygen-isotope exponent on T_c is then measured using

$$\alpha \approx -\frac{\Delta T_c}{T_c} \frac{M}{\Delta M},$$

(6 24)

where ΔT_c and ΔM are the changes in T_c and M upon isotope substitution The isotope effect in these materials is strongly dependent on the the level of hole doping the observed value of α tends to be small in the optimally-doped regime, and increases to larger values as the level of doping is decreased In fact, α can have values greater than $0\,5$ in the deeply underdoped regime The observed isotope effects indicate that phonons are relevant in high-T_c superconductivity

6.5   Isotope exponent on the Effective Mass

Let us define the *isotope exponent on the effective mass* α_{m^*}, in a similar way to that for T_c, as

$$\alpha_{m^*}^{(d)} = \frac{M}{m_d^*} \frac{dm_d^*}{dM} = \frac{d\ln m_d^*}{d\ln M},$$
(6 25)

which, in terms of $m_{0,d}/m_d^*$, takes the form

$$\alpha_{m^*}^{(d)} = -M \frac{m_d^*}{m_{0,d}} \frac{\partial}{\partial M} \left(\frac{m_{0,d}}{m_d^*} \right)$$
(6 26)

(by making use of the quotient rule) Note that the ionic mass enters our formalism via the phonon frequency

$$\omega = \sqrt{\frac{K}{M}},$$
(6 27)

where K is some "spring constant"

In order to relate $\alpha_{m^*}^{(d)}$ to the action, we can substitute the expression we have already derived for $m_{0,d}/m_d^*$, equation (6 10), into equation (6 26) Accordingly, on differentiation of equation (6 10) with respect to M, we see that

$$
\begin{aligned}
\frac{\partial}{\partial M} \left(\frac{m_{0,d}}{m_d^*} \right) &= \frac{1}{2\beta t a^2} \left[\frac{\int_{\text{tw}} \mathcal{D}r \, w_{\text{el}} \, (\Delta r_d)^2 \, \frac{\partial A}{\partial M} e^A}{\int_{\text{tw}} \mathcal{D}r \, w_{\text{el}} e^A} \right. \\
&\qquad\qquad \left. - \frac{\int_{\text{tw}} \mathcal{D}r \, w_{\text{el}} \, (\Delta r_d)^2 \, e^A}{\int_{\text{tw}} \mathcal{D}r \, w_{\text{el}} e^A} \frac{\int_{\text{tw}} \mathcal{D}r \, w_{\text{el}} \frac{\partial A}{\partial M} e^A}{\int_{\text{tw}} \mathcal{D}r \, w_{\text{el}} e^A} \right] \\
&= \frac{1}{2\beta t a^2} \left[\left\langle (\Delta r_d)^2 \frac{\partial A}{\partial M} \right\rangle_0 - \left\langle (\Delta r_d)^2 \right\rangle_0 \left\langle \frac{\partial A}{\partial M} \right\rangle_0 \right] \\
&= -\frac{\omega}{4M\beta t a^2} \left[\left\langle (\Delta r_d)^2 \frac{\partial A}{\partial \omega} \right\rangle_0 - \left\langle (\Delta r_d)^2 \right\rangle_0 \left\langle \frac{\partial A}{\partial \omega} \right\rangle_0 \right],
\end{aligned}
$$
(6 28)

where we have used equation (6 27) to form the identity

$$\frac{\partial A}{\partial M} = \frac{\partial A}{\partial \omega} \frac{\partial \omega}{\partial M} = -\frac{\partial A}{\partial \omega} \frac{\sqrt{K}}{2M\sqrt{M}} = -\frac{\omega}{2M} \frac{\partial A}{\partial \omega}$$
(6 29)

On substitution of equation (6 28) into equation (6 26), the isotope exponent on the effective mass is given by

$$
\begin{aligned}
\alpha_{m^*}^{(d)} &= \frac{\omega}{2} \frac{1}{\left\langle (\Delta r_d)^2 \right\rangle_0} \left[\left\langle (\Delta r_d)^2 \frac{\partial A}{\partial \omega} \right\rangle_0 - \left\langle (\Delta r_d)^2 \right\rangle_0 \left\langle \frac{\partial A}{\partial \omega} \right\rangle_0 \right] \\
&= \frac{\bar{\omega}}{2} \frac{1}{\left\langle (\Delta r_d)^2 \right\rangle_0} \left[\left\langle (\Delta r_d)^2 \frac{\partial A}{\partial \bar{\omega}} \right\rangle_0 - \left\langle (\Delta r_d)^2 \right\rangle_0 \left\langle \frac{\partial A}{\partial \bar{\omega}} \right\rangle_0 \right]
\end{aligned}
$$
(6 30)

Thus, the isotope exponent depends on the partial derivative of A with respect to $\bar{\omega}$ The differentiation must be performed holding the other parameters involved in the model Hamiltonian, equation (6 12), constant, namely λ, $\bar{t}$ and $\bar{\beta}$ This derivative will be evaluated in the following section

Recently, Zhao *et al* made (indirect) measurements of the isotope exponent on the effective mass, for the copper oxide superconducting material $La_{2-x}Sr_xCuO_4$, at different doping levels [14, 52] Here, the isotope dependence of m_{ab}^* (effective supercarrier mass along the CuO_2 planes) is estimated by independently measuring the isotope dependence of the magnetic penetration depth $\Lambda(0)$ and the supercarrier density n_s Since $\Lambda(0) \propto (m_{ab}^*/n_s)^{1/2}$, the isotopic shift in the effective mass may be inferred using

$$\frac{\Delta m_{ab}^*}{m_{ab}^*} \approx 2\frac{\Delta\Lambda(0)}{\Lambda(0)} + \frac{\Delta n_s}{n_s}, \tag{6 31}$$

where Δ denotes the shift in the quantity upon isotope substitution The value of the isotope exponent was found to be very large, $\alpha_{m^*}^{(ab)} = 1\ 9(2)$, in the deeply underdoped regime ($x = 0\ 06$), and much smaller, $\alpha_{m^*}^{(ab)} = 0\ 46(5)$, for optimal doping ($x = 0\ 15$)

6.6 Partial Differentiation of the Action

We have derived expressions for the ground state energy, the number of phonons and the isotope exponent – each involves a partial derivative of the action A with respect to either $\bar{\beta}$ or $\bar{\omega}$ In this section we present the details of the partial differentiation of A, in a brief way In each case, we will formulate the result in terms of the factors $K_1(\bar{\tau}_j, \bar{\tau}_{j-1})$, $K_2(\bar{\tau}_j, \bar{\tau}_{j-1})$ and $K_3(\bar{\tau}_j, \bar{\tau}_{j-1})$, which are defined in equations (5 31), (5 37) and (5 38), respectively As explained in section (5 5), the use of these factors increases the efficiency of the Monte Carlo algorithm by reducing the overall number of exponentials that need to be evaluated during the Monte Carlo simulations

It is convenient to write the action, equation (4 47), in the form

$$A = \frac{\lambda z}{\Phi_0(0,0)} \left\{ \sum_{j=1}^{N_s+1} \left[A_0(\bar{\tau}_j, \bar{\tau}_{j-1})\Phi_0(\mathbf{r}(\bar{\tau}_{j-1}), \mathbf{r}(\bar{\tau}_{j-1})) + A_1(\bar{\tau}_j, \bar{\tau}_{j-1})\Phi_{\Delta\mathbf{r}}(\mathbf{r}(\bar{\tau}_{j-1}), \mathbf{r}(\bar{\tau}_{j-1})) \right] \right.$$

$$+ \sum_{j=1}^{N_s+1} \sum_{k=j+1}^{N_s+1} \left[A_2(\bar{\tau}_j, \bar{\tau}_{j-1}, \bar{\tau}_k, \bar{\tau}_{k-1})\Phi_0(\mathbf{r}(\bar{\tau}_{j-1}), \mathbf{r}(\bar{\tau}_{k-1})) \right.$$

$$\left. \left. + A_3(\bar{\tau}_j, \bar{\tau}_{j-1}, \bar{\tau}_k, \bar{\tau}_{k-1})\Phi_{\Delta\mathbf{r}}(\mathbf{r}(\bar{\tau}_{j-1}), \mathbf{r}(\bar{\tau}_{k-1})) \right] \right\}, \tag{6 32}$$

where $\Phi_{\Delta\mathbf{r}}(\mathbf{r}_1, \mathbf{r}_2)$ is defined by equation (5 39), and

$$A_0(\bar{\tau}_j, \bar{\tau}_{j-1}) = \frac{1}{\bar{\omega}}\left[\bar{\omega}(\bar{\tau}_j - \bar{\tau}_{j-1}) - 1 + e^{-\bar{\omega}(\bar{\tau}_j - \bar{\tau}_{j-1})}\right], \tag{6 33}$$

$$A_1(\bar{\tau}_j, \bar{\tau}_{j-1}) = \frac{1}{\bar{\omega}}e^{-\bar{\omega}(\bar{\beta}+\bar{\tau}_{j-1}-\bar{\tau}_j)}, \tag{6 34}$$

$$A_2(\bar{\tau}_j, \bar{\tau}_{j-1}, \bar{\tau}_k, \bar{\tau}_{k-1}) = \frac{1}{\bar{\omega}}(1 - e^{-\bar{\omega}(\bar{\tau}_j - \bar{\tau}_{j-1})})(1 - e^{-\bar{\omega}(\bar{\tau}_k - \bar{\tau}_{k-1})})e^{-\bar{\omega}(\bar{\tau}_{k-1} - \bar{\tau}_j)} \tag{6 35}$$

$$= \frac{1}{\bar{\omega}}\left[e^{-\bar{\omega}(\bar{\tau}_{k-1} - \bar{\tau}_j)} - e^{-\bar{\omega}(\bar{\tau}_k - \bar{\tau}_j)} - e^{-\bar{\omega}(\bar{\tau}_{k-1} - \bar{\tau}_{j-1})} + e^{-\bar{\omega}(\bar{\tau}_k - \bar{\tau}_{j-1})}\right],$$

and

$$A_3(\bar{\tau}_j, \bar{\tau}_{j-1}, \bar{\tau}_k, \bar{\tau}_{k-1}) = \frac{1}{\bar{\omega}}(1 - e^{-\bar{\omega}(\bar{\tau}_j - \bar{\tau}_{j-1})})(1 - e^{-\bar{\omega}(\bar{\tau}_k - \bar{\tau}_{k-1})})e^{-\bar{\omega}(\bar{\beta} - \bar{\tau}_k + \bar{\tau}_{j-1})} \qquad (6\ 36)$$

$$= \frac{1}{\bar{\omega}}\left[e^{-\bar{\omega}(\bar{\beta} - \bar{\tau}_k + \bar{\tau}_{j-1})} - e^{-\bar{\omega}(\bar{\beta} + \bar{\tau}_{j-1} - \bar{\tau}_{k-1})} - e^{-\bar{\omega}(\bar{\beta} - \bar{\tau}_k + \bar{\tau}_j)} + e^{-\bar{\omega}(\bar{\beta} + \bar{\tau}_j - \bar{\tau}_{k-1})} \right]$$

Let us first consider the expectation value for the isotope exponent $\alpha_{m^*}^{(d)}$, which is given by equation (6 30) We wish to perform the partial differentiation of A, equation (4 47), with respect to $\bar{\omega}$, holding the other model parameters, λ, $\bar{t}$ and $\bar{\beta}$, constant The result is

$$\left.\frac{\partial A}{\partial \bar{\omega}}\right|_\lambda = \frac{\lambda z}{\Phi_0(0,0)}\left\{ \sum_{j=1}^{N_s+1}\left[\left.\frac{\partial A_0}{\partial \bar{\omega}}\right|_\lambda \Phi_0(\mathbf{r}(\bar{\tau}_{j-1}), \mathbf{r}(\bar{\tau}_{j-1})) + \left.\frac{\partial A_1}{\partial \bar{\omega}}\right|_\lambda \Phi_{\Delta \mathbf{r}}(\mathbf{r}(\bar{\tau}_{j-1}), \mathbf{r}(\bar{\tau}_{j-1})) \right] \right.$$

$$\left. + \sum_{j=1}^{N_s+1}\sum_{k=j+1}^{N_s+1}\left[\left.\frac{\partial A_2}{\partial \bar{\omega}}\right|_\lambda \Phi_0(\mathbf{r}(\bar{\tau}_{j-1}), \mathbf{r}(\bar{\tau}_{k-1})) + \left.\frac{\partial A_3}{\partial \bar{\omega}}\right|_\lambda \Phi_{\Delta \mathbf{r}}(\mathbf{r}(\bar{\tau}_{j-1}), \mathbf{r}(\bar{\tau}_{k-1})) \right] \right\}, \quad (6\ 37)$$

where

$$\left.\frac{\partial A_0}{\partial \bar{\omega}}\right|_\lambda = \frac{1}{\bar{\omega}^2} - \left[\frac{1}{\bar{\omega}^2} + \frac{1}{\bar{\omega}}(\bar{\tau}_j - \bar{\tau}_{j-1})\right] e^{-\bar{\omega}(\bar{\tau}_j - \bar{\tau}_{j-1})} \qquad (6\ 38)$$

$$= K_3(\bar{\tau}_j, \bar{\tau}_{j-1})(\frac{1}{\bar{\omega}} + \bar{\tau}_j - \bar{\tau}_{j-1}) - (\bar{\tau}_j - \bar{\tau}_{j-1}),$$

$$\left.\frac{\partial A_1}{\partial \bar{\omega}}\right|_\lambda = -\left[\frac{1}{\bar{\omega}^2} + \frac{1}{\bar{\omega}}(\bar{\beta} + \bar{\tau}_{j-1} - \bar{\tau}_j)\right] e^{-\bar{\omega}(\bar{\beta} + \bar{\tau}_{j-1} - \bar{\tau}_j)} \qquad (6\ 39)$$

$$= -\frac{1}{2}\left[1 + \bar{\omega}(\bar{\beta} + \bar{\tau}_{j-1} - \bar{\tau}_j)\right] K_2(\bar{\tau}_j, \bar{\tau}_{j-1}),$$

$$\left.\frac{\partial A_2}{\partial \bar{\omega}}\right|_\lambda = -\left[\frac{1}{\bar{\omega}^2} + \frac{1}{\bar{\omega}}(\bar{\tau}_{k-1} - \bar{\tau}_j)\right] e^{-\bar{\omega}(\bar{\tau}_{k-1} - \bar{\tau}_j)} + \left[\frac{1}{\bar{\omega}^2} + \frac{1}{\bar{\omega}}(\bar{\tau}_k - \bar{\tau}_j)\right] e^{-\bar{\omega}(\bar{\tau}_k - \bar{\tau}_j)}$$

$$+ \left[\frac{1}{\bar{\omega}^2} + \frac{1}{\bar{\omega}}(\bar{\tau}_{k-1} - \bar{\tau}_{j-1})\right] e^{-\bar{\omega}(\bar{\tau}_{k-1} - \bar{\tau}_{j-1})} - \left[\frac{1}{\bar{\omega}^2} + \frac{1}{\bar{\omega}}(\bar{\tau}_k - \bar{\tau}_{j-1})\right] e^{-\bar{\omega}(\bar{\tau}_k - \bar{\tau}_{j-1})}$$

$$= \left[\bar{\tau}_k e^{-\bar{\omega}(\bar{\tau}_k - \bar{\tau}_j)} - \bar{\tau}_{k-1} e^{-\bar{\omega}(\bar{\tau}_{k-1} - \bar{\tau}_j)}\right] K_3(\bar{\tau}_j, \bar{\tau}_{j-1})$$

$$+ \left\{[\bar{\tau}_j - K_3(\bar{\tau}_j, \bar{\tau}_{j-1})] e^{-\bar{\omega}(\bar{\tau}_{k-1} - \bar{\tau}_j)} - \bar{\tau}_{j-1} e^{-\bar{\omega}(\bar{\tau}_{k-1} - \bar{\tau}_{j-1})}\right\} K_3(\bar{\tau}_k, \bar{\tau}_{k-1}), \qquad (6\ 40)$$

and similarly

$$\left.\frac{\partial A_3}{\partial \bar{\omega}}\right|_\lambda = \left\{\bar{\tau}_k e^{-\bar{\omega}(\bar{\beta} + \bar{\tau}_{j-1} - \bar{\tau}_k)} - \bar{\tau}_{k-1} e^{-\bar{\omega}(\bar{\beta} + \bar{\tau}_{j-1} - \bar{\tau}_{k-1})}\right\} K_3(\bar{\tau}_j, \bar{\tau}_{j-1}) \qquad (6\ 41)$$

$$+ \left\{\bar{\tau}_j e^{-\bar{\omega}(\bar{\beta} - \bar{\tau}_k + \bar{\tau}_j)} - [\bar{\tau}_{j-1} + (\bar{\omega}\bar{\beta} + 1)K_3(\bar{\tau}_j, \bar{\tau}_{j-1})] e^{-\bar{\omega}(\bar{\beta} - \bar{\tau}_k + \bar{\tau}_{j-1})}\right\} K_3(\bar{\tau}_k, \bar{\tau}_{k-1})$$

On substitution of equation (6 37) into equation (6 30), the resulting expression for $\alpha_{m^*}^{(d)}$ depends only on Δr_d and the imaginary times of the kinks (as well as $\bar{\beta}$ and $\bar{\omega}$) Thus, this expression can be implemented into the QMC algorithm

The expression derived for the number of phonons, equation (6 20), requires the differential of the action with respect to $\bar{\omega}$, keeping the product $\lambda\bar{\omega}$ (as well as $\bar{t}$ and $\bar{\beta}$) constant After

differentiation, the result is

$$\frac{\partial A}{\partial \bar{\omega}}\bigg|_{\lambda \bar{\omega}} = \frac{\lambda z}{\Phi_0(0,0)} \Bigg\{ \sum_{j=1}^{N_s+1} \Bigg[\frac{\partial A_0}{\partial \bar{\omega}}\bigg|_{\lambda \bar{\omega}} \Phi_0(\mathbf{r}(\bar{\tau}_{j-1}), \mathbf{r}(\bar{\tau}_{j-1})) + \frac{\partial A_1}{\partial \bar{\omega}}\bigg|_{\lambda \bar{\omega}} \Phi_{\Delta \mathbf{r}}(\mathbf{r}(\bar{\tau}_{j-1}), \mathbf{r}(\bar{\tau}_{j-1})) \Bigg]$$

$$+ \sum_{j=1}^{N_s+1} \sum_{k=j+1}^{N_s+1} \Bigg[\frac{\partial A_2}{\partial \bar{\omega}}\bigg|_{\lambda \bar{\omega}} \Phi_0(\mathbf{r}(\bar{\tau}_{j-1}), \mathbf{r}(\bar{\tau}_{k-1})) + \frac{\partial A_3}{\partial \bar{\omega}}\bigg|_{\lambda \bar{\omega}} \Phi_{\Delta \mathbf{r}}(\mathbf{r}(\bar{\tau}_{j-1}), \mathbf{r}(\bar{\tau}_{k-1})) \Bigg] \Bigg\}, \quad (6\ 42)$$

where

$$\frac{\partial A_0}{\partial \bar{\omega}}\bigg|_{\lambda \bar{\omega}} = \left(\frac{2}{\bar{\omega}} + \bar{\tau}_j - \bar{\tau}_{j-1} \right) K_3(\bar{\tau}_j, \bar{\tau}_{j-1}) - \frac{2(\bar{\tau}_j - \bar{\tau}_{j-1})}{\bar{\omega}}, \quad (6\ 43)$$

$$\frac{\partial A_1}{\partial \bar{\omega}}\bigg|_{\lambda \bar{\omega}} = - \left[1 + \frac{\bar{\omega}}{2} \left(\bar{\beta} - \bar{\tau}_j - \bar{\tau}_{j-1} \right) \right] K_2(\bar{\tau}_j, \bar{\tau}_{j-1}), \quad (6\ 44)$$

$$\frac{\partial A_2}{\partial \bar{\omega}}\bigg|_{\lambda \bar{\omega}} = \left[\bar{\tau}_k e^{-\bar{\omega}(\bar{\tau}_k - \bar{\tau}_j)} - \bar{\tau}_{k-1} e^{-\bar{\omega}(\bar{\tau}_{k-1} - \bar{\tau}_j)} \right] K_3(\bar{\tau}_j, \bar{\tau}_{j-1})$$

$$+ \left\{ [\bar{\tau}_j - 2 K_3(\bar{\tau}_j, \bar{\tau}_{j-1})] e^{-\bar{\omega}(\bar{\tau}_{k-1} - \bar{\tau}_j)} - \bar{\tau}_{j-1} e^{-\bar{\omega}(\bar{\tau}_{k-1} - \bar{\tau}_{j-1})} \right\} K_3(\bar{\tau}_k, \bar{\tau}_{k-1}), \quad (6\ 45)$$

and

$$\frac{\partial A_3}{\partial \bar{\omega}}\bigg|_{\lambda \bar{\omega}} = \left[\bar{\tau}_k e^{-\bar{\omega}(\bar{\beta} + \bar{\tau}_{j-1} - \bar{\tau}_k)} - \bar{\tau}_{k-1} e^{-\bar{\omega}(\bar{\beta} + \bar{\tau}_{j-1} - \bar{\tau}_{k-1})} \right] K_3(\bar{\tau}_j, \bar{\tau}_{j-1})$$

$$+ \left\{ \bar{\tau}_j e^{-\bar{\omega}(\bar{\beta} + \bar{\tau}_j - \bar{\tau}_k)} - \left[\bar{\tau}_{j-1} + (\bar{\omega}\bar{\beta} + 2) K_3(\bar{\tau}_j, \bar{\tau}_{j-1}) \right] e^{-\bar{\omega}(\bar{\beta} + \bar{\tau}_{j-1} - \bar{\tau}_k)} \right\} K_3(\bar{\tau}_k, \bar{\tau}_{k-1}) \quad (6\ 46)$$

Finally, the potential energy, equation (6 9), is the partial derivative of A with respect to β, holding λ, $\bar{\omega}$ and $\bar{t}$ constant The result is given by

$$\frac{\partial A}{\partial \beta} = \frac{\lambda z \bar{\omega}}{2 \Phi_0(0,0)} \Bigg\{ 2 K_3(\beta, \bar{\tau}_{N_s}) \Phi_0(\mathbf{r}(\bar{\tau}_{N_s}), \mathbf{r}(\bar{\tau}_{N_s})) + \bar{\omega} \sum_{j=1}^{N_s} K_2(\bar{\tau}_j, \bar{\tau}_{j-1}) \Phi_{\Delta \mathbf{r}}(\mathbf{r}(\bar{\tau}_{j-1}), \mathbf{r}(\bar{\tau}_{j-1}))$$

$$- 2 \sum_{j=1}^{N_s} K_3(\bar{\tau}_j, \bar{\tau}_{j-1}) \left[e^{-\bar{\omega}(\bar{\beta} - \bar{\tau}_j)} \Phi_0(\mathbf{r}(\bar{\tau}_{j-1}), \mathbf{r}(\bar{\tau}_{N_s})) - e^{-\bar{\omega}(\bar{\beta} - \bar{\tau}_{N_s} + \bar{\tau}_{j-1})} \Phi_{\Delta \mathbf{r}}(\mathbf{r}(\bar{\tau}_{j-1}), \mathbf{r}(\bar{\tau}_{N_s})) \right]$$

$$+ 2 \bar{\omega} \sum_{j=1}^{N_s-1} \sum_{k=j+1}^{N_s} K_3(\bar{\tau}_j, \bar{\tau}_{j-1}) K_3(\bar{\tau}_k, \bar{\tau}_{k-1}) e^{-\bar{\omega}(\bar{\beta} - \bar{\tau}_k + \bar{\tau}_{j-1})} \Phi_{\Delta \mathbf{r}}(\mathbf{r}(\bar{\tau}_{j-1}), \mathbf{r}(\bar{\tau}_{k-1})) \Bigg\}, \quad (6\ 47)$$

where we have considered the end-point segments, involving the imaginary-time range $[\tau_{\bar{N}_s}, \bar{\beta}]$, separately from the internal segments

6.7   Simulation Details

The continuous imaginary time path integral QMC algorithm, presented in chapter (5 1), was programmed using the C++ programming language, and simulations were performed, to double precision, on Hewlett Packard C360 workstations The portable random number generator used

was based on three congruential generators, which for practical purposes is considered to have an infinite period and no sequential correlations [53]

A linked list was used in order to hold the information about the kinks. Each element of this list consisted of six fields: the imaginary time of the kink, the site index (of the start of the kink), the type of kink (left or right), and the three factors $K_1(\bar{\tau}_j, \bar{\tau}_{j-1})$, $K_2(\bar{\tau}_j, \bar{\tau}_{j-1})$ and $K_3(\bar{\tau}_j, \bar{\tau}_{j-1})$, given by equations (5 31), (5 37) and (5 38), respectively. The use of these factors significantly increased the efficiency of the algorithm. In addition to the "local" information held in this list, the program also kept track of two "global" quantities: the number of kinks (of each kind), and the value of $\Delta \mathbf{r} = \mathbf{r}(\beta) - \mathbf{r}(0)$

In this work we study various one-dimensional models, which differ only in the form of the electron-phonon interaction force $f_m(\mathbf{n})$. We only consider the case of $\mathbf{P} = 0$, corresponding to the ground state of the system, where there is no sign problem

For each model, simulations were conducted for various different values of the dimensionless parameters $\bar{\omega}$ and λ. The value of the (dimensionless) inverse temperature $\bar{\beta}$ was chosen such that the low temperature limit $\exp(\bar{\omega}\bar{\beta}) \to \infty$ was sufficiently satisfied. The larger the value of β, the greater the number of kinks, and thus the "slower" the simulation. In practice, values in the range $15 \le \bar{\beta} \le 25$ were found to be sufficient. The upper limit of $\bar{\beta} = 25$ was required for large values of λ, equation (5 14), or small values of $\bar{\omega}$

The physical observables measured were the ground-state energy (both potential and kinetic), the effective mass, the number of phonons and the isotope exponent. The expectation values for these quantities are given by equations (6 9), (6 10), (6 20) and (6 30) respectively. The various partial derivatives of A, appearing in these expressions, are given in section (6 6). The expectation values are a statistical average over the trajectories – corresponding to a simple arithmetic average from within the QMC simulation. Measurements are taken whether or not the Monte Carlo step is accepted, and included in the average according to the Monte Carlo weight. The interaction force $f_m(\mathbf{n})$ was included in the program via the look-up table described in section (5 6)

A typical QMC simulation consisted of a series of between 1,000,000 and 6,000,000 measurements. The measurements were only taken every 10 to 50 Monte Carlo steps, in order to reduce the statistical correlation between successive measurements. For each set of model parameters $(f_m(\mathbf{n}), \bar{\omega}$ and $\lambda)$, between 3 and 6 separate (and therefore statistically independent) Monte Carlo simulations were performed – each using a different value of $\bar{\beta}$

The results of each set of QMC simulations were viewed graphically together, in order to estimate the point at which equilibrium had been reached A typical example is shown in figure (6 1) Only those statistics gathered in equilibrium were included in the averages Viewing the results graphically in this way also allowed us to check for the presence of a finite-temperature error, which would indicate that the condition $\exp(\bar{\omega}\bar{\beta}) \to \infty$ was not sufficiently satisfied In most cases, the Monte Carlo averages were determined to a statistical error of less than one percent
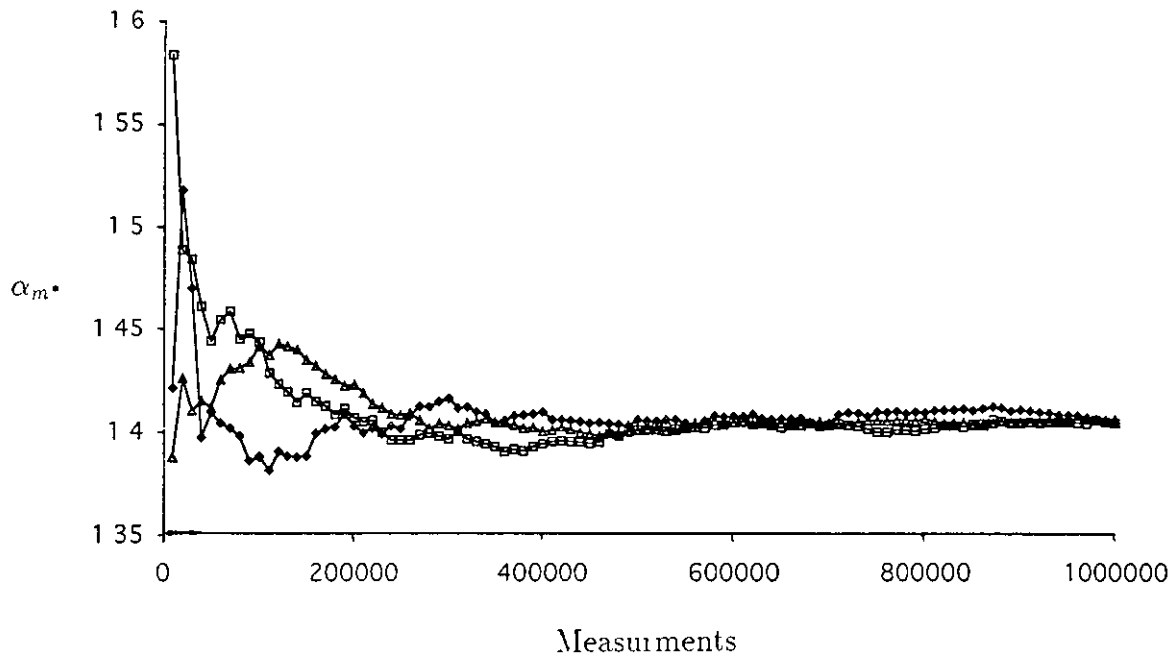
Figure 6 1   A typical example of the simulation output   In this case, the isotope exponent for the Holstein model is measured at $\beta = 15,20$ and 25 at $\omega = 1$ and $\lambda = 2$ and equilibrium was estimated to have been reached after 200,000 measurements

Chapter 7

The Weak-Coupling Limit (Large Polaron)

7.1 Introduction

In 1950 Frohlich considered the ground state of a polaron in the weak-coupling limit $\lambda \ll 1$, using second-order perturbation theory, under the condition that there is never more than one phonon virtually excited [3] The treatment relies on the fact that, in this limit, the (band-electron like) polaron state is much larger than the lattice constant, and thus the discreteness of the lattice is unimportant That is, the free electron term of the Hamiltonian, equation (1 2), may be written as

$$H_{\text{el}} = \frac{\mathbf{k}^2}{2m_0},\tag{7 1}$$

where m_0 is the bare electron mass Note that throughout this chapter, $\mathbf{k}$ represents the momentum (rather than the wavenumber) of the electron

In this chapter, we apply the same treatment to our model Hamiltonian, and determine the energy, effective mass, number of phonons and isotope exponent, in the limit of weak coupling We will use these weak-coupling results in order to check the correctness of our QMC simulations at weak coupling

We start by transforming our model Hamiltonian into momentum representation Standard perturbation theory is then used to determine the ground state energy, in section (7 3), and the number of phonons, in section (7 4) In section (7 5), the effective mass and the isotope exponent

are found by using the perturbation result for the energy

The resulting expressions for the observables involve a summation that we perform numerically, for a given interaction force at a given value of $\bar{\omega}$ The details of this numerical calculation, and the graphical interpretation of the calculated values, is discussed in section (7 6)

7.2   Momentum Representation

In order to apply perturbation theory, it is necessary to transform the electron-phonon term H_{e-ph}, equation (1 12), and the phonon term H_{ph}, equation (1 15), appearing in our model hamiltonian, into momentum representation   In order to do so, we will make use the Fourier transform

$$d^\dagger_{\mathbf{m}} = \frac{1}{\sqrt{N}} \sum_{\mathbf{q}} d^\dagger_{\mathbf{q}} e^{-i\mathbf{q}\,\mathbf{m}/\hbar} \quad , \quad d_{\mathbf{m}} = \frac{1}{\sqrt{N}} \sum_{\mathbf{q}} d_{\mathbf{q}} e^{i\mathbf{q}\,\mathbf{m}/\hbar}, \tag{7 2}$$

where $\mathbf{q}$ represents momentum, and the mathematical identity

$$\frac{1}{N} \sum_{\mathbf{m}} e^{-i\mathbf{m}\,(\mathbf{q}-\mathbf{q}')/\hbar} = \delta_{\mathbf{q},\mathbf{q}'}, \tag{7 3}$$

where $d^\dagger_{\mathbf{q}}$ is the creation, and $d_{\mathbf{q}}$ the destruction operator for a phonon of momentum $\mathbf{q}$

For the present purposes, it is convenient to write the electron-phonon part of the model Hamiltonian, equation (1 12), in the form

$$H_{e-ph} = -\kappa'\hbar\omega \sum_{\mathbf{nm}} \bar{f}_{\mathbf{m}}(\mathbf{n}) c^\dagger_{\mathbf{n}} c_{\mathbf{n}} d^\dagger_{\mathbf{m}} + \text{h c}, \tag{7 4}$$

where $\bar{f}_{\mathbf{m}}(\mathbf{n})$ is the dimensionless *shape* of the interaction, with $\kappa' = (2M\hbar\omega^3)^{-1/2}\kappa$ taking on the dimensionality of force   On application of equation (7 2), then, the electron-phonon term transforms as

$$H_{e-ph} = -\kappa'\hbar\omega \sum_{\mathbf{m},\mathbf{n},\mathbf{k}',\mathbf{k},\mathbf{q}} \bar{f}_{\mathbf{m}}(\mathbf{n}) \, c^\dagger_{\mathbf{k}'} e^{-i\mathbf{k}'\,\mathbf{n}/\hbar} \, c_{\mathbf{k}} e^{i\mathbf{k}\,\mathbf{n}/\hbar} \, d^\dagger_{\mathbf{q}} e^{-i\mathbf{q}\,\mathbf{m}/\hbar} + \text{h c} \tag{7 5}$$

We can properly deal with $\bar{f}_{\mathbf{m}}(\mathbf{n})$ in equation (7 5) by making a shift in the summation variables $\mathbf{m}$ and $\mathbf{n}$ This is possible due to the fact that $\bar{f}_{\mathbf{m}}(\mathbf{n})$ depends on the relative lattice distance $|\mathbf{m} - \mathbf{n}|$, for all the interaction models studied in this work   If we define the new summation variables as $\mathbf{r} = \mathbf{m} - \mathbf{n}$ and $\mathbf{s} = \mathbf{m} + \mathbf{n}$, then the electron-phonon force $\bar{f}_{\mathbf{m}}(\mathbf{n}) = \bar{f}(\mathbf{m} - \mathbf{n}) = \bar{f}_{\mathbf{r}}(0)$ is a function of a single variable only, and equation (7 5) becomes

$$H_{e-ph} = -\kappa'\hbar\omega \frac{1}{N} \sum_{\mathbf{r},\mathbf{s},\mathbf{k}',\mathbf{k},\mathbf{q}} \bar{f}_{\mathbf{r}}(0) c^\dagger_{\mathbf{k}'} c_{\mathbf{k}} d^\dagger_{\mathbf{q}} e^{i(\mathbf{k}-\mathbf{k}')\,(\mathbf{s}-\mathbf{r})/(2\hbar)} e^{-i\mathbf{q}\,(\mathbf{r}+\mathbf{s})/(2\hbar)} + \text{h c}$$

$$= -\kappa'\hbar\omega\frac{1}{N}\sum_{\mathbf{r},\mathbf{s},\mathbf{k}',\mathbf{k},\mathbf{q}}\bar{f}_{\mathbf{r}}(0)c_{\mathbf{k}'}^{\dagger}c_{\mathbf{k}}d_{\mathbf{q}}^{\dagger}e^{\imath(\mathbf{k}-\mathbf{k}'-\mathbf{q})\,\mathbf{s}/(2\hbar)}e^{\imath(\mathbf{k}'-\mathbf{k}-\mathbf{q})\,\mathbf{r}/(2\hbar)} + \text{h c}$$

$$= -\kappa'\hbar\omega\sum_{\mathbf{r},\mathbf{k}',\mathbf{k},\mathbf{q}}\bar{f}_{\mathbf{r}}(0)c_{\mathbf{k}'}^{\dagger}c_{\mathbf{k}}d_{\mathbf{q}}^{\dagger}\delta_{\mathbf{k}',\mathbf{k}-\mathbf{q}}e^{-\imath\mathbf{q}\,\mathbf{r}/\hbar} + \text{h c}$$

$$= -\kappa'\hbar\omega\sum_{\mathbf{k},\mathbf{q}}\tilde{f}_{\mathbf{q}}c_{\mathbf{k}-\mathbf{q}}^{\dagger}c_{\mathbf{k}}d_{\mathbf{q}}^{\dagger} + \text{h c} , \tag{7 6}$$

where we have defined

$$\tilde{f}_{\mathbf{q}} = \sum_{\mathbf{r}}\bar{f}_{\mathbf{r}}(0)e^{-\imath\mathbf{q}\,\mathbf{r}/\hbar} \tag{7 7}$$

The phonon term of the model hamiltonian, given by equation (1 15), transforms as

$$H_{\text{ph}} = \hbar\omega\sum_{\mathbf{q}}d_{\mathbf{q}}^{\dagger}d_{\mathbf{q}} \tag{7 8}$$

Using equations (7 1), (7 6) and (7 8), the model Hamiltonian in the weak-coupling limit can be written in the form

$$H = H_0 + H', \tag{7 9}$$

where

$$H_0 = \frac{\mathbf{k}^2}{2m_0} + \hbar\omega\sum_{\mathbf{q}}d_{\mathbf{q}}^{\dagger}d_{\mathbf{q}}, \tag{7 10}$$

and

$$H' = -\kappa'\hbar\omega\sum_{\mathbf{q},\mathbf{k}}\tilde{f}_{\mathbf{q}}\left(c_{\mathbf{k}-\mathbf{q}}^{\dagger}c_{\mathbf{k}}d_{\mathbf{q}}^{\dagger} + \text{h c}\right) \tag{7 11}$$

In this form, we can directly apply perturbation theory, and thus determine the ground-state energy and the number of phonons

7.3   Energy

The standard second order perturbation expression for the energy is given by

$$E = E_0^{(0)} + H_{00}' + \sum_{n\neq 0}\frac{\mid H_{n0}'\mid^2}{E_0^{(0)} - E_n^{(0)}} \tag{7 12}$$

Here, the matrix element $H_{mn}' = \langle\phi_m^{(0)}\mid H'\mid\phi_n^{(0)}\rangle$, where $\mid\phi_m^{(0)}\rangle$ and $\mid\phi_n^{(0)}\rangle$ are eigenstates of H_0 The energy $E_m^{(0)}$ is the eigenvalue of H_0 corresponding to $\mid\phi_m^{(0)}\rangle$

In our treatment below, as in [3], we consider the perturbation energy corresponding to the creation of a *single* virtual phonon Thus, the initial state $\mid\mathbf{k},0\rangle$ consists of an electron with momentum $\mathbf{k}$ and no phonons The intermediate state, then, consists of an electron with momentum $\mathbf{k}-\mathbf{q}$, and a single phonon of momentum $\mathbf{q}$ – represented by $\mid\mathbf{k}-\mathbf{q},1_{\mathbf{q}}\rangle$ The corresponding

energies are given by

$$E_0^{(0)} = \frac{k^2}{2m_0},$$ (7 13)

and

$$E_n^{(0)} = \frac{(k-q)^2}{2m_0} + \hbar\omega$$ (7 14)

The off-diagonal matrix elements, appearing in equation (7 12), have the form

$$
\begin{aligned}
H_{n0}' &= -\kappa'\hbar\omega \sum_{q,k} \langle k-q, 1_q \mid \tilde{f}_q \left(c_{k-q}^{\dagger} c_k b_q^{\dagger} + \text{h c} \right) \mid k, 0 \rangle \\
&= -\kappa'\hbar\omega \sum_{q} \langle 0, 1_q \mid \tilde{f}_q \mid 0, 1_q \rangle \\
&= -\kappa'\hbar\omega \tilde{f}_q,
\end{aligned}
$$ (7 15)

and the diagonal matrix element H_{00}' is zero, because H' acting on a given state alters the the number of phonons Thus, on substitution of H_{n0}', H_{00}', $E_0^{(0)}$ and $E_n^{(0)}$ into equation (7 12), one can see that

$$E = \frac{k^2}{2m_0} - (\kappa'\hbar\omega)^2 \sum_{q} \frac{\mid \tilde{f}_q \mid^2}{(k-q)^2/2m_0 + \hbar\omega - k^2/2m_0}$$ (7 16)

We will make use of equation (7 16) in section (7 5) in order to calculated the effective mass and the isotope exponent

The ground state energy, occurs at $k = 0$, and is given by

$$E_0 = -(\kappa'\hbar\omega)^2 \sum_{q} \frac{\mid \tilde{f}_q \mid^2}{q^2/2m_0 + \hbar\omega}$$ (7 17)

7.4   Number of Phonons

The number of virtual phonons in the polaron cloud is given by the expectation value of the phonon number operator,

$$N_{\text{ph}} = \sum_{q} \langle 0' \mid d_q^{\dagger} d_q \mid 0' \rangle,$$ (7 18)

where $\mid 0' \rangle$ represents the eigenstate for the perturbed Hamiltonian Using standard first order perturbation theory, this state can be written as

$$
\begin{aligned}
\mid 0' \rangle &= \mid \phi_0^{(0)} \rangle + \sum_{n \neq 0} \frac{H_{n0}'}{E_0^{(0)} - E_n^{(0)}} \mid \phi_n^{(0)} \rangle \\
&= \mid k, 0 \rangle - \kappa'\hbar\omega \sum_{q'} \frac{\tilde{f}_{q'}}{k^2/2m - (k-q')^2/2m - \hbar\omega} \mid k - q, 1_q \rangle,
\end{aligned}
$$ (7 19)

where we have used equations (7 13) to (7 15)

The left-multiplication of equation (7 19) by the phonon destruction operator $d_\mathbf{q}$ yields

$$d_\mathbf{q} \mid 0' \rangle = d_\mathbf{q} \mid \mathbf{k}, 0 \rangle - \kappa' \hbar\omega \sum_{\mathbf{q}'} \frac{\tilde{f}_{\mathbf{q}'} d_\mathbf{q}}{\mathbf{k}^2/2m_0 - (\mathbf{k} - \mathbf{q}')^2/2m_0 - \hbar\omega} \mid \mathbf{k} - \mathbf{q}, 1_\mathbf{q} \rangle$$

$$= -\kappa' \hbar\omega \frac{\tilde{f}_\mathbf{q}}{\mathbf{k}^2/2m_0 - (\mathbf{k} - \mathbf{q})^2/2m_0 - \hbar\omega} \mid \mathbf{k} - \mathbf{q}, 0 \rangle, \tag{7 20}$$

where we have used the fact that, by definition, $d_\mathbf{q} \mid \mathbf{k}, 0 \rangle = 0$ The expectation value given in equation (7 18) is just the quantity $d_\mathbf{q} \mid 0' \rangle$ multiplied by its own Hermitian conjugate – summed over $\mathbf{q}$ Thus, the number of virtual phonons in the polaron cloud is

$$N_{\text{ph}} = \left(\kappa' \hbar\omega \right)^2 \sum_\mathbf{q} \frac{\mid \tilde{f}_\mathbf{q} \mid^2}{\left(\mathbf{k}^2/2m_0 - (\mathbf{k} - \mathbf{q})^2/2m_0 - \hbar\omega \right)^2}, \tag{7 21}$$

which, for the case of $\mathbf{k} = 0$, is given by

$$N_{\text{ph}} = \left(\kappa' \hbar\omega \right)^2 \sum_\mathbf{q} \frac{\tilde{f}_\mathbf{q}^2}{\left(\mathbf{q}^2/2m_0 + \hbar\omega \right)^2} \tag{7 22}$$

7.5   Effective Mass and the Isotope Exponent

From this point on, we restrict ourselves to the one-dimensional case, because we are only considering the QMC results for one-dimensional models in this work In section (7 3), we determined the second-order perturbation expression for the energy We can now use this result in order to find the effective mass, which is defined as

$$\frac{m_0}{m^*} = m_0 \left. \frac{\partial^2 E_k}{\partial k^2} \right|_{k \to 0} \tag{7 23}$$

If we expand the square in the denominator of equation (7 16),

$$E_k = \frac{k^2}{2m_0} - \left(\kappa' \hbar\omega \right)^2 \sum_q \frac{\mid \tilde{f}_q \mid^2}{q^2/2m_0 - kq/m_0 + \hbar\omega}, \tag{7 24}$$

we see that the partial differentiation is easily performed, to give

$$\frac{m_0}{m^*} = 1 - \left(\kappa' \hbar\omega \right)^2 \sum_q \frac{2q^2}{m_0} \frac{\mid \tilde{f}_q \mid^2}{\left(q^2/2m_0 - kq/m_0 + \hbar\omega \right)^3}$$

$$= 1 - 4 \left(\kappa' \hbar\omega \right)^2 \sum_q \frac{\mid \tilde{f}_q \mid^2 q^2/2m_0}{\left(q^2/2m_0 - kq/m_0 + \hbar\omega \right)^3} \tag{7 25}$$

Thus, the inverse effective mass, which is defined at $k = 0$, is given by

$$\frac{m_0}{m^*} = 1 - 4 \left(\kappa' \hbar\omega \right)^2 \sum_{\mathbf{q} \neq 0} \frac{\mid \tilde{f}_q \mid^2 q^2/2m_0}{\left(\mathbf{q}^2/2m_0 + \hbar\omega \right)^3} \tag{7 26}$$

We would also like to obtain a weak-coupling expression for the isotope exponent on the effective mass, in order to check our QMC results The definition of the effective mass, equation

(6 26), involves the partial derivative of the effective mass with respect to the ionic mass M Using the fact that $\omega \propto M^{-1/2}$, then

$$\frac{\partial}{\partial M} = \frac{\partial \omega}{\partial M}\frac{\partial}{\partial \omega} = -\frac{\omega}{2M}\frac{\partial}{\partial \omega},$$

(7 27)

and so the isotope exponent may be written, in one-dimension, as

$$\alpha_{m^*} = \frac{m^*}{m_0}\frac{\omega}{2}\frac{\partial}{\partial \omega}\left(\frac{m_0}{m^*}\right)$$

(7 28)

The differentiation of equation (7 26) with respect to ω yields

$$\frac{\partial}{\partial \omega}\left(\frac{m_0}{m^*}\right) = -8\kappa'^2\hbar^2\omega\sum_q\frac{|\tilde{f}_q|^2\, q^2/2m_0}{\left(q^2/2m_0 + \hbar\omega\right)^3} + 12\kappa'^2\hbar^3\omega^2\sum_q\frac{|\tilde{f}_q|^2\, q^2/2m_0}{\left(q^2/2m_0 + \hbar\omega\right)^4},$$

(7 29)

and so the isotope exponent is given by

$$\alpha_{m^*} = 2\left(\kappa'\hbar\omega\right)^2\sum_q\left\{\frac{3\hbar\omega\,|\tilde{f}_q|^2\, q^2/2m_0}{\left(q^2/2m_0 + \hbar\omega\right)^4} - \frac{2\,|\tilde{f}_q|^2\, q^2/2m_0}{\left(q^2/2m_0 + \hbar\omega\right)^3}\right\}\frac{m^*}{m_0}$$

(7 30)

7.6   Numerical Analysis

We have determined the energy, the number of phonons, the effective mass and the isotope exponent in the weak-coupling limit $\lambda \ll 1$ In this section, we express these perturbation results in a form that allows us to directly compare them with our QMC results

We wish to measure the energy with respect to the bottom of the free-electron band Accordingly, by equating the two expressions for the free-electron dispersion given by equations (1 6) and (4 15), we see that, for small k

$$\frac{k^2}{2m_0} = 2t - 2t\cos(ka/\hbar),$$

(7 31)

where $m_0 = \hbar^2/2ta^2$, and a is the lattice constant Thus, we must substitute equation (7 31) into the perturbation result for each observable

On substitution of equation (7 31) into equation (7 17), the energy (measured with respect to the bottom of the free-electron band) is given by

$$\frac{1}{t}E_0 = -2 - \frac{2\lambda\bar{\omega}}{\sum_m \bar{f}_m^2(0)}\sum_{\bar{q}}\frac{|\tilde{f}_{\bar{q}}|^2}{2 - 2\cos\bar{q} + \bar{\omega}},$$

(7 32)

where we have converted to the dimensionless representation used in our QMC scheme, which was discussed in section (5 4) Here, the momentum $\bar{q} = q\hbar/a$ should only take on the (discrete)

values allowed on a chain of N sites In this form, equation (7 32) relates directly to the QMC measurement of the ground-state energy

It is convenient, for the purposes of numerical calculation, to write equation (7 32) in the form

$$\frac{1}{t}E_0 = -2 - \lambda \Upsilon_{E_0}(\bar{f}, \bar{\omega}),\tag{7 33}$$

where $\Upsilon_{E_0}(\bar{f}, \bar{\omega})$ is the coefficient of the linear term in λ, which must be determined numerically We can write this as

$$\Upsilon_{E_0}(\bar{f}, \bar{\omega}) = \sum_{\bar{q}} F(\bar{q}, \bar{f}) \Omega_{E_0}(\bar{q}, \bar{\omega}),\tag{7 34}$$

where the "model dependence" is contained within the factor

$$F(\bar{q}, \bar{f}) = \frac{\left[\sum_{\mathbf{m}} \bar{f}_{\mathbf{m}}(0)\right]^2}{N \sum_{\mathbf{m}} \bar{f}_{\mathbf{m}}^2(0)},\tag{7 35}$$

and the dependence on $\bar{\omega}$ is contained within

$$\Omega_{E_0}(\bar{q}, \bar{\omega}) = \frac{2\bar{\omega}}{2 - 2\cos\bar{q} + \bar{\omega}}\tag{7 36}$$

In a similar manner, the number of phonons, the effective mass and the isotope exponent, given by equations (7 22), (7 26) and (7 30), can be expressed as

$$N_{\mathrm{ph}} = \lambda \Upsilon_{N_{\mathrm{ph}}}(\bar{f}, \bar{\omega}),\tag{7 37}$$

$$\frac{m_0}{m^*} = 1 - \lambda \Upsilon_{m^*}(\bar{f}, \bar{\omega}),\tag{7 38}$$

and

$$\alpha_{m^*} = \frac{\lambda}{m_0/m^*} \Upsilon_{\alpha_{m^*}}(\bar{f}, \bar{\omega}),\tag{7 39}$$

Here, the coefficients of the linear term in λ take the general form

$$\Upsilon_X(\bar{f}, \bar{\omega}) = \sum_{\bar{q}} F(\bar{q}, \bar{f}) \Omega_X(\bar{q}, \bar{\omega}),\tag{7 40}$$

where $F(\bar{q}, \bar{f})$ is defined in equation (7 35), and $\Omega_X(\bar{q}, \bar{\omega})$ is given by

$$\Omega_{N_{\mathrm{ph}}}(\bar{q}, \bar{\omega}) = \frac{2}{(2 - 2\cos\bar{q} + \bar{\omega})^2},\tag{7 41}$$

$$\Omega_{m^*}(\bar{q}, \bar{\omega}) = \frac{8\bar{\omega}\,(2 - 2\cos\bar{q})}{(2 - 2\cos\bar{q} + \bar{\omega})^3},\tag{7 42}$$

or

$$\Omega_{\alpha_{m^*}}(\bar{q}, \bar{\omega}) = \frac{12\bar{\omega}^2\,(2 - 2\cos\bar{q})}{(2 - 2\cos\bar{q} + \bar{\omega})^4} - \frac{4\bar{\omega}\,(2 - 2\cos\bar{q})}{(2 - 2\cos\bar{q} + \bar{\omega})^3}\tag{7 43}$$

The value of $\Upsilon(\bar{f}, \bar{\omega})$ was numerically calculated for each pair of $\bar{f}_{\mathbf{m}}(\mathbf{n})$ and $\bar{\omega}$ used in the QMC simulations In table (7 1) we present the results of the numerical calculation for each interaction model at $\bar{\omega} = 1$

Table 7 1   The numerically calculated value of the coefficient of the linear term in λ, equation
(7 40), for each interaction model at $\bar{\omega} = 1$ For example, the ground state energy of the Holstein
polaron, equation (7 33), is given by $E_0/t = -2 - 0\ 894\lambda$

Interaction Model	$\sum_{\mathbf{m}} \bar{f}_{\mathbf{m}}^2(0)$	Υ_{E_0}	$\Upsilon_{N_{ph}}$	Υ_{m_0/m^*}	$\Upsilon_{\alpha_{m^*}}$
Holstein ($R_{sc} \to 0$)	1 000	0 894	0 537	0 572	0 143
Screened Frohlich ($R_{sc} = 1$)	1 034	1 079	0 736	0 637	0 219
Screened Frohlich ($R_{sc} = 3$)	1 133	1 257	0 937	0 670	0 283
Non-screened Frohlich ($R_{sc} \to \infty$)	1 269	1 394	1 400	0 844	0 405

The values that $\Upsilon_X(\bar{f},\bar{\omega})$ take can be understood graphically   In figure (7 1) we plot $\Omega_X(\bar{q},\bar{\omega})$,
corresponding to each of the observables, against $\bar{q}$ at $\bar{\omega} = 1$ In figure (7 2) we plot $F(\bar{q},\bar{f})$,
equation (7 35), against $\bar{q}$ for the interaction models studied in this work, which were discussed
in section (1 4)   The value of $\Upsilon_X(\bar{f},\bar{\omega})$ for a given $\bar{f}$ and $\bar{\omega}$, then, is simply the summation over
$\bar{q}$ of the product of the relevant curves for $\Omega_X(\bar{q},\bar{\omega})$ and $F(\bar{q},\bar{f})$

The graphical interpretation can explain some of the trends we see in table (7 1)   For example,
as we increase the "spread" of the interaction from the Holstein to the non-screened Frohlich
interaction (by increasing R_{sc}), the value of $\Upsilon_X(\bar{f},\bar{\omega})$ increases "smoothly" for all the observables
(at $\bar{\omega} = 1\ 0$)   This is because the peak in $F(\bar{q},\bar{f})$ becomes more sharp as R_{sc} increases, as can be
seen from figure (7 2)   Note how rapidly the value of $\Upsilon_{N_{ph}}(\bar{f},\bar{\omega})$ increases with increasing R_{sc}

Thus, we observe that the polaron properties in the weak-coupling limit are strongly dependent
on the precise nature of the shape of the electron-phonon interaction in Fourier-space, as well as
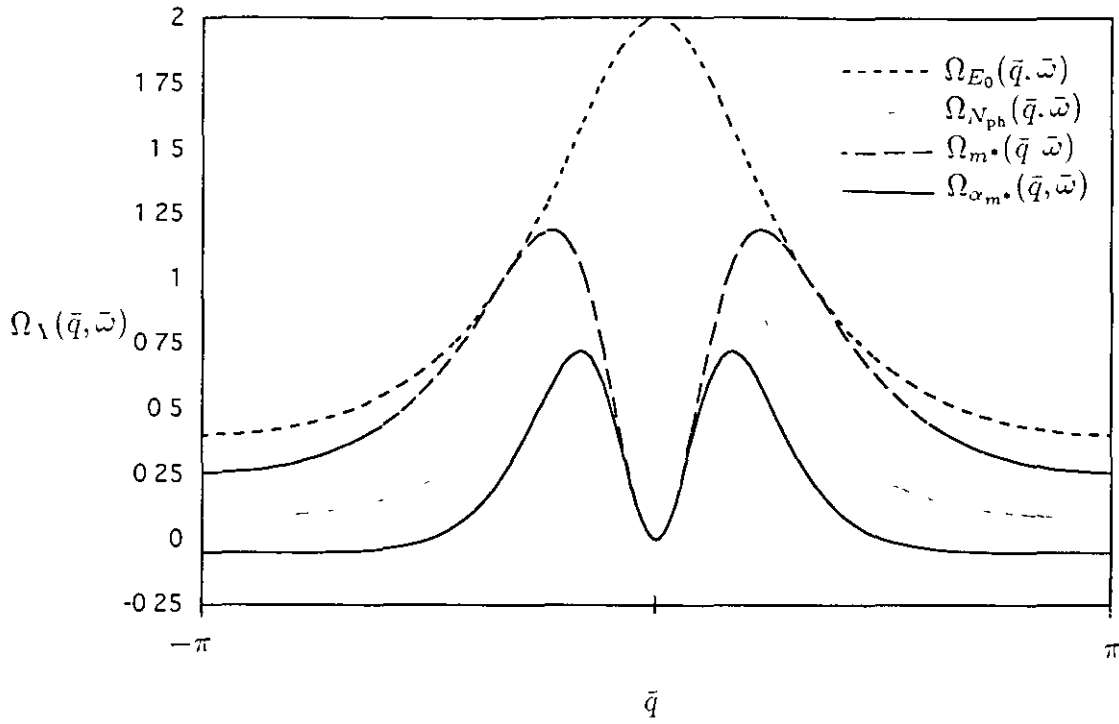on the value of $\bar{\omega}$

Figure 7 1 The variation of $\Omega_X(\bar{q},\bar{\omega})$, corresponding to each of the observables, with $\bar{q}$ at $\bar{\omega} = 1\,0$
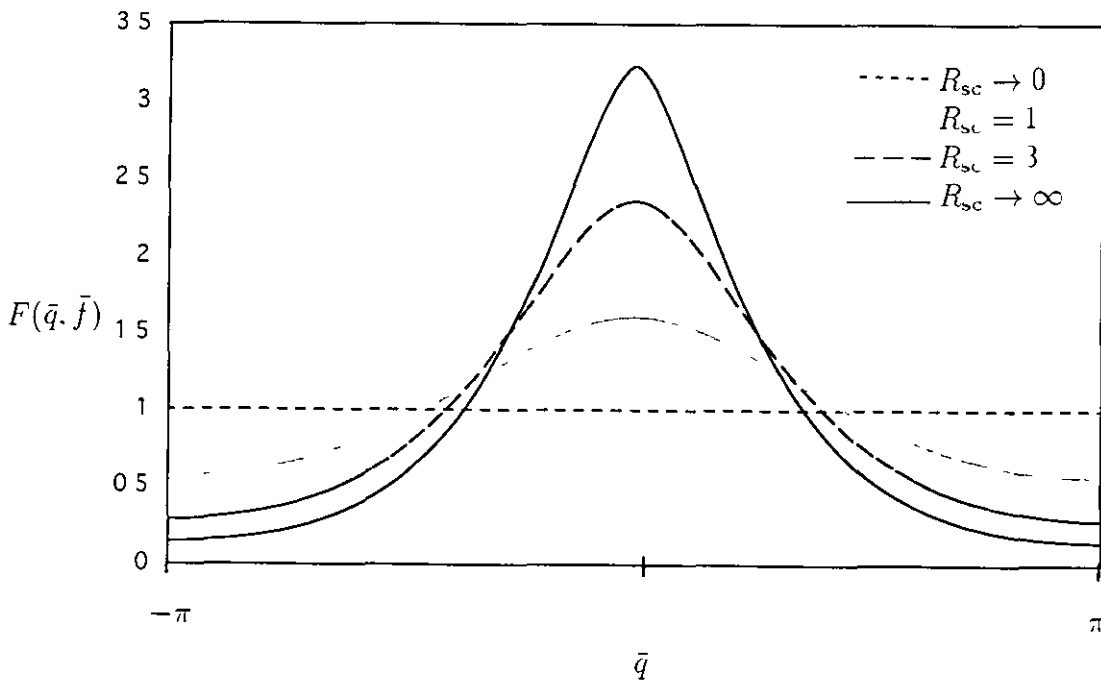

Figure 7 2 The variation of $F(\bar{q},\bar{f})$, equation (7 35), with $\bar{q}$ for the screened Frohlich model at the screening lengths R_{sc} studied in this work

Chapter 8

The Strong-Coupling Limit (Small Polaron)

8.1 Introduction

When the electron-phonon coupling is strong, the electron becomes "trapped" in a potential well created by the induced lattice distortion. In which case, the "size" of the polaron state is comparable with the lattice constant, and the term "small polaron" is used. A small polaron can exist if the polaronic energy-level shift E_p (due to the induced lattice deformation) is comparable or greater than the half bandwidth zt (for a hyperbolic lattice), where z is the coordination number. The ratio of these two quantities defines the electron-phonon coupling constant λ. Thus, the condition for small polaron formation is [4]

$$\lambda = \frac{E_p}{zt} \geq 1, \qquad (8\ 1)$$

which is referred to as the strong-coupling regime. In this regime it is energetically favourable for localised states to exist – the electron is trapped in a potential well of depth E_p. The small polaron can move from site to site (at zero temperature) through the action of zero-point motion.

An analytical method to determine the effective mass and energy dispersion in the strong-coupling regime, for a lattice polaron with a general electron-phonon interaction force $f_m(n)$, has recently been published by Alexandrov and Kornilovitch [31]. The method is based on the Lang-Firsov canonical transformation [9], followed by a second-order perturbation technique that uses $1/\lambda$ as a small parameter [10]. Note that, at large values of λ, the "size" of the the polaronic

state of of the order of the lattice constant, even though the lattice distortion (polaron cloud) may extend over a large number of sites

In this chapter, we will present the strong-coupling results for the energy and effective mass, following [31] In sections (8 4) and (8 5), we will use these results in order to determine the number of phonons and the isotope exponent in the strong-coupling regime The results of this chapter will allow us to check the correctness of our QMC results for large values of λ

In section (8 6), we will discuss the mechanism by which the small polaron can *tunnel* from site to site through the lattice at large λ An understanding of this mechanism will be of use when we come to consider the effects of long-range electron-phonon interactions

8.2   Exact Solution for Extreme-Coupling

The model Hamiltonian may be solved analytically in the extreme-coupling limit, by making use of the Lang-Firsov canonical transformation [9] The hopping term of the resulting transformed Hamiltonian vanishes in the limit $\lambda \to \infty$, rendering the transformed Hamiltonian diagonal

Our starting point is to transform the phonon operators, $d_{\mathbf{m}}^{\dagger}$ and $d_{\mathbf{m}}$, appearing in our model Hamiltonian, into Fourier-space Using the transform

$$d_{\mathbf{m}}^{\dagger} = \frac{1}{\sqrt{N}} \sum_{\mathbf{q}} d_{\mathbf{q}}^{\dagger} e^{-i\mathbf{q}\cdot\mathbf{m}} \quad , \quad d_{\mathbf{m}} = \frac{1}{\sqrt{N}} \sum_{\mathbf{q}} d_{\mathbf{q}} e^{i\mathbf{q}\cdot\mathbf{m}} \tag{8 2}$$

(where $\mathbf{q}$ represnets the wave number), and the identity $\sum_{\mathbf{m}} e^{i\mathbf{m}(\mathbf{q}-\mathbf{q}')} = N\delta_{\mathbf{q},\mathbf{q}'}$ – the model Hamiltonian, equation (1 1), may be written in the form

$$H = -\sum_{\mathbf{nn}'} t_{\mathbf{nn}'} c_{\mathbf{n}'}^{\dagger} c_{\mathbf{n}} + \hbar\omega \sum_{\mathbf{q}} d_{\mathbf{q}}^{\dagger} d_{\mathbf{q}} - \sum_{\mathbf{m},\mathbf{n},\mathbf{q}} f_{\mathbf{m}}(\mathbf{n}) c_{\mathbf{n}}^{\dagger} c_{\mathbf{n}} \left[u_{\mathbf{m}}(\mathbf{q}) d_{\mathbf{q}} + u_{\mathbf{m}}^{*}(\mathbf{q}) d_{\mathbf{q}}^{\dagger} \right], \tag{8 3}$$

with

$$u_{\mathbf{m}}(\mathbf{q}) = \frac{\hbar\omega}{(2MN\hbar\omega^3)^{1/2}} e^{i\mathbf{q}\cdot\mathbf{m}}, \tag{8 4}$$

where the hopping term in equation (8 3) is not restricted to nearest-neighbour hopping

Now let us apply the Lang-Firsov canonical transformation, which is given by

$$\tilde{H} = e^{S} H e^{-S} \tag{8 5}$$

where

$$S = -\frac{1}{\hbar\omega} \sum_{\mathbf{m},\mathbf{n},\mathbf{q}} f_{\mathbf{m}}(\mathbf{n}) c_{\mathbf{n}}^{\dagger} c_{\mathbf{n}} \left[u_{\mathbf{m}}(\mathbf{q}) d_{\mathbf{q}} - u_{\mathbf{m}}^{*}(\mathbf{q}) d_{\mathbf{q}}^{\dagger} \right] \tag{8 6}$$

By making use of the "standard" formula

$$\tilde{a} = e^S a e^{-S} = a + [S,a] + \frac{1}{2}[S,[S,a]] + \quad , \tag{8 7}$$

where a represents a general operator, the phonon operator transforms as

$$\tilde{d}_{\mathbf{q}} = d_{\mathbf{q}} - \frac{1}{\hbar\omega} c_{\mathbf{n}}^{\dagger} c_{\mathbf{n}} f_{\mathbf{m}}(\mathbf{n}) u_{\mathbf{m}}^{*}(\mathbf{q}), \tag{8 8}$$

and the electron operator transforms as

$$\tilde{c}_{\mathbf{n}} = c_{\mathbf{n}} \exp \left\{ \frac{1}{\hbar\omega} \sum_{\mathbf{m},\mathbf{q}} f_{\mathbf{m}}(\mathbf{n}) \left[u_{\mathbf{m}}(\mathbf{q}) d_{\mathbf{q}} - u_{\mathbf{m}}^{*}(\mathbf{q}) d_{\mathbf{q}}^{\dagger} \right] \right\} \tag{8 9}$$

On substitution of these transformed operators into equation (8 3), and after some algebraic manipulation, the transformed Hamiltonian may be written as

$$\tilde{H} = -\sum_{\mathbf{n},\mathbf{n}'} \sigma_{\mathbf{n}\mathbf{n}'} c_{\mathbf{n}'}^{\dagger} c_{\mathbf{n}} + \hbar\omega \sum_{\mathbf{q}} d_{\mathbf{q}}^{\dagger} d_{\mathbf{q}} - \sum_{\mathbf{n}} E_{\mathrm{p}} c_{\mathbf{n}}^{\dagger} c_{\mathbf{n}}, \tag{8 10}$$

where we define the *polaronic shift* in energy as

$$E_{\mathrm{p}} = \frac{1}{2NM\omega^2} \sum_{\mathbf{m},\mathbf{m}',\mathbf{q}} f_{\mathbf{m}}(\mathbf{n}) f_{\mathbf{m}'}(\mathbf{n}) e^{-i\mathbf{q}(\mathbf{m}-\mathbf{m}')}, \tag{8 11}$$

and the transformed hopping amplitude,

$$\sigma_{\mathbf{n}\mathbf{n}'} = t_{\mathbf{n}\mathbf{n}'} \exp \left\{ \frac{1}{\hbar\omega} \sum_{\mathbf{m},\mathbf{q}} [f_{\mathbf{m}}(\mathbf{n}) - f_{\mathbf{m}}(\mathbf{n}')] \left[u_{\mathbf{m}}(\mathbf{q}) d_{\mathbf{q}} - u_{\mathbf{m}}^{*}(\mathbf{q}) d_{\mathbf{q}}^{\dagger} \right] \right\}, \tag{8 12}$$

now also depends on the phonon operators

In the limit of extreme-coupling $\lambda \to \infty$, the hopping term may be neglected, and so the energy is simply given by

$$E = -\sum_{\mathbf{n}} E_{\mathrm{p}} n_{\mathbf{n}} + \hbar\omega \sum_{\mathbf{q}} n_{\mathbf{q}}, \tag{8 13}$$

where $n_{\mathbf{q}} = 0, 1, 2, \quad, \infty$ is the phonon occupation number, and $n_{\mathbf{n}} = 0, 1$ is the electron occupation number

Thus, in the limit $\lambda \to \infty$, the transformed Hamiltonian, equation (8 10), describes localised polarons (trapped in a potential well of "depth" E_{p}) and independent phonons   The phonon term in equation (8 10), which involves $\tilde{d}_{\mathbf{q}}$ as given in equation (8 8), represents lattice vibrations around new shifted equilibrium positions

8.3   Strong-Coupling Perturbation

In the strong-coupling regime $\lambda \geq 1$, we can treat the transformed hopping term in equation (8 10) as a perturbation, when there is originally no hopping, using $1/\lambda$ as a small parameter [4]

Thus, we define $\tilde{H} = \tilde{H}_0 + \tilde{H}'$, where

$$\tilde{H}_0 = \hbar\omega \sum_{\mathbf{q}} d_{\mathbf{q}}^\dagger d_{\mathbf{q}} - \sum_{\mathbf{n}} E_{\mathrm{p}} c_{\mathbf{n}}^\dagger c_{\mathbf{n}}, \qquad (8\ 14)$$

and

$$\tilde{H}' = -\sum_{\mathbf{n},\mathbf{n}'} \sigma_{\mathbf{n}\mathbf{n}'} c_{\mathbf{n}'}^\dagger c_{\mathbf{n}} \qquad (8\ 15)$$

Let us consider a single electron   The appropriate set of N degenerate Bloch eigenstates of $\tilde{H}_0$, which corresponds to the lowest energy level $-E_{\mathrm{p}}$, is given by

$$|\mathbf{k},0\rangle = \frac{1}{\sqrt{N}} \sum_{\mathbf{n}} c_{\mathbf{n}}^\dagger e^{i\mathbf{k}\cdot\mathbf{n}} |0\rangle, \qquad (8\ 16)$$

where $|0\rangle$ is the vacuum state   Applying standard second-order perturbation theory, equation (7 12), the result for the lowest energy levels reads [31]

$$E(\mathbf{k}) = -E_{\mathrm{p}} - \varepsilon_{\mathrm{p}}(\mathbf{k}) - \sum_{\mathbf{k}',n_{\mathbf{q}}} \frac{|\langle \mathbf{k},0 \mid \sum_{\mathbf{n}\mathbf{n}'} \hat{\sigma}_{\mathbf{n}\mathbf{n}'} c_{\mathbf{n}'}^\dagger c_{\mathbf{n}} \mid \mathbf{k}',n_{\mathbf{q}}\rangle|^2}{\hbar\omega \sum_{\mathbf{q}} n_{\mathbf{q}}}, \qquad (8\ 17)$$

where $n_{\mathbf{q}}$ is the number of phonons with wave vector $\mathbf{q}$, and $\mid \mathbf{k}',n_{\mathbf{q}}\rangle$ is an excited state of $\tilde{H}_0$ that consists of a single electron with wave vector $\mathbf{k}'$ and one or more phonons   Let us discuss each term of equation (8 17) separately below

The first term E_{p} is the polaronic energy-level shift, corresponding to the solution in the limit of extreme-coupling $\lambda \to \infty$, given by equation (8 11)   The second term appearing in equation (8 17) – linear with respect to the bare hopping amplitude $t_{\mathbf{n}\mathbf{n}'}$ – is the small-polaron dispersion

$$\varepsilon_{\mathrm{p}}(\mathbf{k}) = \sum_{\mathbf{n}\neq 0} t_{\mathbf{n}0} e^{-g^2(\mathbf{n})} e^{-i\mathbf{k}\cdot\mathbf{n}}, \qquad (8\ 18)$$

where g^2 is known as the (zero temperature) *mass renormalisation exponent*, which is given by

$$g^2(\mathbf{n}) = \frac{1}{2NM\hbar\omega^3} \sum_{\mathbf{m},\mathbf{m}',\mathbf{q}} [f_{\mathbf{m}}(0)f_{\mathbf{m}'}(0) - f_{\mathbf{m}}(0)f_{\mathbf{m}'}(\mathbf{n})] e^{-i\mathbf{q}\cdot(\mathbf{m}-\mathbf{m}')} \qquad (8\ 19)$$

The final term of equation (8 17) is quadratic with respect to the bare hopping amplitude $t_{\mathbf{n}\mathbf{n}'}$, and produces a negative correction to the energy   It is of order of $1/\lambda^2$ and is almost *independent* of $\mathbf{k}$ [31]   The intuitive interpretation of this term is discussed in section (8 6)

8.4   Energy and the Number of Phonons

The strong-coupling perturbation result, presented in previous section, was derived without placing any restrictions on the interaction force $f_{\mathbf{m}}(\mathbf{n})$, or on the hopping integral $t_{\mathbf{n}\mathbf{n}'}$ In this work,

we consider nearest-neighbour hopping only, and forms of $f_m(n)$ that depend on the relative lattice distance $|m - n|$ Under these restrictions, equations (8 11), (8 18) and (8 19) reduce to

$$E_p = \frac{1}{2M\omega^2} \sum_m f_m^2(0),$$
(8 20)

$$\varepsilon_p(k) = t \sum_{n \neq 0} e^{-g^2(1)} e^{-ik \cdot n},$$
(8 21)

and

$$g^2(1) = \frac{1}{2M\hbar\omega^3} \sum_m \left[f_m^2(0) - f_m(0)f_m(1) \right],$$
(8 22)

where we have used the identity $\sum_q e^{-iq \cdot (m-m')} = N\delta_{m,m'}$, and made a shift in the summation indices The electron-phonon coupling constant λ is defined as the ratio of E_p to the bare-electron half-bandwidth zt Thus, for the models we study in this work, the coupling constant is given by

$$\lambda = \frac{1}{2M\hbar\omega^2 zt} \sum_m f_m^2(0)$$
(8 23)

We only conduct our QMC simulations for the case when $k = 0$, which corresponds to the ground state of the system   At $k = 0$, the value of $\varepsilon_p(k)$ is real and small compared with $-E_p$, and so the energy in equation (8 17) is dominated by the polaron shift $-E_P$ Thus, the strong-coupling result for the ground state energy at $k = 0$ is given by

$$E(0) = -\frac{1}{2M\omega^2} \sum_m f_m^2(0)$$
(8 24)

Due to the fact that $E_p = N_{ph}\hbar\omega$, it immediately follows that the number of phonons in the polaron cloud at $k = 0$ is given by

$$N_{ph}(0) = \frac{1}{2M\hbar\omega^3} \sum_m f_m^2(0)$$
(8 25)

Finally, we wish to express equations (8 24) and (8 25) in the dimensionless representation used in our QMC scheme   In terms of λ and $\bar{\omega}$, defined by equations (8 23) and (5 13) respectively, the ground state energy is written as

$$\frac{E_0}{t} = z\lambda,$$
(8 26)

and the number of virtual phonons in the polaron cloud as

$$N_{ph} = \frac{z\lambda}{\bar{\omega}}$$
(8 27)

8.5   Effective Mass and the Isotope Exponent

The perturbation result, given by equation (8 17), can be used in order to determine the effective mass and the isotope exponent on the effective mass, in the strong coupling regime For simplicity, in this section we will restrict ourselves to the the one-dimensional case

The inverse effective mass is defined by equation (7 23) Assuming that the third term in equation (8 17) is *completely* independent of k, then the effective mass is simply the second partial derivative of $\varepsilon_p(k)$, equation (8 21), with respect k, as $k \rightarrow 0$ Thus, the inverse effective mass is given by

$$\frac{m_0}{m^*} = e^{-g^2(1)}, \qquad (8\ 28)$$

where $m_0 = \hbar^2/2ta^2$ is the bare electron mass, and $g^2(1)$ is defined in equation (8 22) It is convenient to expressed this result in terms of the polaron shift E_p, equation (8 20), so that

$$\frac{m_0}{m^*} = \exp\left(-\frac{\gamma E_p}{\hbar \omega}\right), \qquad (8\ 29)$$

where the dimensionless constant

$$\gamma \equiv 1 - \frac{\sum_m f_m(0) f_m(1)}{\sum_m f_m^2(0)} \qquad (8\ 30)$$

depends only on the *shape* of the electron-phonon interaction force In the dimensionless representation used in our QMC simulations, equation (8 29) is written

$$\frac{m_0}{m^*} = \exp\left(\frac{-2\gamma\lambda}{\bar{\omega}}\right) \qquad (8\ 31)$$

Now let us consider the isotope exponent on the effective mass α_{m^*}, which is expressed as a partial derivative of m_0/m^* with respect to ω in equation (7 28) Using equation (7 28) and (8 31), the isotope exponent is given in dimensionless representation as [54]

$$\alpha_{m^*} = \frac{m^*}{m_0} \frac{\bar{\omega}}{2} \frac{\partial}{\partial \bar{\omega}} \left[\exp\left(-\frac{2\gamma\lambda}{\bar{\omega}}\right)\right]$$
$$= \frac{\gamma\lambda}{\bar{\omega}} \qquad (8\ 32)$$

The dimensionless constant $0 \leq \gamma \leq 1$, which is defined by equation (8 30), must in general be determined numerically In table 8 1, we present the numerically calculated value of γ for each of the one-dimensional interaction models studied in this work, which were introduced in section (1 4)

8.6   Small-Polaron Tunneling Mechanism

The perturbation result for the energy, given by equation (8 17), is valid in the strong-coupling regime, where the polaronic shift E_p is large compared with the energy of the bottom of the bare-electron band zt As we discussed in the section (8 3), the third term in equation (8 17) represents a negative correction to $-E_p$ which is of the order of $1/\lambda^2$ and almost independent

Table 8 1   Values of the dimensionless parameter $\gamma = 1 - \sum_m f_m(0) f_m(1)/ \sum_{m'} f_{m'}^2(0)$ for the one-dimensional models studied in this work, where γ depends only on the *shape* of the interaction force

Interaction Model	γ
Holstein	1 000
Screened Frohlich ($R_{sc} = 1$)	0 745
Screened Frohlich ($R_{sc} = 3$)	0 531
Non-screened Frohlich	0 387

of $\mathbf{k}$ This term represents a much larger correction to $-E_p$ than does the second term, due to the small exponent in $\varepsilon_p(\mathbf{k})$, equation (8 21)   Because a way has not been found to evaluate the matrix elements in the third term of equation (8 17) exactly, we discuss its interpretation as a second-order virtual hopping process [4], which allows the polaron to tunnel from site to site through the lattice in a narrow band   In this section, we will restrict the discussion to the case of the (on site) Holstein model

The polaron is initially localised in a potential well of "depth" E_p, at a particular site $\mathbf{n}$ The electron undergoes a *virtual* hop to a neighbouring site $\mathbf{n}'$ – whereupon it directly returns $(E_p \gg zt)$, as illustrated in figure 8 1a   The term "virtual" is used because the process occurs too quickly for the lattice deformation around site $\mathbf{n}$ to follow the electron   Thus, this virtual hopping does not significantly alter the effective mass of the polaron

The electron continues to virtually hop backwards and forwards between site $\mathbf{n}$ and its neighbour   Upon each virtual hop, a small amount of lattice deformation is induced around site $\mathbf{n}'$, reducing the energy of this site by a small amount $\sim t^2/E_p$ (figure 8 1b)   After many virtual hops, the energy associated with site $\mathbf{n}'$ is reduced to the extent that the electron is able to tunnel from site $\mathbf{n}$ to $\mathbf{n}'$, as shown in figure 8 1c   The polaron is now localised in a potential well of depth E_p at site $\mathbf{n}'$, and the lattice deformation associated with site $\mathbf{n}$ starts to relax back (figure 8 1d), and the tunneling process can now start again

Thus, at zero temperature the polaron tunnels from site to nearest-neighbour site in a narrow band – behaving like a heavy particle with a large effective mass given by equation (8 31)   We will extend this mechanism to the case of the long-range interaction later in chapter (10)
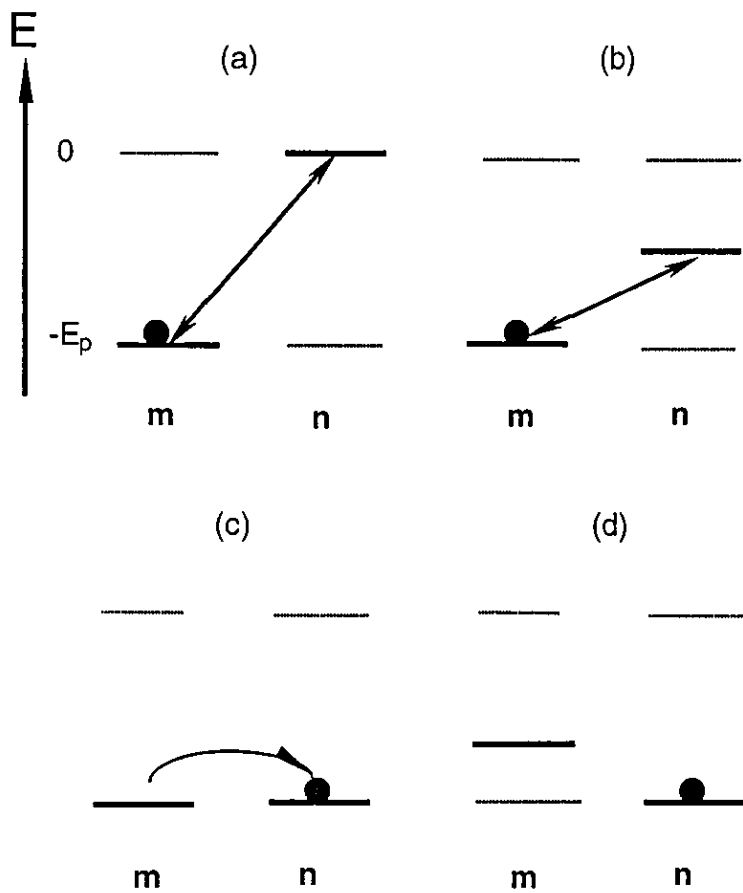
Figure 8 1   The small-polaron tunneling mechanism from site **m** to **n**   (a) The electron virtually hops from **m** to **n**, and immediately back again, without the deformation on **m** following   (b) Each virtual hop induces a small amount of deformation at site **n**   (c) When enough deformation has accumulated at **n**, the electron tunnels from **m** to **n**   (d) The deformation around **m** starts to relax back

Chapter 9

Holstein Interaction

9.1 Introduction

In this chapter, we consider the one-dimensional molecular crystal model introduced in 1959 by Holstein [7] [8] The Holstein model is the simplest interaction model we study in this work, because the electron interacts only with the oscillator it currently occupies ("short-range" interaction) The Holstein model is a particular case of our generalised model Hamiltonian, equation (1 1), with the electron-phonon interaction force being described by

$$f_{\mathbf{m}}(\mathbf{n}) = -\kappa \delta_{\mathbf{mn}} \tag{9 1}$$

Our aim is to use our quantum Monte Carlo (QMC) scheme, presented in chapter (5), in order to identify the properties of the Holstein polaron These results will allow us to infer what effects increasing the range, and changing the shape of $f_{\mathbf{m}}(\mathbf{n})$ have on the polaron properties The QMC simulations directly and independently measure the expectation value of the ground-state energy (both kinetic and potential), the number of phonons, the effective mass and the isotope exponent All the QMC measurements presented here were determined to within a statistical error of less than one percent

The ground state energy and effective mass of the one-dimensional Holstein polaron have been previously studied, using the present QMC scheme, by Kornilovitch [30] The QMC results were found to be in excellent agreement with those obtained by independent methods (such as exact diagonalisation and variational calculations), showing that the present QMC scheme is free from systematic errors

In this chapter we reproduce the results of [30], and extend the study to include our new physical observables the number of phonons in the polaron cloud, and the isotope exponent on the effective mass We perform QMC simulations at various values of the dimensionless phonon frequency $\bar{\omega}$ For each value of $\bar{\omega}$, we will compare the QMC results with both the weak-coupling perturbation (WCP) expressions, given in chapter (7), and the strong-coupling perturbation (SCP) results, given in chapter (8)

We start in section (9 2) by presenting the QMC results for the ground state energy, and use these results in order to identify the large-polaron, small-polaron and transition regions In section (9 3) we examine how the boundaries of these regions alter with changing $\bar{\omega}$ The QMC results for the number of phonons, the effective mass and the isotope exponent are discussed in sections (9 4) and (9 5) Finally, the dependence of the effective mass on the number of phonons is examined in section (9 6), and explained in terms of the small-polaron tunneling mechanism in section (9 7)

9.2   Potential, Kinetic and Total Energy

The potential energy (PE), the kinetic energy (KE) and the total energy (TE) of the ground state were calculated using QMC for the one-dimensional Holstein model A typical example of the variation of these energies with the coupling constant λ is shown in figure (9 1), for a fixed (dimensionless) phonon frequency of $\bar{\omega} = 1$ As can be seen, the TE curve tends to the the WCP result from below as $\lambda \to 0$, and to the SCP result of $E(0)/t = 2\lambda$ as $\lambda \to \infty$

Note that the QMC potential energy is actually the sum of the potential energy of the electron-phonon interaction and the elastic energy of the lattice Similarly, the QMC kinetic energy is the of the kinetic energy of the electron, together with the kinetic energy of the lattice vibrations This lattice contribution to the energy corresponds with the phonon term H_{ph}, equation (1 14), that appears in the model Hamiltonian

Three separate regions can clearly be distinguished in figure (9 1)   At weak-coupling we observe large-polaron (band-electron-like) behavior, at strong-coupling we see small-polaron (self-trapped) behavior, and in between we observe a *smooth* transition region The coupling constant was defined, in chapter (8), as the ratio of the polaronic energy level shift E_p to the energy at the bottom of the bare-electron band zt This means that, by design, λ naturally characterises these three separate regions Note that E_p, and therefore λ, are independent of the phonon frequency $\bar{\omega}$ Thus, λ and $\bar{\omega}$ are independent dimensionless control parameters

Let us discuss the three regions evident in figure (9 1) in more detail   These are

1   The *large-polaron region* at weak-coupling ($\lambda = 0$ to $\lambda \approx 1$ in this case)   We define this
   region as the range of λ in which the behavior of the system is accurately described by WCP
   theory, which was given in chapter (7)   [1]   At $\lambda = 0$ the TE is entirely kinetic and represents
   the bottom of the bare-electron band, with energy $-zt$ As λ increases within this region,
   we see that the KE increases but remains large compared with the PE, resulting from the
   fact that the the motion of the electron is only slightly affected by the electron-phonon
   interaction   As the term "large-polaron" suggests, in this region we only have "extended"
   (band-electron type) states

2   The *small-polaron region* at strong-coupling (in this case $\lambda \approx 2\,5$ to $\lambda \to \infty$)   Here, the PE
   is much greater than the KE   This region is defined as the range of λ in which the SCP
   theory provides an accurate description of the behavior of the system, which was given in
   chapter (8)   As the term "small-polaron" suggests, in this region there exists only localised
   (self-trapped) polaronic states

3   The *transition region* at intermediate coupling ($\lambda \approx 1$ to $\lambda \approx 2\,5$ in this case)   The smooth
   transition from large to small polaron starts at $\lambda \approx 1$, where the energy of the electron-
   phonon interaction becomes comparable with the kinetic energy of the electron, meaning
   that it is energetically favorable for localised states to form   Note that this does not occur
   at exactly $\lambda = 1$ due to the contribution in energy from the lattice, as mentioned above
   As λ increases, we see a large decrease in the PE (due to the increased lattice deformation)
   and an comparatively small increase in the KE (due to the localisation of the polaron)

The actual values of λ that mark the end of the large-polaron region and the beginning of the
small-polaron region are considered in more detail later in section (9 4)

9.3   Variation of Energy with Phonon Frequency

In this section, we investigate the way in which the properties of the Holstein polaron are affected
by altering the value of the dimensionless phonon frequency $\bar{\omega}$, as defined in section (5 4)   This
quantity is also known as the *adiabatic ratio*, and is often used as a parameter in analytical
approaches to the polaron problem   The *adiabatic regime* is defined for the case when $\bar{\omega} < 1$,
and the anti-adiabatic regime when for the case when $\bar{\omega} > 1$

---

[1] Note that the term "large-polaron" has historically been connected with the results of one-dimensional adia-
batic theory   In this work, however, we use the term only as defined above

In addition to the phonon frequency of $\bar{\omega} = 1$, the PE, the KE and the TE of the one-dimensional Holstein model were also computed for $\bar{\omega} = 0.5$ and $\bar{\omega} = 3$. The QMC results for all three values of $\bar{\omega}$ are presented together in figure (9 2) against λ. The QMC results are in excellent agreement with both the WCP results (not shown) and the SCP expression (which is $\bar{\omega}$-independent) for the energy at all three values of $\bar{\omega}$. As can be seen from figure (9 2), changing the value of $\bar{\omega}$ has the effect of shifting the boundaries of the three regimes identified in the previous section

Consider the variation of the KE with phonon frequency $\bar{\omega}$. In the large-polaron region, we observe from figure (9 2) that the KE has almost the same value for each $\bar{\omega}$. This is because the KE is mainly due to that of the electron. As $\lambda \to \infty$, the KE curves appear to tend to a small negative value – corresponding with the energy of the lattice vibrations [2] At intermediate values of λ, we see from figure (9 2) that the KE decreases as $\bar{\omega}$ increases

As a consequence of the above variation of the KE with phonon frequency $\bar{\omega}$, we see that as $\bar{\omega}$ increases

1 The start of the transition region shifts to higher λ, because the transition from large to small polaron begins when the KE becomes comparable with the PE, at which point it is energetically favourable for self-trapped states to exist

2 The transition region becomes broader – the start of the small-polaron region is also shifted to larger λ. This is because small-polaron behaviour occurs when the KE is very much smaller than the PE

3 The PE curve approaches the line representing the SCP result over the *full range* of λ. This is as one would expect, due to the fact that in the limit $\bar{\omega} \to \infty$, the hopping term of the model Hamiltonian can be neglected, and thus the SCP theory is valid

The values of λ that mark the start and end of the transition region are estimated in the following section

---

[2] In order to estimate the lattice kinetic energy, one could in principle compute the KE at very large values of λ However, this would be computationally difficult because, as λ increases, the acceptance rate of the QMC algorithm becomes increasingly small

9.4 Number of Phonons

The induced lattice distortion in the vicinity of the polaron is quantified, in a intuitive way, by the number of phonons in the polaron cloud N_{ph} This is a quantity of interest, because the mass enhancement of the polaron, compared with the bare-electron mass, is due to the surrounding phonon cloud

The expectation value of N_{ph} was directly computed using the QMC algorithm for the one-dimensional Holstein interaction The variation of N_{ph} with λ, for phonon frequencies of $\bar{\omega} = 0\ 5$, $\bar{\omega} = 1$ and $\bar{\omega} = 3$, is presented in figure (9 3) The QMC results for N_{ph} tend to the WCP results at small λ (not shown), and to the SCP result of $N_{ph} = 2\lambda/\bar{\omega}$ at large λ, for each value of $\bar{\omega}$ It is apparent from figure (9 3) that, for all couplings, N_{ph} decreases as the value of $\bar{\omega}$ increases Loosely speaking, it is simply "harder" to create phonons of higher frequency

The smooth transition from large to small polaron, which was observed in the energy curves, is again clearly visible in the QMC results for N_{ph} We observe from figure (9 3) that as the value of $\bar{\omega}$ increases

1 The start of the transition region shifts to higher λ

2 The transition region becomes broader

3 The curves representing N_{ph} move towards the SCP solution of $N_{ph} = 2\lambda/\bar{\omega}$ over the *entire range* of λ

The above three characteristics are the same as those observed in the QMC results for the PE, discussed in the previous section In fact, the values of λ that correspond to the edges of the transition region in figure (9 3), appear to match the corresponding values in figure (9 2) It should be stressed that, because λ is independent of phonon frequency $\bar{\omega}$, the above shifts in the transition region boundaries are entirely due to changing the value of $\bar{\omega}$, and not in the way the observables are measured

In table (9 1) we present the values of λ that mark the estimated start and end of the transition region for $\bar{\omega} = 0\ 5, \bar{\omega} = 1$ and $\bar{\omega} = 3$ These estimations are based on the QMC results for N_{ph}, PE, KE and TE In order distinguish more clearly the value of λ at which the "trend" of the curves altered -- the deviation of each observable from the corresponding SCP and WCP result was plotted against λ A careful inspection of the slopes of these graphs (not shown) allowed us to make a reasonable estimate of the transition-region boundaries

The QMC results for the effective mass and the isotope exponent were excluded from these estimates, because, as we shall see, they tend to the SCP solution at a slower rate than those for the energy and N_{ph}

Table 9 1   The boundaries of the transition region for the one-dimensional Holstein model, at various values of the (dimensionless) phonon frequency $\bar{\omega}$ The estimates are based on the QMC results for N_{ph}, PE, KE and TE

$\bar{\omega}$	End of large-polaron region/λ	Start of small-polaron region/λ
0 5	$(1\ 1 \pm 0\ 1)$	$(2\ 0 \pm 0\ 2)$
1	$(1\ 3 \pm 0\ 1)$	$(2\ 7 \pm 0\ 3)$
3	$(2\ 1 \pm 0\ 1)$	$(5\ 5 \pm 0\ 6)$

9.5   Effective Mass and the Isotope Exponent

As discussed in chapter (4), the use of twisted (rather than periodic) boundary conditions in imaginary time allows dynamic properties, such as the effective mass and the isotope exponent, to be directly extracted from the QMC simulations

The quantity m_0/m^*, the ratio of the bare-electron mass, $m_0 = \hbar^2/2ta^2$, to the effective mass of the polaron m^*, was measured for the one-dimensional Holstein polaron, at phonon frequencies of $\bar{\omega} = 0\ 5, \bar{\omega} = 1$ and $\bar{\omega} = 3$ The results are presented against λ in figures (9 4) and (9 5)

Let us first consider the effective mass in the large-polaron region   We see from figure (9 4) that, for each value of $\bar{\omega}$, the QMC results tend to the WCP solution as λ becomes small   As $\bar{\omega}$ is increased, the effective mass m^* is reduced   Note that an important feature of figure (9 4) is that m_0/m^* reduces almost *linearly* with λ in the large-polaron region   We will see in the following chapter that this is *not* the case for the long-range interaction models

In order to see the transition from large to small polaron more clearly, we present the QMC results for the effective mass as a plot of $\ln(m^*/m_0)$ versus λ in figure (9 5)   The transition is smooth, and we again observe that as $\bar{\omega}$ increases   the start of the transition region moves to higher λ, the transition region becomes broader, and the curve moves closer to the line representing the SCP result of $\ln(m^*/m_0) = 2\lambda/\bar{\omega}$

In the small-polaron region, the effective mass is dramatically reduced as the value of $\bar{\omega}$ increases   It is apparent from figure (9 5) that the QMC results for $\ln(m^*/m_0)$ appear to tend to the SCP solution at a slower rate (in λ) than does the energy or N_{ph}, which are shown in figures

(9 2) and (9 3) respectively   The origin of this feature is discussed in section (9 7)

The exponent of the isotope effect on the effective mass, α_{m^*}, was also directly computed using the QMC algorithm   The variation of α_{m^*} with λ for $\bar{\omega} = 0\ 5, \bar{\omega} = 1$ and $\bar{\omega} = 3$ is shown in figure (9 6)   We see that the results are in excellent agreement with the WCP results at small λ (not shown), and the SCP solution of $\alpha_{m^*} = \gamma\lambda/\bar{\omega}$ at large λ

The shape of the curves of α_{m^*} versus λ, in figure (9 6), can be understood with reference to the corresponding plots of $\ln(m^*/m_0)$, shown in figure (9 5)   Using the definition of the isotope exponent, equation (6 26), wee see that the relationship between α_{m^*} and m^*/m_0 is given by

$$\alpha_{m^*} = \frac{m^*}{m_0}\frac{\bar{\omega}}{2}\frac{\partial}{\partial\bar{\omega}}\left(\frac{m_0}{m^*}\right),\tag{9 2}$$

where we have used the fact that $\bar{\omega} \propto M^{-1/2}$ Equation (9 2) is valid for all values of λ Thus, one can justify the variation of α_{m^*} with λ, seen in figure (9 6), by considering the effect that equation (9 2) has on the QMC results for $\ln(m^*/m_0)$, as given in figure (9 5)

9.6   Dependence of Effective Mass on Phonons

We are particularly interested in comparing the QMC results for m^* and N_{ph}, because the mass enhancement is a result of the phonon field around the polaron   This fact leads one to think about the possibility that a simple approximate relation between m^* and N_{ph} may exist   The SCP theory relates m^*, equation (8 31), and N_{ph}, equation (8 27), via the expression

$$\ln\left(\frac{m^*}{m_0}\right) = \gamma N_{\mathrm{ph}},\tag{9 3}$$

which tends to the value of $2\gamma\lambda/\bar{\omega}$ as $\lambda \to \infty$ There is a conjecture that equation (9 3) may approximately hold for all λ, for all forms of interaction, and for all values of $\bar{\omega}$ [55]   The fact that the QMC scheme computes m_0/m^* and N_{ph} in a direct, independent and numerically "exact" manner allows us to test the validity of the above conjecture   This is done below for the Holstein interaction at $\bar{\omega} = 0\ 5, \bar{\omega} = 1$ and $\bar{\omega} = 3$, and in the following chapter for the long-range interactions

The values of $\ln(m^*/m_0)$ and γN_{ph}, determined using QMC, are explicitly plotted against λ in figure (9 7), for the Holstein model at $\bar{\omega} = 0\ 5, \bar{\omega} = 1$ and $\bar{\omega} = 3$ For each value of $\bar{\omega}$ studied, the general shape of the $ln(m^*/m_0)$ and γN_{ph} curves are similar   We again notice that the $ln(m^*/m_0)$ curves tend to the SCP result at a slower rate than those for γN_{ph} Having said this, however, it is evident from figure (9 7) that the relation given by equation (9 3) is indeed

approximately true for the one-dimensional Holstein interaction over the *full range* of λ, and for each $\bar{\omega}$ studied

The approximation becomes more exact as the value of $\bar{\omega}$ is increased Over the range of λ shown in figure (9 7), the average percentage difference between $ln(m^*/m_0)$ and γN_{ph} was found to be $(20 \pm 10)\%$, $(13 \pm 7)\%$ and $(9 \pm 4)\%$ for $\bar{\omega} = 0\ 5$, $\bar{\omega} = 1$ and $\bar{\omega} = 3$ One can clearly see that, for each value of $\bar{\omega}$, the percentage difference is largest in the transition region Thus, it is a result of the fact that the transition region shifts to higher λ as $\bar{\omega}$ increases (moving both N_{ph} and m^* closer to the SCP solution), that the approximation becomes more exact with increasing $\bar{\omega}$

9.7   Small-Polaronic Second-Order Processes

We have noticed that the QMC effective mass tends to the SCP result at a slower rate in λ than does the number of phonons, as can be clearly seen from figure (9 7) This was also found to be true for the energy (not shown) Thus the QMC results, which in principle are numerically "exact", appear to show that the SCP expression for the effective mass, derived in section (8 5) to be

$$\frac{m^*}{m_0} = \exp\left(\frac{2\gamma\lambda}{\bar{\omega}}\right),\tag{9 4}$$

overestimates the effective mass at intermediate values of coupling – where at the same time the energy and N_{ph} are in good agreement In this section we discuss the origin of this feature in terms of the tunneling mechanism introduced in section (8 6) for the Holstein model

The quantity m_0/m^* is defined in equation (7 23) as the second partial derivative of the energy with respect to k, for $\mathbf{k} \rightarrow 0$ In forming the SCP result for m_0/m^*, it was assumed that the second-order term of $E(\mathbf{k})$, equation (8 17), was *completely* k-independent, thus allowing it to be neglected when calculating the effective mass

This assumption is only strictly true in the limit $\lambda \gg 1$, where, in terms of the tunneling mechanism introduced in section (8 6), the electron undergoes virtual hopping from the occupied site to its nearest neighbour The *immediate* return of the electron is "guaranteed" because, in this limit, the "depth" of the potential well E_p is much larger than the energy of the bottom of the bare-electron band zt, and thus the third term of equation (8 17) is entirely k-independent However, at the values of λ corresponding with the *start* of the transition region, the electron is no longer "guaranteed" to immediately fall back into the potential well It may, for example, virtually hop to the next-nearest site before returning to the occupied site These more compli-

cated second-order processes, which were neglected in the derivation of equation (9 4), introduce a slight k-dependence in the second-order term, and thus if taken into account, would have the effect of reducing the SCP effective mass

The SCP results for E_0 and N_{ph}, on the other hand, are *not* affected by the second-order term in equation (8 17), because they are both evaluated at $k = 0$ This is the reason why the QMC results for m^* appear to tend more slowly to the SCP solution than does the E_0 or the N_{ph}

Thus, if the SCP approach is extended into the intermediate coupling regime, then the SCP result for the effective mass is overestimated   This feature has previously been observed for the Holstein model, using the technique of numerical diagonalisation, for a several-site vibrating cluster with a single electron [18]   Our results, then, appear to confirm this for the case of the one-dimensional *infinite*-lattice Holstein model, using the present QMC technique
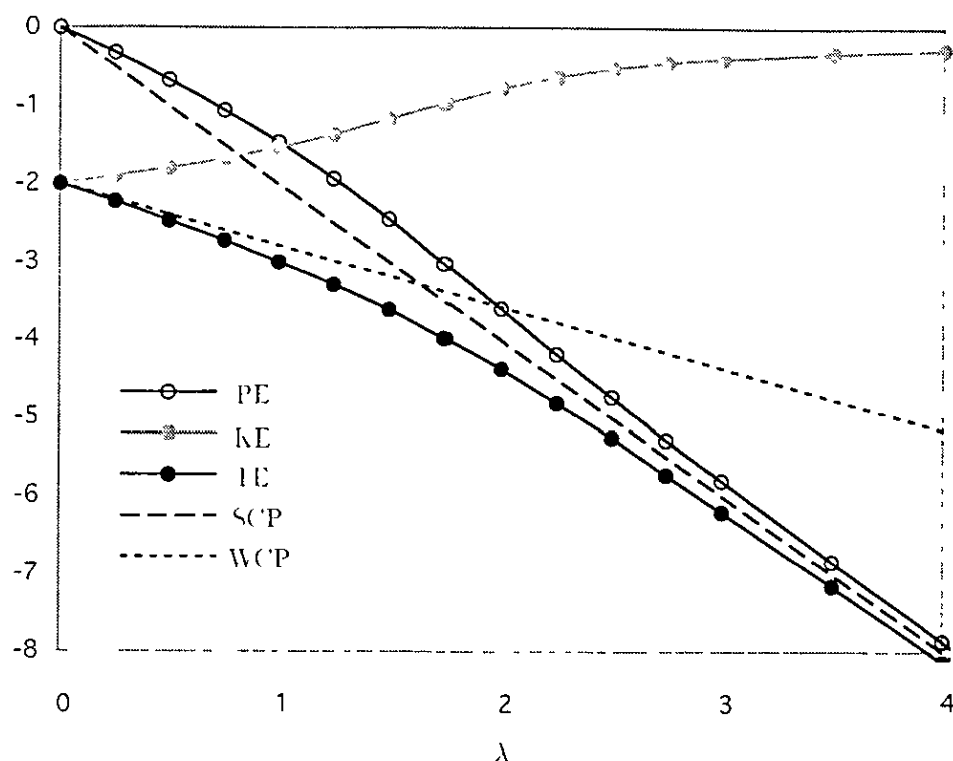
Figure 9 1 The variation of potential energy (PE), kinetic energy (KE) and total energy (TE) with λ for the one-dimensional Holstein model at $\bar{\omega} = 1$ The dashed line is the strong coupling perturbation (SCP) result and the dotted line the weak-coupling perturbation (WCP) result One can clearly distinguish the large-polaron transition and small-polaron regions
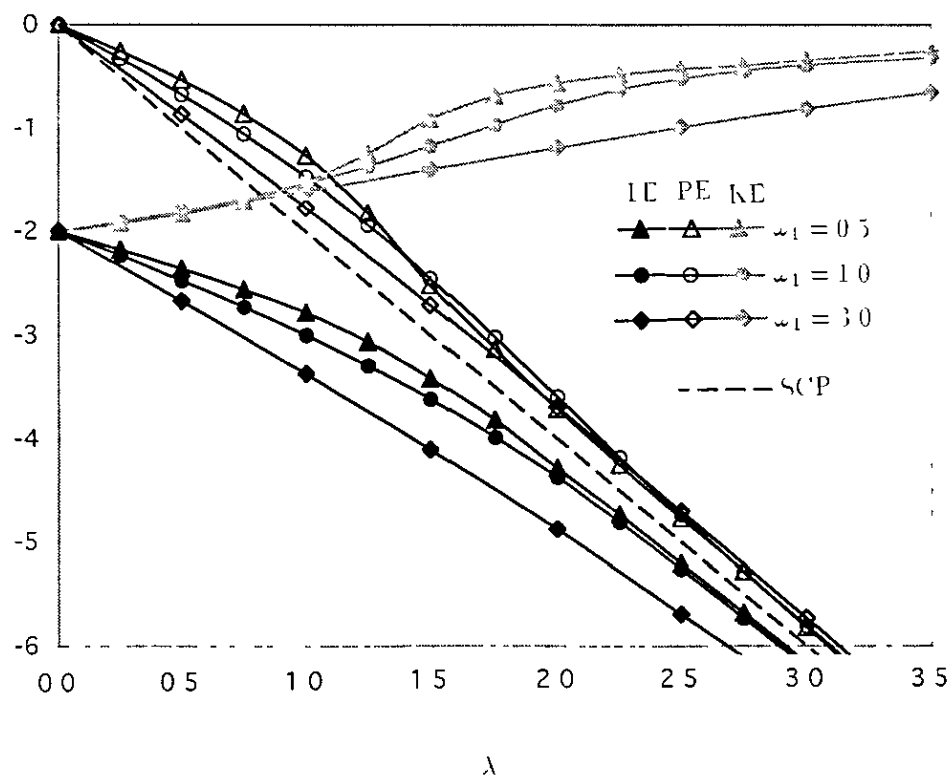
Figure 9 2 The PE, KE and TE for the one-dimensional Holstein model against λ at $\bar{\omega} = 0\ 5$, 1 0 and 3 0 As $\bar{\omega}$ increases the transition region shifts to higher λ and becomes broader
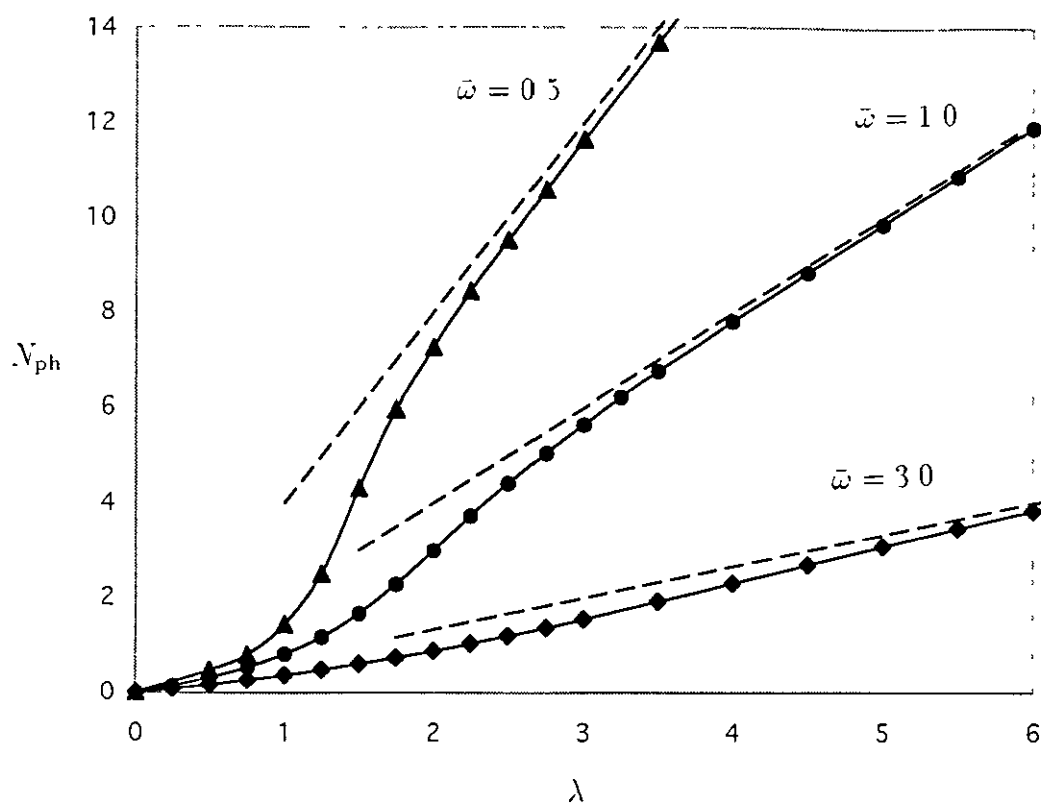
Figure 9 3   The number of phonons for the Holstein model at $\bar{\omega} = 0\,5$, $1\,0$ and $3\,0$ The dashed line shows the SCP result $N_{\mathrm{ph}} = 2\lambda/\bar{\omega}$
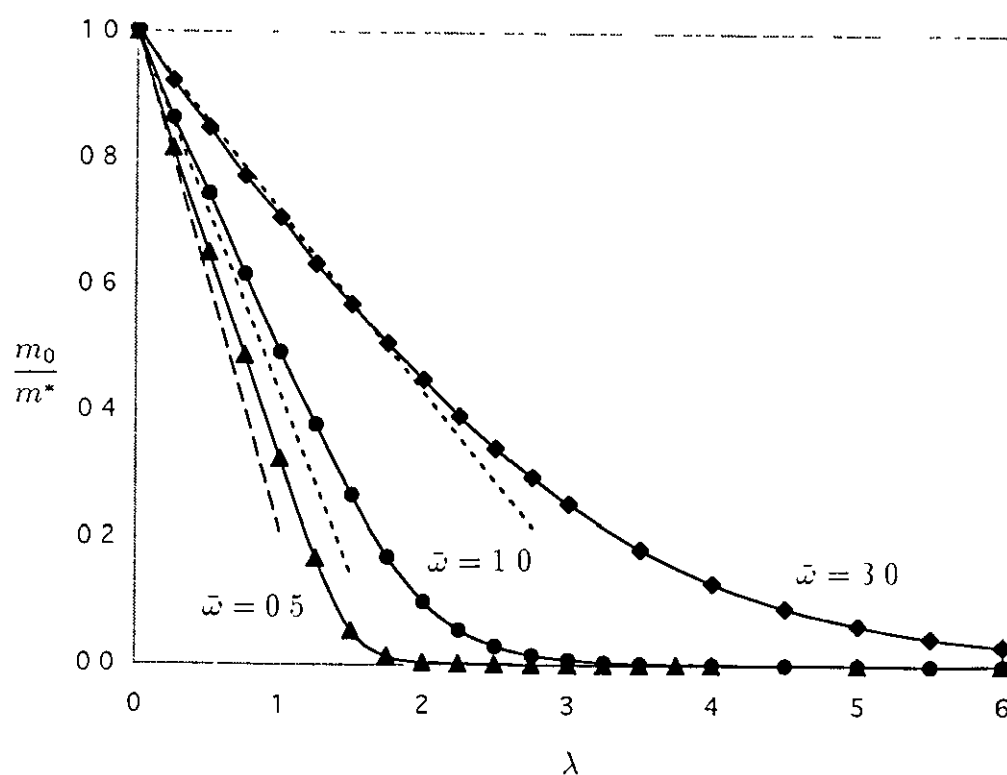

Figure 9 4   Inverse effective mass for the Holstein model at $\bar{\omega} = 0\,5$ $1\,0$ and $3\,0$ The dotted line shows the WCP results
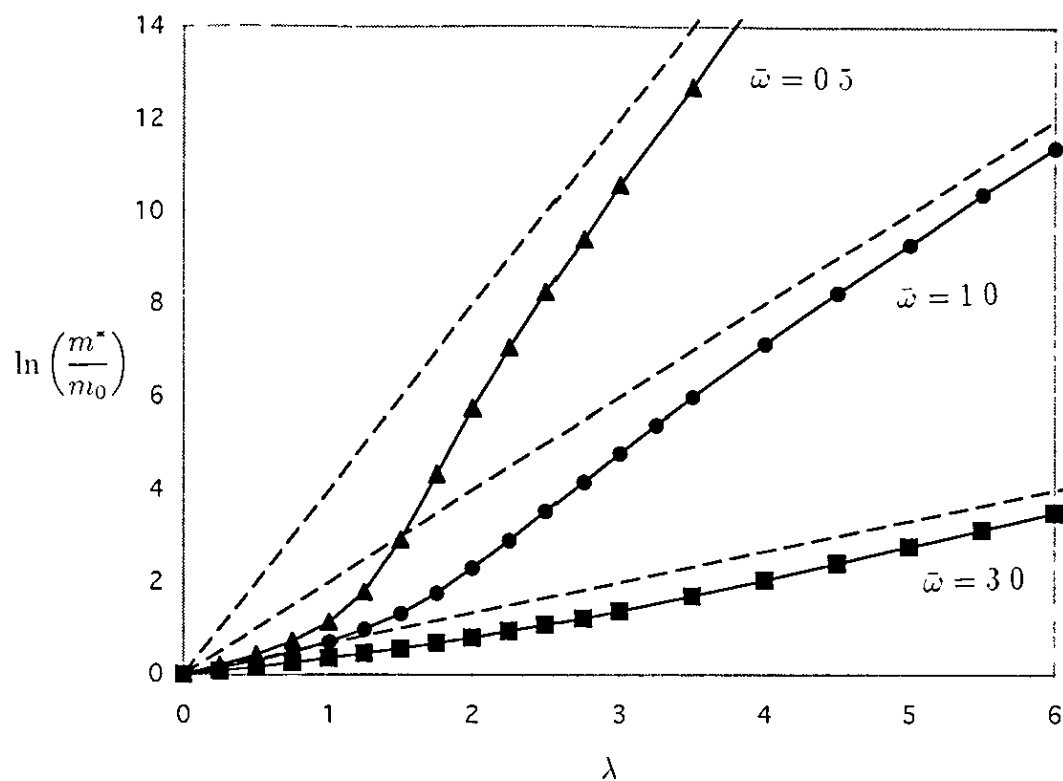
Figure 9 5 The effective mass for the Holstein model at $\bar{\omega}$ =0 5, 1 0 and 3 0 The dashed line shows the SCP result of $\ln(m^*/m_0) = 2\lambda/\bar{\omega}$
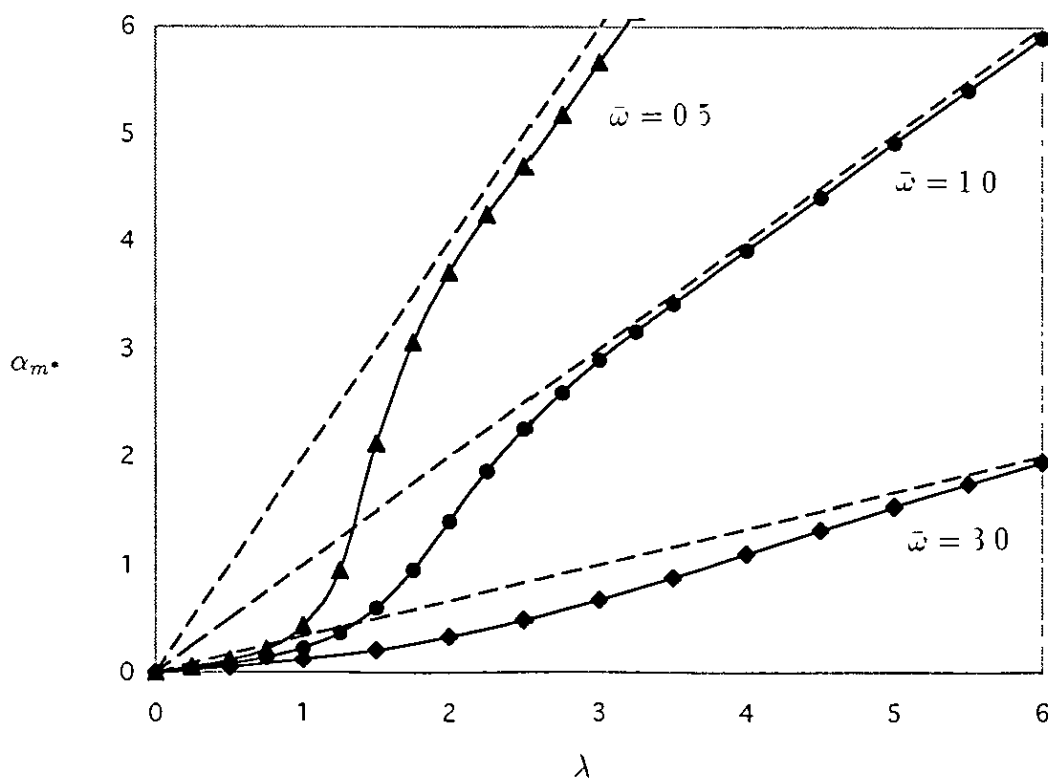

Figure 9 6 The isotope exponent for the Holstein model at $\bar{\omega}$ =0 5, 1 0 and 3 0 The dashed line shows the SCP result, and the dotted line the WCP result
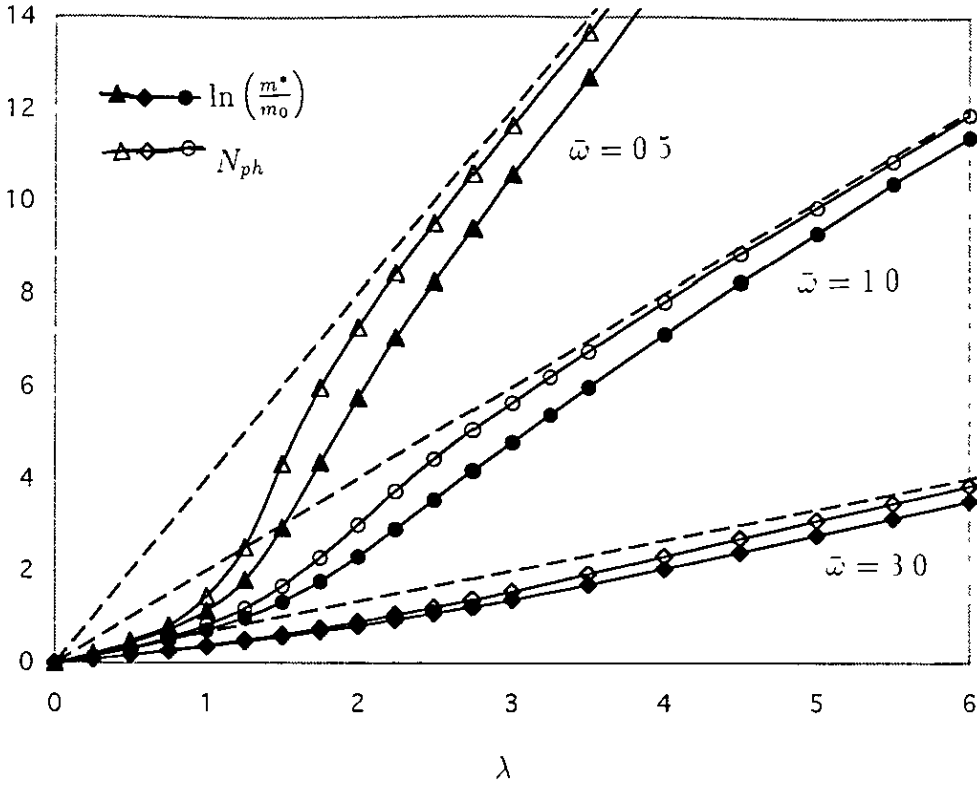
Figure 9 7 Comparison of the λ dependence of the number of phonons and the logarithm of the effective mass for the Holstein model at $\bar{\omega} =0\ 5,\ 1\ 0$ and $3\ 0$ The number of phonons converges more quickly to the $\lambda \rightarrow \infty$ result (dashed lines)

Chapter 10

Screened Fröhlich Interaction

10.1 Introduction

In the previous chapter, we studied the properties of the *short-range* Holstein model. In this chapter, we will consider several *long-range* interaction models, which are based on the discrete (non-screened) Fröhlich model – recently introduced by Alexandrov and Kornilovitch [31] – which mimics the interaction between a hole and the apical oxygen ions in high-T_c superconducting materials.

Our primary objective is to investigate the way in which the *shape* of the long-range electron-phonon interaction affects the properties of the polaron. It is therefore interesting, from a theoretical point of view, to study the *screened* Fröhlich model, in which the screening effect due to the presence of other electrons in the lattice is taken into account from within $f_m(n)$ [1]. The short-range Holstein interaction may be regarded as a special case of the screened Fröhlich interaction with an infinite amount of screening. Thus, by altering the amount of screening (via a single parameter), we can easily transverse from the Holstein model, through the screened Fröhlich model, to the non-screened Fröhlich model, in a universal manner.

The discrete (non-screened) Fröhlich model is presented in section (10 2), and the effect of screening is included in section (10 3). The QMC results for the ground state energy, the number of phonons, the effective mass, and the isotope exponent of the screened Fröhlich model, with

---

[1] The amount of screening we impose here is far greater than that expected in the high-T_c compounds – based on calculations involving the dynamic properties of the polaron response [57]

various amounts of screening, are given in sections (10 4) to (10 6)   As we will see, at strong coupling the Holstein polaron is "heavier" than the screened Frohlich polaron   This will be discussed in terms of the tunneling mechanism in section (10 7)

Note that in this chapter we restrict our investigations to a fixed dimensionless phonon frequency (adiabatic ratio) of $\bar{\omega} = 1$ This intermediate value of $\bar{\omega}$ was chosen in order to include some non-adiabatic polaron properties   All the QMC results presented in this chapter were determined to a statistical error of less than one percent

10.2   Fröhlich Interaction Force

Let us consider the long-range discrete Frohlich interaction proposed by [31] as being an appropriate model to describe the polaronic behavior in certain high-T_c cuprates   The model is depicted in figure (10 1) for the one-dimensional case   The mobile charge-carrier (electron or hole) may hop from site to nearest-neighbour site along the lower chain   The chain consists of an infinite number of lattice sites separated by the lattice constant a The electron interacts with *all* the ions which reside at the lattice sites of a similar chain, that is parallel to the first   The separation of the two chains is also equal to a lattice constant a We assume in this model that the vibrations of the ions are polarized in a direction that is perpendicular to the chains   Furthermore, the ions do not interact with one-another, and so vibrate with the same characteristic frequency

We wish to find an expression for the the interaction force $f_{\mathbf{m}}(\mathbf{n})$ – between the mobile charge-carrier on site $\mathbf{n}$ (of the lower chain) and the m'th ion (of the upper chain) – such that the the generalised model Hamiltonian will describe the discrete Frohlich model described above   Since both m and n are measured in units of a, we choose from this point on to take $a = 1$ The presence of the charge-carrier displaces the m'th ion by a *small* distance $\xi_{\mathbf{m}}$ in a direction perpendicular to the chain, as shown in figure (10 1)   The distance between the charge-carrier and the *original* position of the ion is given by

$$r_{\mathbf{mn}}^2 = |\mathbf{m} - \mathbf{n}|^2 + 1, \tag{10 1}$$

and the distance between the charge-carrier and the *displaced* ion is

$$\mathbf{r}_{\mathbf{mn}}'^2 = |\mathbf{m} - \mathbf{n}|^2 + (1 - \xi_{\mathbf{m}})^2 \approx |\mathbf{m} - \mathbf{n}|^2 + 1 - 2\xi_{\mathbf{m}}, \tag{10 2}$$

where only the first order terms in $\xi_{\mathbf{m}}$ of the binomial expansion of $(1 - \xi_{\mathbf{m}})^2$ have been retained Using Coulombs law, the difference in the mutual potential energy due to the change of radial distance r_{mn} to r_{mn}' is given by

$$\delta U_{\mathbf{mn}} = \frac{Q_{\mathbf{m}} Q_{\mathbf{n}}}{4\pi\epsilon_0} \left(\frac{1}{r_{nm}'} - \frac{1}{r_{nm}} \right), \tag{10 3}$$

where Q_m and Q_n denote the charge of the ion and the charge-carrier respectively We may use the binomial expansion again for the quantity $1/r'_{nm}$, appearing in equation (10 3), to give

$$\frac{1}{(|m-n|^2 + 1 - 2\xi_m)^{1/2}} = \frac{1}{r_{nm}} \left(1 - \frac{2\xi_m}{r_{nm}^2}\right)^{-1/2} \approx \frac{1}{r_{nm}} + \frac{\xi_m}{r_{nm}^3},\qquad(10\ 4)$$

where again we have kept only the first order terms in ξ_m Thus, the difference in potential energy, which is due to the electron-phonon interaction *only*, can be written as

$$\delta U_{mn} \approx \frac{Q_m Q_n}{4\pi\epsilon_0} \frac{\xi_m}{(|m-n|^2 + 1)^{3/2}}\qquad(10\ 5)$$

From first principles we can think of δU_{mn} as being the work done, by the internal forces, in taking the ion from its original position to its displaced position We may write $\delta U_{mn} = f_m(n)\xi_m$, where $f_m(n)$ is interpreted as the z-projection of the Coulomb force on the ion due to the presence of the charge-carrier Thus, we deduce that the Hamiltonian for the discrete Frohlich model is that of our generalised model Hamiltonian, equation (1 1), with the electron-phonon interaction force having the form

$$f_m(n) = \frac{\kappa}{(|m-n|^2 + 1)^{3/2}}\qquad(10\ 6)$$

Physically, this model was proposed in order to represent the interaction between a hole in the copper-oxygen layer (lower chain) and the apical oxygens in the ionic layer (upper chain) contained within the structure of certain doped high-T_c superconductors such as $YBa_2Cu_3O_{6+x}$ [31] These materials are highly anisotropic due to the fact that the holes are sharply localised in the copper-oxygen layer – giving rise to poor conduction in the c-direction (normal to copper-oxygen layer) This leads to very poor screening of the electron-phonon interaction in the c-direction, and almost complete screening in the a-b plane Thus, it is assumed that the ions vibrate only in a direction that is perpendicular to the chains, and so the above model mimics the electron-phonon interaction in these materials

10.3   Screened Fröhlich Force

Imagine that a positive charge is introduced into a free electron gas The presence of the positive charge will attract electrons in its immediate vicinity producing a surplus of electronic charge around it This acts to reduce – or *screen* – the field of the positive charge Consider, for example, the force exerted by an electron in a metal It is well known from solid state theory that, to a reasonable approximation, the Coulomb force is screened by other electrons according to [56]

$$\mathbf{F} = \frac{e^2\mathbf{r}}{4\pi\epsilon_0 r^3} \exp\left(\frac{-r}{R_{\text{sc}}}\right),\qquad(10\ 7)$$

where R_{sc} is known as the *screening length* That is, the screened force is the non-screened force multiplied by an exponential damping factor The screening length in a typical metal, having a very large electron density ($\geq 10^{28} m^{-3}$), is of the order of a lattice constant, and so the screening effects are very important A typical semiconductor, on the other hand, has a relatively low carrier density and so the screening length is large compared with a lattice constant It is often a reasonable approximation to neglect the effects of screening for a semiconductor

Consider now the interaction force of the discrete Frohlich model, given by equation (10 6) Our aim is to investigate the way in which the *shape* of the long-range electron-phonon interaction affects the properties of the polaron Accordingly, let us define the interaction force for the *screened Frohlich model* as

$$f_m(n) = \frac{\kappa}{\left(|m - n|^2 + 1\right)^{3/2}} \exp\left(-\frac{|m - n|}{R_{sc}}\right),$$ (10 8)

where R_{sc} is the screening length Increasing the value of R_{sc} decreases the screening effect and thus increases the width ("spread") of the interaction force In this chapter we consider equation (10 8), in one dimension, for the following four cases

1 The Holstein model $(f_m(n) = \delta_{n,m})$, with $R_{sc} \to 0$

2 The screened Frohlich model, with $R_{sc} = 1$

3 The screened Frohlich model, with $R_{sc} = 3$

4 The non-screened Frohlich model, equation (10 6), with $R_{sc} \to \infty$

In practice, then, we can move from the Holstein model, through the screened Frohlich models, to the non-screened Frohlich model, simply by changing the value of the parameter R_{sc} The shape of the electron-phonon interaction force $f_m(n)$ for each of the above screening lengths are shown in figure (10 2)

Note that, based on an analysis that takes into account the dynamic properties of the polaron response, the screening length in superconducting cuprates is expected to be close to $R_{sc} \to \infty$ [4] We have chosen the above values of R_{sc} simply in order to investigate the way in which the properties of the polaron are affected by the shape of the electron-phonon interaction force

10.4 Transition Region Boundaries

The QMC algorithm was used to compute the potential energy (PE), the kinetic energy (KE) and the total energy (TE) for the one-dimensional screened Frohlich model, equation (10 7) with a (dimensionless) phonon frequency of $\bar{\omega} = 1$ Figure (10 3) shows these energies as a function of the coupling constant λ for all four different screening lengths $R_{sc} \to 0$ (Holstein interaction), $R_{sc} = 1$, $R_{sc} = 3$, and $R_{sc} \to \infty$ (non-screened Frohlich interaction) One can see from figure (10 3) the existence of the self-trapping transition for all values of R_{sc} Let us discuss the small-polaron, large-polaron and transition regions separately below [2]

In the small-polaron region, the TE, for each value of R_{sc}, tends to the same strong-coupling perturbation (SCP) result of $E_0/t = -2\lambda$ That is, changing the screening length does not alter the energy in the limit $\lambda \to \infty$ (the SCP result is independent of γ) In the large-polaron region, the QMC results were found to be in excellent agreement with the weak-coupling perturbation (WCP) results, presented in chapter (7), for all values of R_{sc} (not shown)

At intermediate values of coupling, one can clearly see from figure (10 3) that, as the value of R_{sc} increases, the KE increases less rapidly with λ As a result of this

1 The start of the transition region – the point at which it becomes energetically favorable for localised states to exist – shifts to higher λ

2 The transition region broadens, because the small-polaron region begins when the KE is small compared with the PE

3 The PE versus λ curve moves closer to the line representing the SCP result over the *full range* of λ

In the previous chapter, we observed very similar behaviour in the Holstein model as $\bar{\omega}$ increased However, in the present case – with the phonon frequency $\bar{\omega}$ fixed – the increase in KE with λ is due only to changing the shape of $f_m(n)$

The QMC results for the number of phonons in the polaron cloud N_{ph}, using the same four interaction lengths, are presented against λ in figure (10 4) They are in excellent agreement with the WCP results at small λ (not shown), and with the (γ-independent) SCP result of $N_{ph} = z\lambda/\bar{\omega}$ at large λ

---

[2] We define the large-polaron (small-polaron) region as the range of λ in which the behaviour of the polaron is accurately described by strong-coupling (weak-coupling) perturbation theory

Interaction Model	Start of transition/λ	End of transition/λ
Holstein ($R_{sc} \to 0$)	($1\ 1 \pm 0\ 1$)	($2\ 0 \pm 0\ 2$)
Screened Frohlich ($R_{sc} = 1$)	($1\ 7 \pm 0\ 1$)	($3\ 8 \pm 0\ 4$)
Screened Frohlich ($R_{sc} = 3$)	($2\ 2 \pm 0\ 1$)	($4\ 7 \pm 0\ 4$)
Non-screened Frohlich ($R_{sc} \to \infty$)	($2\ 9 \pm 0\ 2$)	($6\ 3 \pm 0\ 5$)

Table 10 1   The boundaries of the transition region for the one-dimensional screened Frohlich interaction, at various screening lengths R_{sc} (measured in units of the lattice constant)   The estimates are based on the QMC results for N_{ph}, PE, KE and TE

The transition region boundaries are again discernible, and appear to correspond with the boundaries observed in the energy curves   Table (10 1) shows the values of λ that mark the estimated start and end of the transition region for each value of R_{sc} The estimates are based on the QMC results for N_{ph}, PE, KE and TE, and found using the method described in section (9 4)

It is rather interesting to compare the curves of N_{ph} versus λ for the long-range interactions ($R_{sc} > 0$) with the curve for the (short-range) Holstein model ($R_{sc} \to 0$)   This is done in figure (10 5), where we plot the ratio of N_{ph} for each R_{sc} to the value of N_{ph} for the Holstein model, against λ The plot reveals that changing the screening length (at fixed $\bar{\omega} = 1$) produces large fractional differences in the values of N_{ph} in the large-polaron region   The ratios are largest in the limit $\lambda \to 0$, having values of $\approx 2\ 1$ for $R_{sc} \to \infty$, $\approx 1\ 8$ for $R_{sc} = 3$, and $\approx 1\ 4$ for $R_{sc} = 1$

10.5   Effective Mass and the Isotope Exponent

The QMC results for the effective mass of the screened Frohlich model, at screening lengths of $R_{sc} \to 0$ (Holstein interaction), $R_{sc} = 1$, $R_{sc} = 3$ and $R_{sc} \to \infty$ (non-screened Frohlich interaction), are presented as graphs of m_0/m^* and $\ln(m^*/m_0)$, versus λ, in figures (10 6) and (10 7) respectively

Let us first consider the effective mass in the small-polaron region   As can be seen from figure (10 7), the QMC results for each R_{sc} tend to the SCP result of $\ln(m^*/m_0) = 2\gamma\lambda/\bar{\omega}$, where γ is defined by equation (8 30)   Thus, unlike the PE and the N_{ph}, the SCP result for the effective mass is "model dependent"   It is evident from figure (10 7), that in the small-polaron region, increasing R_{sc} decreases the effective mass by a large amount   For example the non-screened Frohlich polaron is over 1000 times "lighter" than the Holstein polaron at $\lambda = 4$, and over

10000 times at $\lambda = 5$ The origin of this rather surprising feature is discussed in terms of the small-polaron tunneling mechanism later in section (10 7)

Let us now consider the results for the effective mass in the large-polaron region, where the QMC results tend to the WCP results for all R_{sc} (not shown) In the case of the Holstein interaction ($R_{sc} \rightarrow 0$), one can see from figure (10 6) that m_0/m^* decreases approximately linearly with λ in this region At the same time, the decrease is approximately exponential for the other screening lengths As a consequence, the effective mass found for the long-range interaction is actually *larger* than that found for the Holstein (short-range) interaction In fact, at around $\lambda \approx 0\ 5$, the effective mass for the long-range interaction models ($R_{sc} > 0$) in the range of 5% to 10% larger than that of the Holstein (short-range) interaction This is in line with our QMC results for N_{ph} shown in figure (10 5) Thus, as the "spread" of the interaction is increased, the number of phonons in the polaron cloud is increased, which in turn tends to increase the effective mass of the polaron

The direct QMC results for the isotope exponent on the effective mass α_{m^*} are presented against λ for the same four values of R_{sc} in figure (10 8) In the small-polaron region we see that the isotope exponent tends to the SCP result of $\alpha_{m^*} = \gamma\lambda/\bar{\omega}$ Thus for large λ the value of α_{m^*} for each R_{sc} is approximately a fraction γ that of the Holstein model The values of γ for each model were presented in table (8 1) In the large-polaron region, the values of α_{m^*} for the different screening lengths appear in the reverse order of the small-polaron region, as predicted by the WCP theory in section (7)

10.6 Dependence of Effective Mass on Phonon Cloud

In the previous chapter, we observed that the effective mass of the Holstein polaron tended to the SCP result at a slower rate, in λ, than did N_{ph} or TE In figure (10 7), we plot both $\ln(m^*/m_0)$ and γN_{ph} against λ for all values of the screening length R_{sc} We observe that the same behavior is present in the QMC results for *all* values of R_{sc} That is, SCP expression for the effective mass, derived in chapter (8), slightly overestimates its value, for the screened and non-screened Frohlich polaron in the small-polaron region

In section (9 6), we considered the conjecture that the the SCP relation between the effective mass and the number of phonons, given by equation (9 3), may approximately hold over all λ, for all values of $\bar{\omega}$ and for all forms of $f_m(n)$ Let us now test the validity of this conjecture for the screened Frohlich model In figure (10 7), the QMC results for $\ln(m^*/m_0)$ and γN_{ph} are

plotted together, against λ, for all the values of R_{sc} (at $\bar{\omega} = 1$) We see that equation (9 3) is approximately correct for *all* the values of R_{sc} studied For the range of coupling shown in figure (10 7), the percentage difference between $\ln(m^*/m_0)$ and γN_{ph} was found to be $(13 \pm 7)\%$, $(6 \pm 3)\%$, $(11 \pm 8)\%$ and $(30 \pm 20)\%$ for $R_{sc} \to 0$, $R_{sc} = 1$, $R_{sc} = 3$ and $R_{sc} \to \infty$ respectively In the small-polaron region, we see that the conjecture becomes more valid as the value of R_{sc} increases This is a consequence of the fact that the both N_{ph} and m^* move closer to the SCP solution with increasing R_{sc} However, this is not the case in the large-polaron region, where we know from our WCP calculations, presented in chapter (7), that the values of N_{ph} and m^* depends on the precise nature of the shape of the interaction force in Fourier space

10.7 Tunneling Mechanism for Long-Range Interaction.

We have observed that, in the small-polaron region, both E_0 and N_{ph} tend to the corresponding "model independent" SCP result, which are given by equations (8 26) and (8 27), respectively At the same time, m^* and α_{m^*} tend to the corresponding "model dependent" (γ-dependent) SCP result given by equations (8 31) and (8 32), respectively Here, the "mass enhancement factor" γ, defined in equation (8 30), depends only on the shape of the interaction force For example, in the limit $\lambda \to \infty$, the Holstein small-polaron ($\gamma = 1$) has the same ground state energy, but is much "heavier", than the non-screened Frohlich small-polaron ($\gamma = 0\ 387$) We presented the value of γ for each model studied in table (8 1)

In section (8 6), we discussed the tunneling mechanism of the Holstein small-polaron, where the electron interacts only with the site it currently occupies The polaron is localised in a potential well at a particular site (created by the induced lattice distortion around it) The polaron *slowly* tunnels through the lattice by means of a virtual hopping process – the rapid back-forth motion between the occupied site and its nearest-neighbour On each virtual hop, the energy of the nearest-neighbour site is reduced by a small amount Only after a sufficient number of virtual hops have taken place, can the electron "coherently" tunnel to the nearest-neighbour site

Now let us consider the case for the long-range interaction models Compared with the case of the Holstein model, the energy of the nearest-neighbour site (and beyond) is reduced by an amount that depends on the shape of interaction force $f_m(n)$, as depicted in figure (10 7) Thus, the number of virtual hops required before the polaron can tunnel to the nearest-neighbour site is reduced The resulting increase in the hopping frequency reduces the effective mass of the polaron Increasing the value of R_{sc} in the screened Frohlich model has the effect of increasing the interaction force exerted on the nearest-neighbour site $f_m(1)$ Hence, in the small-polaron

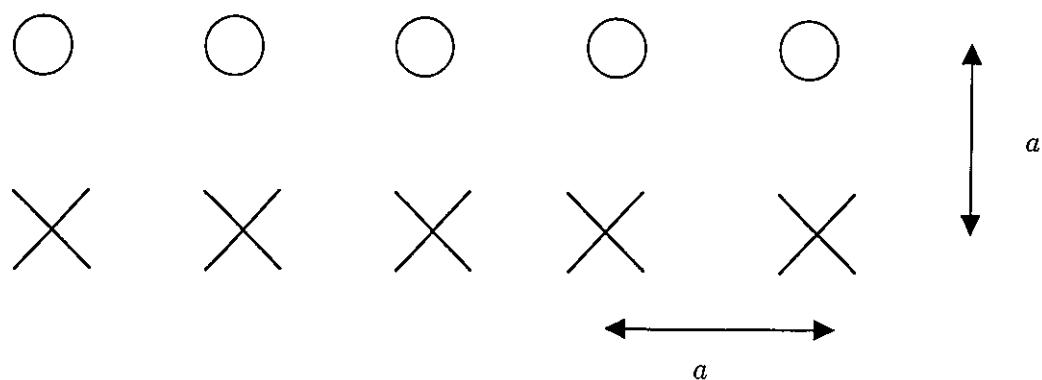region, the effective mass becomes smaller as R_{sc} is increased

Figure 10 1   Geometry of the Frohlich model shown in one dimension The mobile charge-carrier moves on the lower chain and interacts with all the ions of the upper chain The vibrations of the ions are polarized in a direction that is perpendicular to the chains
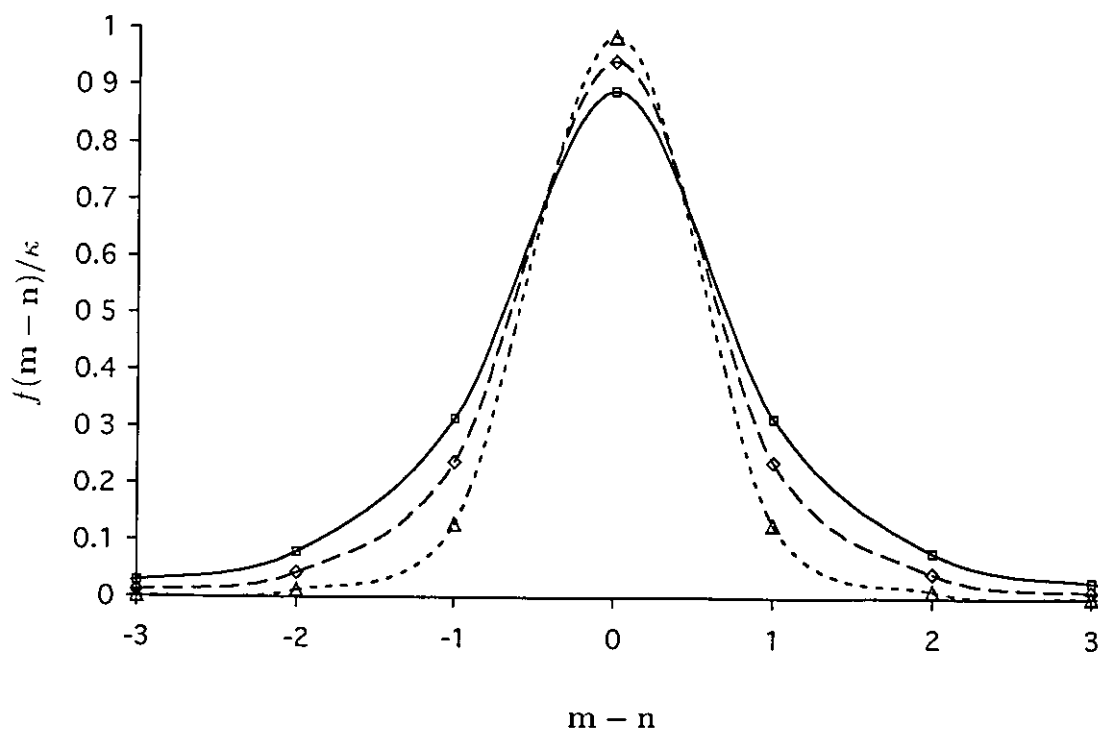

Figure 10 2   The shape of the screened Frohlich interaction force, equation (10 8), at screening lengths of $R_{sc} \to 0$ (Holstein interaction), $R_{sc} = 1$, $R_{sc} = 3$ and $R_{sc} \to \infty$ (non-screened Frohlich interaction)
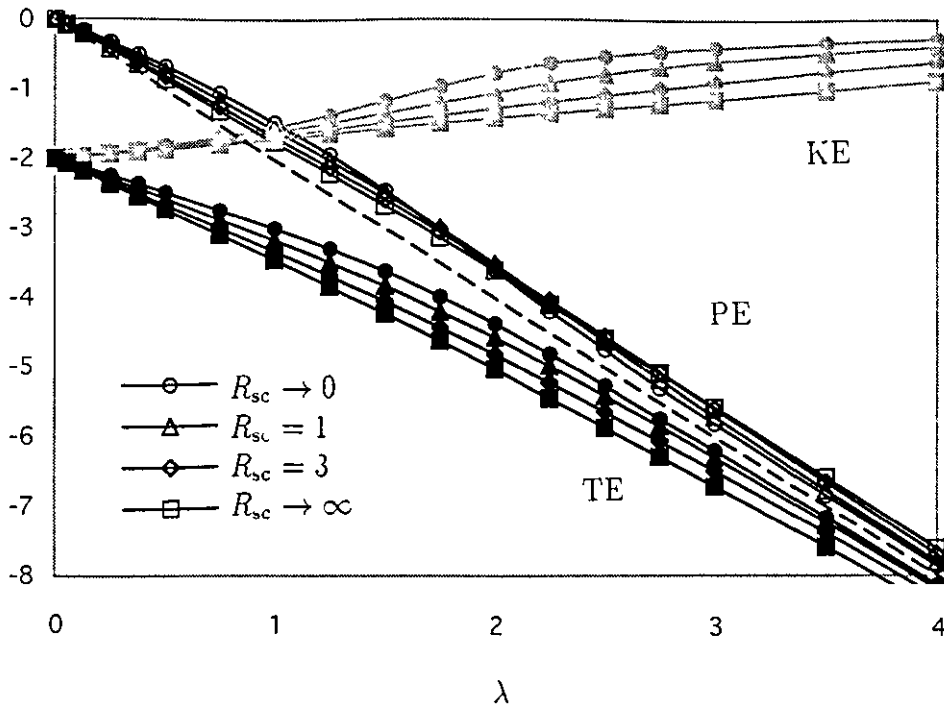
Figure 10 3 The potential energy (PE), kinetic energy (KE) and total energy (TE) of the one-dimensional screened Frohlich model at $\bar{\omega} = 1$, versus λ, for the various screening lengths R_{sc} The TE (and PE) curves tend to the same strong coupling perturbation (SCP) result of $E_0/t = -2\lambda$ (dashed line) as $\lambda \to \infty$
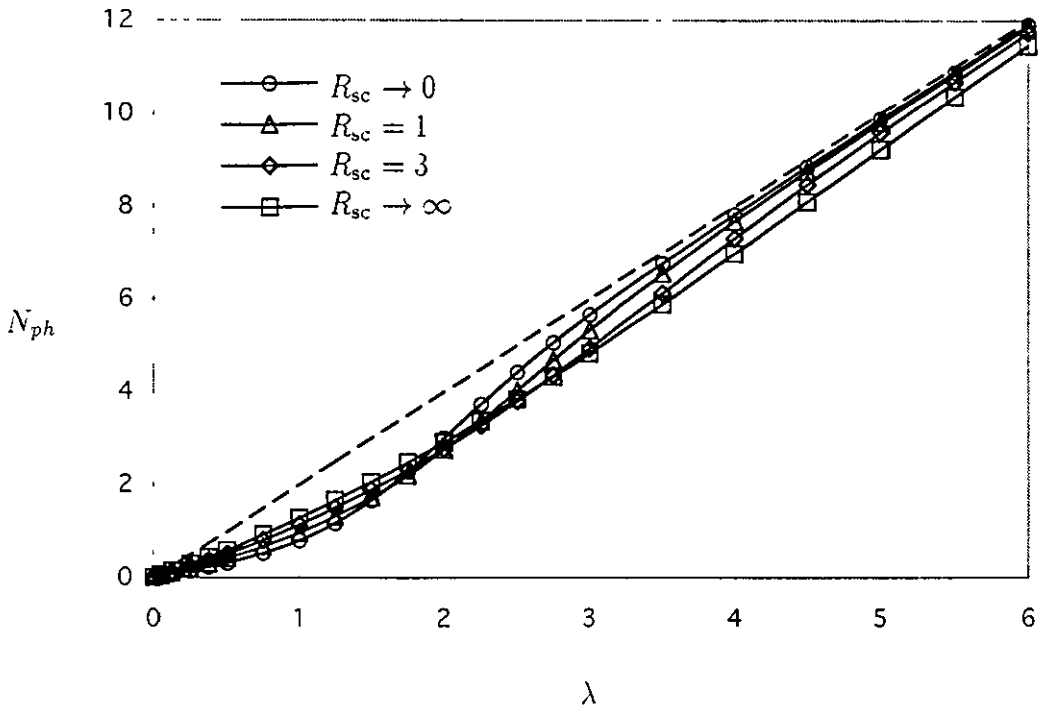

Figure 10 4 The number of phonons in the cloud N_{ph} versus λ for each R_{sc}, at $\bar{\omega} = 1$ The curves tend to the same SCP result of $N_{ph} = z\lambda/\bar{\omega}$, represented by the dashed line, as $\lambda \to \infty$

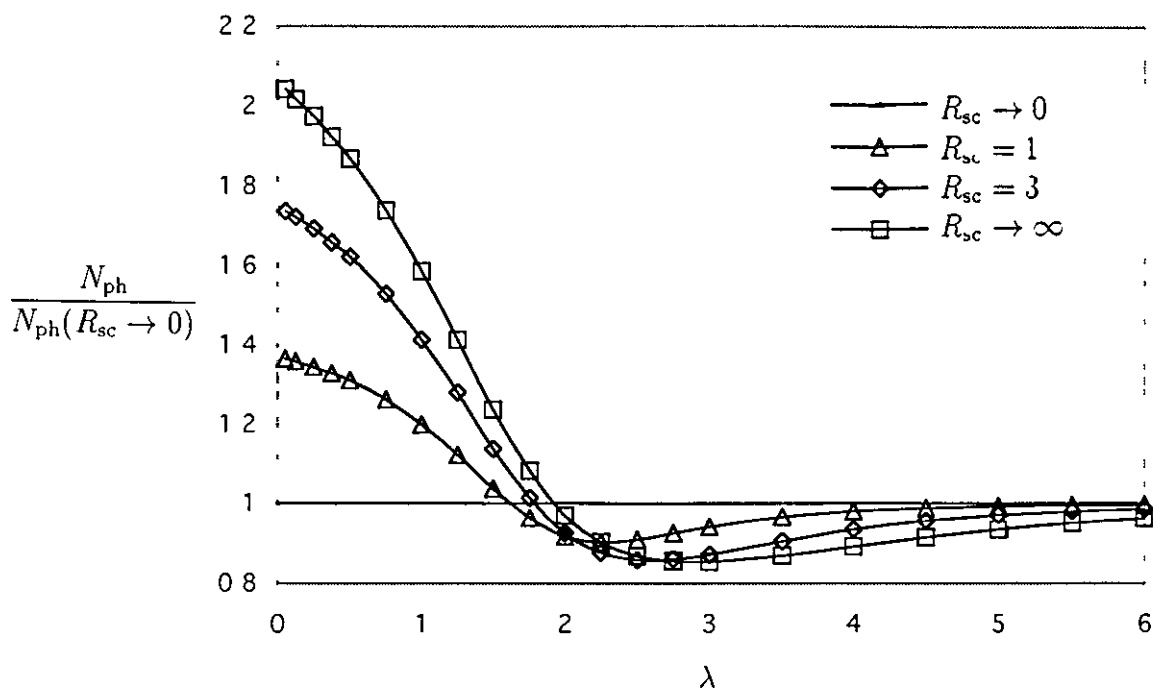Figure 10 5   The ratio of N_{ph} for each value of R_{sc} to the number of phonons for the Holstein model ($R_{sc} \to 0$) versus λ, at $\bar{\omega} = 1$
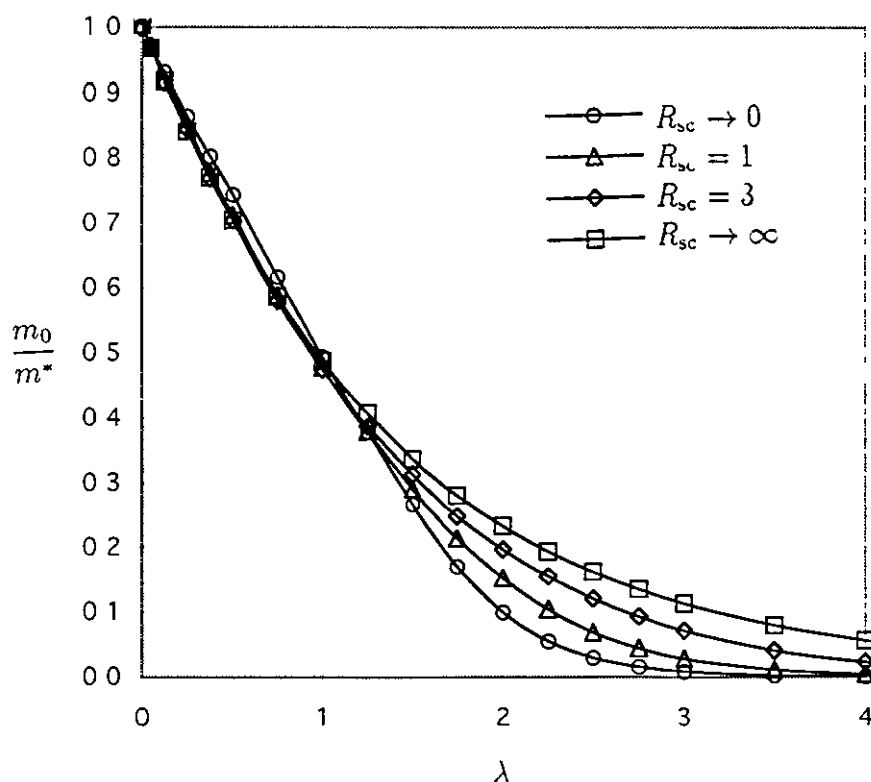

Figure 10 6   The inverse effective mass, m_0/m^*, for each R_{sc}, versus λ, at fixed $\bar{\omega} = 1$ For weak coupling ($\lambda < 1$) the Holstein large-polaron has a slightly smaller m^* than the long-range interactions
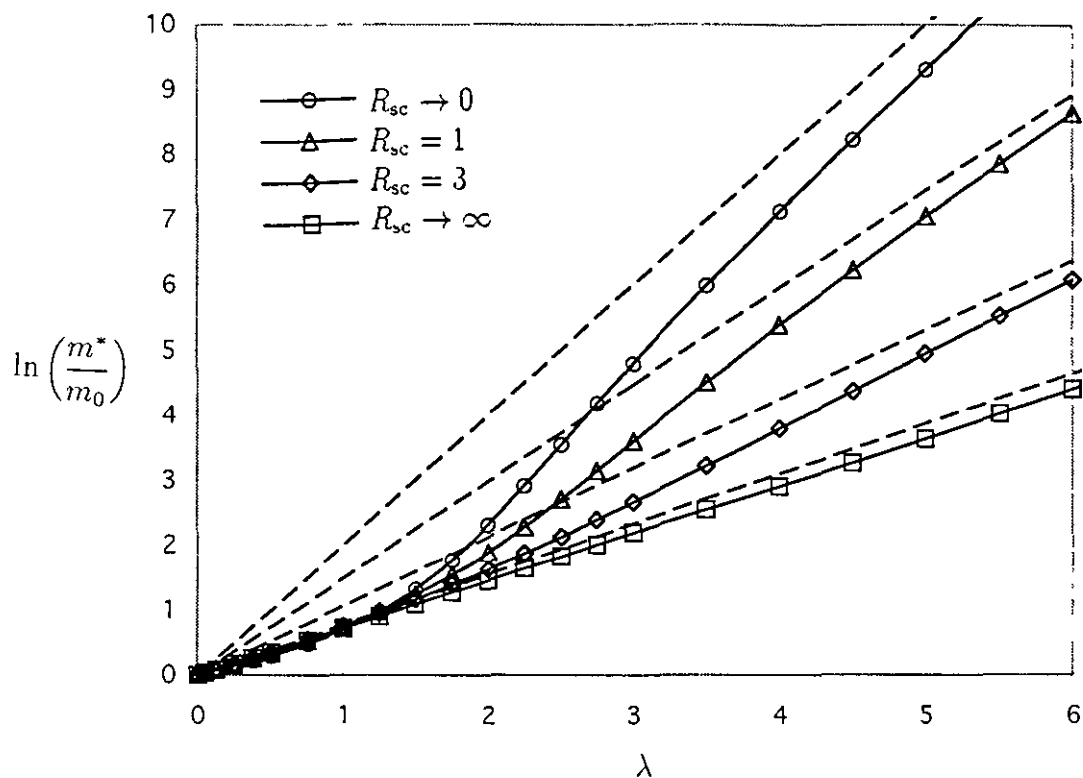
Figure 10 7   The logarithm of the effective mass versus λ, at $\bar{\omega} = 1$ For strong coupling an increase in R_{sc} dramatically reduces the effective mass   The curves tend to the SCP result (dashed lines) at a slower rate than does the TE and N_{ph}
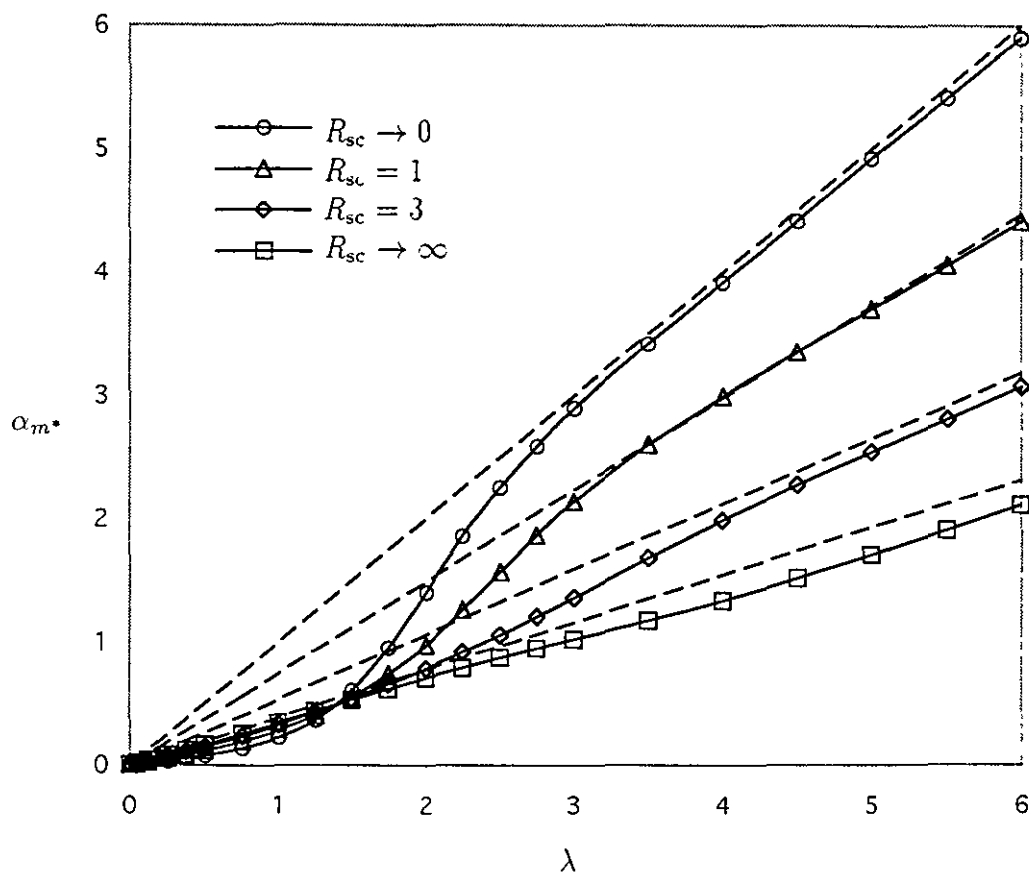

Figure 10 8   The isotope exponent (on effective mass) versus λ, for each R_{sc}, at $\omega_l = 1$
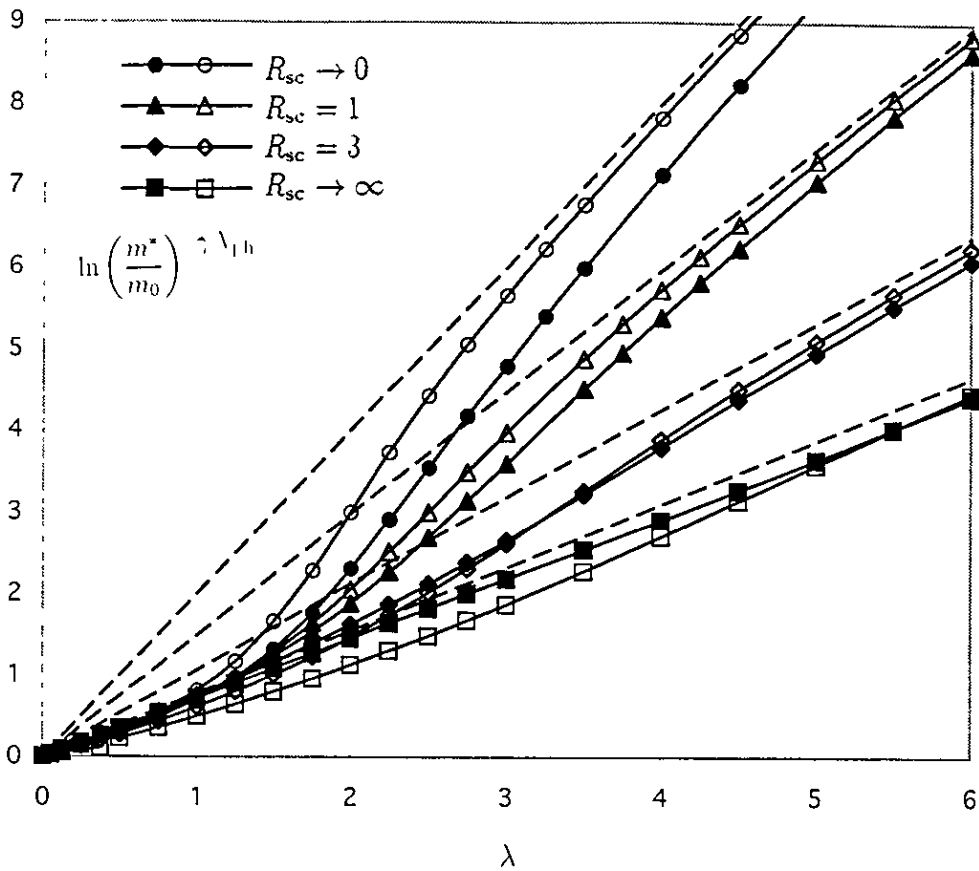
Figure 10 9 Comparing the values of $\ln(m^*/m_0)$ with γN_{ph} over λ, at $\bar{\omega} = 1$ The dashed line represents the SCP result of $\ln(m^*/m_0) = \gamma N_{\mathrm{ph}} = 2\lambda/\bar{\omega}$
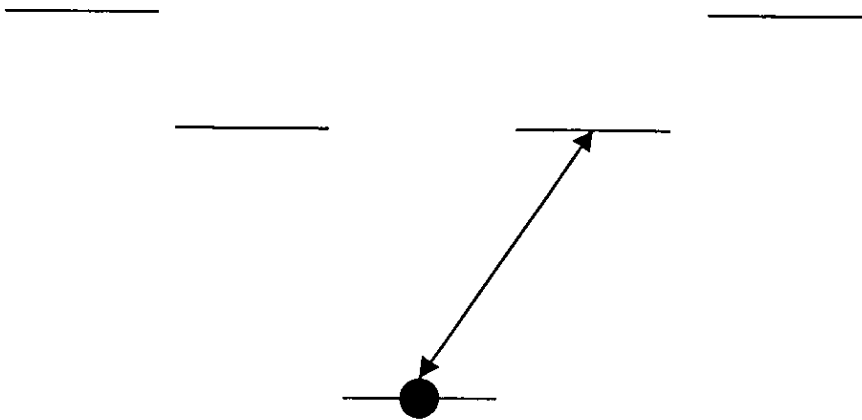

Figure 10 10 The small-polaron tunneling mechanism for long-range electron-phonon interactions Compared with the Holstein model, the nearest-neighbour site is at a lower energy, which increases the tunneling frequency, and thus reduces the effective mass

Chapter 11

Conclusions and Further Work

11.1 Conclusions

The general aim of this work was to investigate the way in which the *shape* of the long-range electron-phonon interaction governs the physical properties of the lattice polaron, particularly in the – physically most realistic – intermediate range of coupling The understanding of this is of considerable current interest due to the fact that there is an increasing amount of experimental evidence to suggest that polarons are present in the high-temperature metal-oxide superconducting materials, and the magneto-resistance manganites

We have performed an extensive numerical study of the ground state properties of the long-range screened Frohlich polaron, equation (10 8), in one dimension, over a wide range of coupling We used the continuous-time path-integral quantum Monte Carlo (QMC) method, which has recently been developed by Kornilovitch [30] The phonon degrees of freedom were analytically integrated out – leaving only the electron coordinates to be simulated The partition function was represented as a path integral with *twisted* boundary conditions in imaginary time [29] This allowed us to *directly* extract dynamic properties from the imaginary-time simulation There were no systematic errors due to finite-size, finite-time-step or finite-temperature

The screened Frohlich interaction was studied at various values of the screening length R_{sc}, which changes the width or "spread" of the interaction, in a controlled manner We studied the following four interaction models (characterised by different values of R_{sc})

1 The Holstein model, with $R_{sc} \rightarrow 0$

2 The screened Frohlich model, with $R_{sc} = 1$

3 The screened Frohlich model, with $R_{sc} = 3$

4 The non-screened Frohlich model, with $R_{sc} \rightarrow \infty$

For each interaction model, the QMC algorithm was used to make accurate measurements the ground-state energy (kinetic and potential), the effective mass, the number of phonons in the polaron cloud, and the isotope exponent on the effective mass In addition, we performed strong-coupling perturbation (SCP) and weak-coupling perturbation (WCP) calculations, in order to supplement the numerical results

For each interaction model, we determined the variation of the above observables with the coupling constant λ, at a fixed (dimensionless) phonon frequency (adiabatic ratio) of $\bar{\omega} = 1$ In the case of the Holstein model, in addition to $\bar{\omega} = 1$, we also performed simulations at $\bar{\omega} = 0\,5$ and $\bar{\omega} = 3$ The main findings of this investigation are summarised below

1 We observed the presence of the self-trapping transition for *all* the values of R_{sc} studied In each case, the following three regions were identified

(a) The large-polaron region at weak coupling, in which the behaviour of the system is accurately described by WCP theory This region is characterised by delocalised, band-electron-like states

(b) The small-polaron region at strong coupling, in which the behaviour is accurately described by SCP theory This region is characterised by localised ("self-trapped") polaronic states

(c) The transition region at intermediate coupling We observed a smooth cross-over from large- to small- polaron, in all the observables measured

2 At intermediate coupling, we saw that, as the value of R_{sc} increased, the kinetic energy increased less rapidly with λ, and as a result

(a) The start of the transition region – the point at which it becomes energetically favorable for localised states to exist – shifts to higher λ

(b) The transition region broadens, because the small-polaron region starts when the kinetic energy is much smaller than the potential energy

(c) The values of each observable moves closer to the corresponding SCP result over the *entire* range of λ

The values of λ that mark the transition-region boundaries, for each R_{sc}, were presented in table (10 1)

3 In the large polaron region, the effective mass for the long-range interactions ($R_{sc} > 1$) were found to be up to 10% larger than that for the Holstein interaction ($R_{sc} \to 0$) This corresponds with a large increases in the number of phonons at small coupling Thus, at weak coupling, the long-range interactions induce more lattice distortion, which has the effect of increasing the effective mass

4 At strong-coupling, both the effective mass and the isotope exponent tend to SCP results that are "model dependent" (which involve the "mass enhancement factor" γ) At the same time, the ground-state energy and the number of phonons tend to SCP results that are "model independent" As a result, at large λ we observed that, as the value of R_{sc} increased, the effective mass was reduced by a large amount, but the energy and number of phonons were not significantly affected This was interpreted in terms of the small-polaron tunnelling mechanism An interaction with a greater width induces more lattice distortion on the nearest-neighbour site, increasing the tunneling frequency, and thus reducing the effective mass

5 For all the interaction models, we observed that the SCP approach slightly overestimated the effective mass, at the beginning of the small-polaron region This was also explained in terms of the small-polaron tunneling mechanism At the values of λ corresponding to the start of the small-polaron region, there are complicated second-order processes present that are neglected in the SCP derivation of the effective mass Even with this feature present, we found that the SCP relation between the effective mass and the number of polarons, equation (9 3), held approximately true over all coupling

6 We also studied the way in which the phonon frequency $\bar{\omega}$ affected the polaron properties for the Holstein model We confirmed that, as the value of $\bar{\omega}$ increases, the KE increases less rapidly with λ As a result we observed that the transition region shifts to higher λ, the transition region became broader, and the value of the observables move toward the corresponding SCP result We presented the values of λ that marked the edges of the transition region for each value of $\bar{\omega}$ studied in table (9 1)

11.2 Recommendations for Further Work

The investigation presented in this work could immediately be extended to higher dimensionality, which is more physically realistic In particular, it would be useful to investigate the isotope

exponent on the effective mass in a two- or three-dimensional system, as this would allow a valid comparison to be made with the experimentally measured values discussed in section (6 5)

Another immediate extension of our investigation would be to perform QMC stimulations at non-zero value of the total momentum   It has already been demonstrated that the polaron spectrum can be determined using the present QMC scheme [30]   The drawback to this is the presence of the sign problem at non-zero total momentum

We found that the simulation becomes more computationally demanding at large λ or small ω, as β must be increased in order to satisfy the condition $\exp(\hbar\omega\beta) \gg 1$ Given this restriction, and also the fact that increasing the dimensionality or dealing with the sign problem also require substantially more computational effort, it would be advantageous to make an attempt at increasing the efficiency of the algorithm   One way in which this could done is to consider a "menu" of processes that propose the change to the trajectory on each Monte Carlo step   For example, allowing the kinks to shift in imaginary-time might well have the effect of improving the efficiency at large λ

The continuous-time path-integral QMC approach is much more efficient than the traditional discrete-time algorithm   Thus, the continuous-time method can be applied to to almost any quantum model that has previously been studied using QMC, where computational effort has been a problem

It is the twisted boundary conditions in imaginary time that allows the effective mass and the isotope exponent to be measured   In principle, the method may be applied to any quantum object that can be assigned an effective mass, such as defects in quantum liquids

References

[1] A von Hippel, Z Phys **68** 309 (1931)

[2] L D Landau, Z Phys **3** 664 (1933)

[3] H Frohlich, H Pelzer and S Zienau, Phil Mag **41** 221 (1950)

[4] A S Alexandrov and N F Mott, *Polarons and Bipolarons*, World Scientific (Singapore, 1995)

[5] H Frohlich, Adv Phys **3**, 325 (1954)

[6] S I Pekai, Sov Phys JETP **19** 796 (1949)

[7] T Holstein, Ann Phys **8**, 325 (1959)

[8] T Holstein Ann Phys **8**, 343 (1959)

[9] I G Lang and Yu A Firsov, Sov Phys JETP **16** 1301 (1963)

[10] A S Alexandrov, H Capellmann and U Gobel, Phys Rev B **46** 4374 (1992)

[11] E K H Salje, A S Alexandrov and W Y Liang, *Polarons and Bipolarons in High Temperature Superconductors and Related Materials*, Cambridge Univ Press (Cambridge, 1995)

[12] X X Bi and P C Eklund, Phys Rev Lett **70**, 2625 (1993)

[13] A Paolone and P Roy, Phys Rev B **53**, 2756 (1996)

[14] G M Zhao, K Conder, H Keller and K A Muller, J Phys Condens Matter **10** 40 (1999)

[15] M Jaime, H T Hardner, M R M B Salamon P Dorsey and D Emin, Phys Rev Lett **78**, 951 (1997)

[16] A J Millis, P B Littlewood and B I Shraiman, Phys Lett **74** 5144 (1995)

[17] A Lanzara, Phys Rev Lett **81** 878 (1998)

[18] A S Alexandrov, V V Kabanov and D K Ray, Phys Rev B **49** 9915 (1994)

[19] G Wellein and H Fehske, Phys Rev B **56** 4513 (1997)

[20] J Ranninger and U Thibblin, Phys Rev B **45** 7730 (1992)

[21] J Bonca, S A Trugman and I Batistić, Phys Rev B **60** 1633 (1999)

[22] E Jackelmann and S R White, Phys Rev B **57** 6376 (1998)

[23] H de Raedt and A Lagendijk, Phys Rev Lett **49**, 1522 (1982)

[24] H de Raedt and A Lagendijk, Phys Rev B **27**, 6097 (1983)

[25] E Berger, P Valásek and W v d Linden, Phys Rev B **52** 4806 (1995)

[26] J E Hirsch, R L Sugar, D J Scalapino and R Blankenbecler, Phys Rev B **26**, 5033 (1982)

[27] J E Hirsch and E Fradkin, Phys Rev B **27**, 4302 (1983)

[28] S R White, D J Scalapino, R L Sugar, E Y Loh, J E Gubernatis, Phys Rev B **40**, 506 (1989)

[29] P E Kornilovitch and E R Pike, Phys Rev B **55**, R8634 (1997)

[30] P E Kornilovitch, Phys Rev Lett **81**, 5382 (1998)

[31] A S Alexandrov and P E Kornilovitch, Phys Rev Lett **82**, 807 (1999)

[32] H Kleinert *Path Integrals in Quantum Mechanics, Statistics and Polymer Physics* (World Scientific, Singapore, 1990)

[33] R P Feynman, Phys Rev **97**, 660 (1955)

[34] N V Prokof'ev, B V Svistunov and I S Tupitsyn JETP Lett **64**, 911 (1996)

[35] N V Prokof'ev, B V Svistunov and I S Tupitsyn JETP **87** 310 (1998)

[36] B B Beard and U J Wiese Phys Rev Lett **77** 5130 (1996)

[37] R P Feynman *Statistical Mechanics* (Benjamin, Reading MA, 1972)

[38] J Mathews and R L Walker *Mathematical Mathods of Physics* (Benjamin, California, 1973)

[39] P E Kornilovitch, Phys Rev B **60**, 3237 (1999)

[40] K Binder and D W Heermann 1988 *Monte Carlo Simulation in Statistical Physics An Introduction* (Berlin Springer)

[41] N Metropolis, A N Rosenbluth, M N Rosenbluth, A H Teller and E Teller, J Chem Phys **21** 1087 (1953)

[42] N V Prokof'ev, B E Svistunov and I S Tupitsyn, J E P T Lett **87** 310 (1998)

[43] B B Beard and U J Wiese, Phys Rev Lett **77**, 5130 (1996)

[44] E Farhi and S Gutmann, Ann Phys (N Y) **213**, 182 (1992)

[45] P E Kornilovitch, Phys Rev Lett **84** 1551 (2000)

[46] E Maxwell, Phys Rev **78** 477 (1950)

[47] C A Reynolds, B Serin, W H Wright and N Nesbitt, Phys Rev **78** 487 (1950)

[48] J Bardeen, L N Cooper and J R Schrieffer, Phys Rev **108**, 1175 (1957)

[49] S Hoen, W N Creager, L C Bourne, M F Crommie, T W Barbee III, M L Cohen, A Zettl, L Bernardez and J Kinney, Phys Rev B **39** 2269 (1989)

[50] M K Crawford, M N Kunchur, W E Farneth, E M McCarron III and S J Poon, Phys Rev B **41** 282 (1990)

[51] H J Bornemann and D E Morris, Phys Rev B **44**, 5322 (1991)

[52] G M Zhao, M B Hunt, H Keller and K A Muller, Nature (London) **385** 236 (1997)

[53] W H Press, B P Flannery, S A Teukolsky, W T Vetterling, *Numerical Recipes, the Art of Scientific Computing*, Cambridge University Press (New York, 1986)

[54] A S Alexandrov, Phys Rev B **46** 14932 (1992)

[55] P E Kornilovitch, (private communication)

[56] J S Blakemore, *Solid State Physics*, Cambridge University Press (Malta, 1974)

[57] A S Alexandrov and N F Mott, *High Temperature Superconductors and other Superfluids*, Taylor and Francis (London, 1994)